MASTERARBEIT

Titel der Masterarbeit

„Interferometric tests of quantum physics on curved space-time“

Verfasser

Christopher Karl Hilweg, BSc.

angestrebter akademischer Grad

Master of Science (MSc.)

Wien, 2014

Studienkennzahl lt. Studienblatt:	A 066 876
Studienrichtung lt. Studienblatt:	Masterstudium Physik
Betreuer:	Assoz. Prof. Dr. Philip Walther

Acknowledgements

Writing this thesis would never have been possible without the guidance from many people who supported me in different ways and making it an unforgettable experience for me.

First of all, I would like to thank my supervisor Assoz. Prof. Dr. Philip Walther, who offered continuous advice and new ideas throughout the whole thesis. I thank him for his guidance and the great effort he put into making me a better scientist.

I would also like to thank Dr. Piotr T. Chrusciel, who guided me through the difficult field of general relativity with ease. He also inspired me with new ideas and new ways to calculate general relativistic effects, which I have used throughout this thesis.

Very sincere gratitudes go to Magdalena Zych, Fabio Costa and Igor Pikovski who introduced me to the subject of the thesis and always supported me with their advise.

I acknowledge my gratitude to Amir Moqanaki and the rest of my research group for experimental insights to the field of quantum optics.

I also want to express my very sincere gratitude to my parents, my grandparents and my siblings for their endless support - both spiritually and materially. I also would like to thank my best friend, Marianne, for guiding me always through difficult times. And finally, I would like to express my deepest sense of gratitude to my life companion Alexandra, who always supports me with love and patience.

Contents

Abstract

Quantum mechanics and general relativity are two fundamentally different theories and have both been tested independently with very high precision. Quantum mechanics allows to describe nature at very small scales whereas general relativity gives access to descriptions at very large scales. But even after a century of research, an interplay of these two very different theories has never been tested experimentally. The ongoing search for a unified framework, capable of combining all known forces of nature, suffers from this lack of experimental guidance. Even regimes where quantum mechanics applies and general relativity is treated classically has not been verified experimentally. This work investigates experimental possibilities that probe the interface of quantum mechanics and general relativity at the level of single photons. Those ideally suited quantum systems examine the influence of both, gravity and non-inertial motion, on interference effects. This can be achieved by using different types of interferometers whose paths are subject to different gravitational or centripetal potentials. Those potential differences allows to test, depending on the experimental configuration, the gravitational or inertial mass-energy equivalence which is the main focus of this thesis. To this end, after a short introduction to basic principles, the work starts by investigating properties of optical fibers substituting the arms of the interferometers and the limitations they impose on experimental results. It is shown that Michelson interferometers are ideally suited to test inertial effects on single photons, but are not beneficial to reveal gravitationally induced relative phases. Several schemes of Mach-Zehnder interferometers for testing the inertial and gravitational mass-energy equivalence principle are studied and the feasibility and limitations of those set-ups is discussed.

The results of this thesis show that gravitationally induced phase shifts in single particle wave functions are due to technical limitations hard to observe. If the arms of the interferometers are subject to different gravitational and inertial potentials however, present day technology allows to test for mass-energy equivalence and provides furthermore a experimental guideline towards testing genuine general relativistic effects on single quantum systems.

Zusammenfassung

Quantenmechanik und allgemeine Relativitätstheorie sind zwei grundsätzlich verschiedene physikalische Theorien, welche unabhängig voneinander mit sehr hoher Präzission experimentell geprüft wurden. Die Theorie der Quantenmechanik beschreibt Naturprozesse auf kleinen Skalen während die allgemeine Relativitätstheorie Beschreibungen auf großen Skalen ermöglicht. Jedoch ist es auch nach einem Jahrhundert intensiver Forschung nicht gelungen, ein Zusammenspiel dieser verschiedenen Theorien experimentell zu erforschen. Die andauernde Suche nach einer vereinheitlichten Theorie, welche alle bekannten Naturkräfte vereint, wird durch diese fehlende experimentelle Führung erheblich erschwert. Selbst Prozesse in denen die Quantenmechanik ihre Anwedung findet und die Gravitation klassisch beschrieben wird, wurden noch nicht im Labor überprüft. Diese Arbeit untersucht verschiedene Möglichkeiten, um die Schnittstelle zwischen Quantenmechanik und allgemeiner Relativitätstheorie auf dem Niveau einzelner Photonen zu testen. Diese Quantensysteme prüfen sowohl den Einfluss von gravitativen als auch nicht-inertialen Bewegungen auf Interferenz-Effekte durch den Einsatz verschiedener Interferometer deren Arme verschiedenen gravitativen und zentripetalen Potentialen unterliegen. Diese Potentialunterschiede erlauben es, je nach experimenteller Anordnung, das Äquivalenzprinzip zwischen träger/schwerer Masse und Energie zu überprüfen, was den Schwerpunkt der vorliegenden Arbeit darstellt. Zu diesem Zweck werden, nach einer kurzen Einleitung in die benötigten Grundlagen, die Eigenschaften und experimentellen Beschränkungen von optischen Lichtwellenleitern studiert, welche als Arme der Interferometer fungieren. Es wird gezeigt, dass sich Michelson Interferometer bestens zur Untersuchung von Trägheitseffekten von Einzelphotonen eignen, während sie sich für den Nachweis gravitativ induziierter Phasenschübe als nicht vorteilhaft erweisen. Weiters werden verschiedene Anordnungen eines Mach-Zehnder Interferometers zur Erforschung der Äquivalenz von Energie und träger/schwerer Masse studiert und die experimentellen Beschränkungen aufgezeigt.

Wie die Ergebnisse dieser Arbeit zeigen, ist es aufgrund technischer Einschränkungen überaus schwierig Phasenschübe durch gravitativen Einfluss auf die Wellenfunktion eines

einzelnen Teilchens nachzuweisen. Weisen die Arme eines Interferometers jedoch unterschiedliche Gravitations- und/oder Zentripetalpotentiale auf, so ist es im Rahmen heutiger technologischer Standards möglich die Masse-Energie Äquivalenz zu testen. Solche Tests können einen ausgezeichneten Leitfaden für Experimente darstellen, welche allgemein relativistische Effekte auf einzelne Quantensysteme nachweisen wollen, die im Rahmen der klassichen Gravitationstheorie nicht erklärt werden können.

1 Introduction

The theory of general relativity describes gravity as a manifestation of space-time geometry [1] - it predicts that a massive object stretches space and slows down time. The general relativistic time dilation, which follows from the Einstein equivalence principle (Chapter 2.1), describes that clocks far away from gravitating bodies ticks slower. The consequences of this prediction, like the gravitational redshift and the Shapiro delay, have been tested in various classical experiments ([2],[3],[4]), where the occurring general relativistic effects can be fully understood by the laws of classical physics. On the other hand, the influence of gravity on single-particle quantum wavefunctions was first tested by Colella, Overhauser and Werner in the renown COW experiment [5]. The experiment was performed with single neutrons, prepared in a superposition of two locations at different heights above the earth in an interferometer which results, due to gravity, in a relative phase shift between the different paths when the amplitudes are brought to interfere. Although this phase shift can be interpreted as a result of the general relativistic time dilation, one can also fully describe this with non-relativistic quantum mechanics in flat space-time. In a recent work [6], the authors proposed an experiment that allows to make a genuine test of general relativistic time dilation in quantum mechanics. They suggested to use massive single particles in a Mach-Zehnder type interferometer which, in conjunction with a relative phase shift, display a reduction in the visibility of the interference pattern which is caused by the quantum complementarity between the which path-information and the interference. The novelty of this scheme, compared to the COW experiment, was to use an additional internal degree of freedom serving as a clock which keeps track of the elapsed time, therefore giving

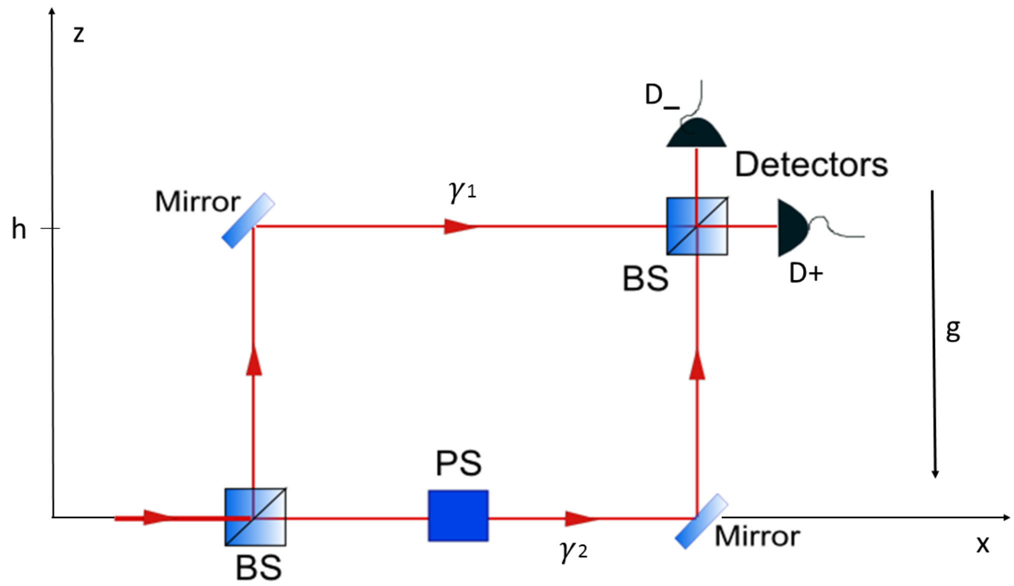

Figure 1.1: Mach-Zehnder interferometer placed vertically inside earth's gravitational field, which is homogeneous by assumption. The set-up consists of two beam splitters (BS), two Mirrors and two detectors $D_{\pm}$. A phase shifter (PS) is placed in the lower path to control the relative phase difference between the two trajectories.

information about the path chosen and reducing the interferometric visibility by the accessible amount of which-path information. A quantum-optic version of this experiment was suggested in [7], where the massive particle is replaced by single photons. In the next chapter I want to present this proposal in a short but consistent way, and take this as a starting point to motivate this thesis.

1.1 Quantum interference of single photons influenced by gravity

We consider a Mach-Zehnder interferometer which is placed vertically inside the gravitational field of the earth (see Figure (1.1)). The wave packet of a single photon is split by the first beam splitter and is travelling in a coherent superposition along the two trajectories γ_1 and γ_2.

As explained in chapter 2.1, the geometry for this particular situation can be modeled by the Schwarzschild metric [1]. For small enough interferometers[1], all points along the x-axis are approximately on the same radial coordinate distance r and a two-dimensional approximation of the Schwarzschild metric can be used for which the line element reads $c^2 d\tau^2 = \left(1 + \frac{2V(r)}{c^2}\right) c^2 dt^2 - r^2 d\theta^2$, where $V(r) = -\frac{GM}{r}$ is the gravitational potential with M the mass of the earth and G the gravitational constant. The coordinate time t and the polar angle θ are the proper time and the polar coordinate as measured by a far away observer, whereas the latter is actually the same for a local observer at r. For light-like trajectories ($d\tau^2 = 0$), a coordinate length in x-direction given by l and incorporating general relativistic time dilation, the proper time difference for an observer located at the upper path at $r + h$ is given by

$$\Delta\tau = \sqrt{1 + \frac{2V(r+h)}{c^2}}(t_r - t_{r+h}) \tag{1.1}$$

This equation shows, that the arrival time of the photon at the second beam splitter depends on its radial distance r. For symmetry reasons, the propagation along the radial direction is the same for both of the paths and can be neglected in the proper time difference. If we approximate $V(r+h) - V(r) \approx gh$, with $g = \frac{GM}{r^2}$ the gravitational acceleration on earth, we can write the total difference in the photons arrival times for free space propagation as

$$\Delta\tau \approx \frac{lgh}{c^3} \tag{1.2}$$

With the above approximations, $\Delta\tau$ only depends on the enclosed area $A = lh$ of the interferometer. For an ideal single photon source, the state of a photon moving in the +x-direction at a radial distance r in the considered metric can be described by [8]: $|1\rangle_f = a_f^\dagger |0\rangle = \int d\nu f(\nu) e^{i\frac{\nu}{c}(x_r - c\tau_r)} a_\nu^\dagger |0\rangle$ defined with respect to a local observer [2] at r, where $f(\nu)$ is the mode function, ν is the angular frequency defined with respect to the

[1] As compared to the radial distance from the center of the earth.

[2] So the proper time is given by $\tau_r = \sqrt{1 + \frac{2V(r)}{c^2}}t$.

local coordinates and $a_\nu^\dagger$ is a single frequency bosonic creation operator. From this the detection probabilities for the two detectors $D_\pm$ reads [7]

$$P_{f\pm} = \frac{1}{2}\left(1 \pm \int d\nu |f(\nu)|^2 cos(\nu\Delta\tau)\right) \tag{1.3}$$

where $\Delta\tau$ is given by equation (1.2). For $\Delta\tau$ small with respect to the frequency width of the normalized mode function ($\int d\nu|f(\nu)|^2 = 1$) the cosine term is almost constant for the relevant frequency range and can be taken out of the integral to give the phase shift term $cos(\nu_0 \frac{lgh}{c^3})$, with the central frequency of the mode function ν_0. In this situation the interferometric visibility defined by $\mathcal{V} \equiv \frac{Max_\varphi P_\pm - Min_\varphi P_\pm}{Max_\varphi P_\pm + Min_\varphi P_\pm}$ remains maximal and the gravitational time dilation is negligible although there is a relative phase shift between the two paths. This phase shift is, as stated before, fully compatible with non-relativistic quantum mechanics in flat space-time and therefore not a genuine test for general relativistic time dilation. Nevertheless, within this limit an experiment can probe the mass-energy equivalence between the photons energy and its gravitational mass.
In the limit where time dilation dominates over the width of the mode function, the amplitude of the phase shift term decreases (compare equation (1.3)) which results in a complete loss of the visibility if $\Delta\tau$ is larger than the width of the mode function. Therefore the visibility indicates that the two modes reach the second beam splitter at distinct times (the center of the wave packets gets shifted), which cannot be explained without general relativistic time dilation and would therefore be the first genuine test of general relativistic effects at the level of single quanta. A sketch of the two different situations can be found in Figure (1.2)

1.2 This thesis

A substantial loss of the interferometric visibility can be observed when the time dilation is comparable with the photon's coherence time, denoted by t_c. Equation (1.2) reveals under this circumstances, that the area enclosed by the interferometer to observe general relativistic time dilation is approximately

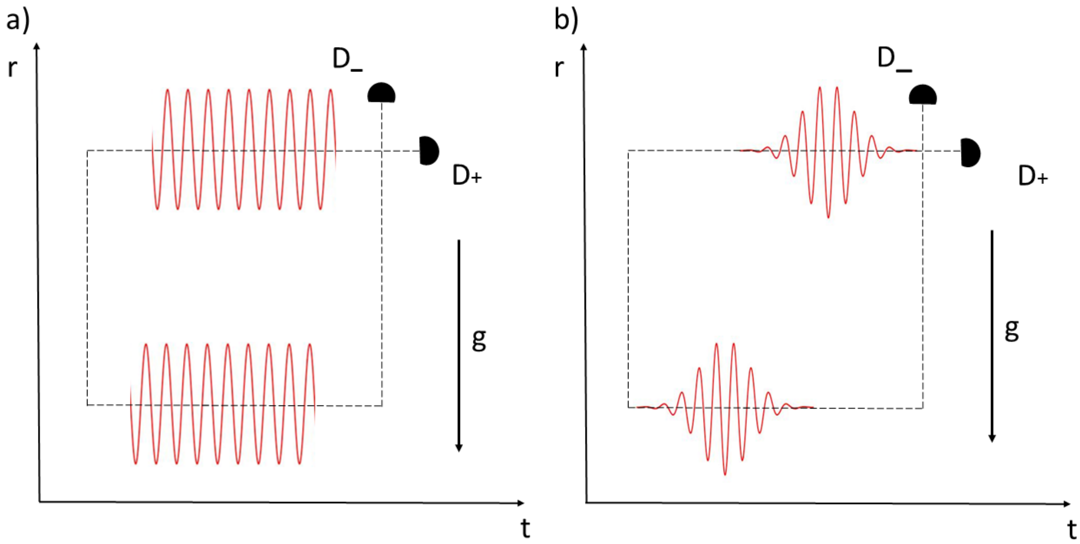

Figure 1.2: Sketch of the two different regimes of the general relativistic effects as described in [7]. Single photon wave packets with different coherence times (described by the width of the mode function) travelling in superposition along two paths at different heights in a homogeneous gravitational field and gets detected by the detectors $D_{\pm}$. a) Wave packet with long coherence time as compared to $\Delta\tau$ will give, in principle, perfect interference. b) Short coherence times of the wave packet as compared to the time dilation will not overlap in a coherent way, resulting in a loss of interference.

$$A_{td} \approx \frac{t_c\, c^3}{g} \tag{1.4}$$

Because the c^3 term is of order 10^{25}, the area needed to see a full loss of the interferometric visibility is very large. Even if one considers femtosecond optical pulses, A_{td} would still be of the order $10^3 km^2$. One of the advantages of using photons as a quantum system for testing general relativistic effects is that optical fibers can be used for transmission, therefore making experiments confined in a laboratory feasible. But as we will see in chapter 3, limitations for the performance of optical fibers make it very challenging to observe a loss in the visibility. Fortunately, experimental parameters for gravitationally induced phase shifts, thus probing mass-energy equivalence, are much less demanding. The gravitational phase shift for the considered Mach-Zehnder type interferometer is given by $\Delta\phi = \nu_0 \frac{lghN}{c^3}$, where N is the group refractive index of the optical fiber. Using a central angular frequency of the visible spectrum $\nu_0 = 10^{15} \frac{rad}{s}$ and fixing the height[3] to a value $h = 1m$ for easy implementation in a laboratory experiment, a length $l = 1000km$ for the optical fibers would result in a phase shift of $10^{-4} rad$. Such parameters are feasible with present day technologies [9].

In this thesis, the experimental proposal of [7] is examined to check its feasibility and strategies for possible improvements for gravitationally induced phase shifts will be given. Additionally, tests for inertial mass-energy equivalence and combined tests for inertial and gravitational mass-energy equivalence are under investigation. Experiments testing the general relativistic time dilation by a drop in the interferometric visibility are, due to present day technical limitations, not the primary target of this work. I will start with a short introduction to general relativity (section 2.1) and fiber optics (section 2.2) to acquire the tools to understand the mathematical description of the physical effects. The limitations of optical fibers for this type of experiments will be discussed in chapter 3. As a preliminary step to test gravitational effects on single photons, in chapter 4 an experiment including a Michelson interferometer to test inertial mass energy-equivalence

[3] To be precise, there are tiny general relativistic corrections to this value because the formula refers to coordinate length as seen by a far away observer and not to a length as measured in the laboratory.

is briefly discussed. Chapter 5 is the main part of the thesis, where several modifications of the original proposal are under investigation and their use for revealing gravitationally induced phase shifts is explored.

2 Basic principles

2.1 General relativity

To understand the proposed experiment, one has to understand the key concepts of general relativity first. Due to its importance for this thesis, I want to derive some of the basic concepts where I follow mainly the description of [1] as otherwise stated. Newton described gravity at the end of his famous Pricipia ([10]) as cause, that operates on the sun and planets according to the quantity of solid matter which they contain and propagates at all sides to immense distances decreasing always as the inverse square law. The theory of general relativity describes gravity as a manifestation of space-time geometry. It predicts that in the presence of a massive object the flow of time is slowed down whereas the space around it is stretched. This is encoded in the space-time metric tensor $g_{\mu\nu}$, that includes all information about the geometry of space-time. At the heart of general relativity is the principle of equivalence of gravitation and inertia (or Einstein equivalence principle (EEP)) [11]. In a famous Gedankenexperiment, Einstein concluded that it should be impossible for a physicist in a freely falling elevator to detect an external homogeneous gravitational field, because all included objects (elevator, test bodies, experimentalist) respond to gravity in the same way. From this can be deduced, that there should exist coordinate systems, where the influence of gravity in small enough regions of space-time can be transform away. From that observation we can introduce one formulation of the equivalence principle ([1],[12])

At every point in space-time within an arbitrary gravitational field exists a locally inertial coordinate system, in which all laws of nature - within a

sufficiently small region around that point - takes on the form of special relativity.

This means that in this locally inertial frames the laws of nature are the same as in an unaccelerated, cartesian coordinate system with no gravity present. Because Newtonian theory can predict a plethora of astronomical observations in the appropriate limits to a very high precision, a new theory of gravity should include Newtonian gravity in the limiting case. Gravity described by the Newtonian theory should therefore only be a limiting case of the general relativistic description ([12],[13]) and we require:

In the limiting case of static, weak gravitational fields and slowly moving particles, the equations of general relativity should reduce to those of Newtonian gravity.

2.1.1 Curved space-time dynamics

Here we apply the principle of equivalence together with the requirement of the Newtonian limit stated above to arrive at a accurate description for the trajectory of a particle in curved space-time. For this we consider a particle freely falling in a homogeneous gravitational field. According to the principle of equivalence we can find a locally inertial system, where the influence of gravity is absent and therefore the particle is moving on a straight line as in flat space. A point in this inertial coordinate system is denoted by the coordinates ξ^α and the equation of motion is

$$\frac{d^2\xi^\alpha}{d\tau^2} = 0 \tag{2.1}$$

where the proper time $d\tau$ is used as the parameter to describe the curve $\xi^\alpha(\tau)$ with [1]

$$d\tau^2 = \eta_{\alpha\beta} d\xi^\alpha d\xi^\beta \tag{2.2}$$

Here and in all following chapters, Greek induces run from 0 to 3 and describe four-

[1]Throughout this thesis a metric with signature -2 is used.

vectors, whereas Latin indices run from 1 to 3 and describe spatial three-vectors and the Einstein summation convention is understood. The proper time (as otherwise stated, $c = 1$ in this chapter) can also be expressed in an arbitrary 'laboratory' coordinate system with coordinates [2] x^μ

$$d\tau^2 = \eta_{\alpha\beta} d\xi^\alpha d\xi^\beta = \eta_{\alpha\beta} \frac{\partial \xi^\alpha}{\partial x^\mu} dx^\mu \frac{\partial \xi^\beta}{\partial x^\nu} dx^\nu = g_{\mu\nu} dx^\mu dx^\nu \tag{2.3}$$

by defining the metric tensor $g_{\mu\nu}$ as

$$g_{\mu\nu} = \eta_{\alpha\beta} \frac{\partial \xi^\alpha}{\partial x^\mu} \frac{\partial \xi^\beta}{\partial x^\nu} \tag{2.4}$$

However if the test particle is subject to gravity, equation (2.1) does not apply. Because the coordinates of the freely falling coordinate system are functions of the coordinates in the laboratory frame, $\xi^\alpha = \xi^\alpha(x^\mu)$, we can write

$$\frac{d^2\xi^\alpha}{d\tau^2} = \frac{d}{d\tau}\left(\frac{d\xi^\alpha}{d\tau}\right) = \frac{d}{d\tau}\left(\frac{d\xi^\alpha}{dx^\mu}\frac{dx^\mu}{d\tau}\right) = \frac{\partial \xi^\alpha}{\partial x^\mu}\frac{d^2x^\mu}{d\tau^2} + \frac{\partial^2 \xi^\alpha}{\partial x^\mu \partial x^\nu}\frac{dx^\mu}{d\tau}\frac{dx^\nu}{d\tau} = 0 \tag{2.5}$$

What we want is something similar to Newton's gravitational law $\mathbf{a} = -\nabla\phi$. We can achieve this by multiplying both sides with $\frac{\partial x^\lambda}{\partial \xi^\alpha}$ and using the general relation for the matrix $\frac{\partial x^\nu}{\partial x^\mu} = \delta^\nu_\mu$, so we arrive at a form that looks similar to the Newtonian case

$$\frac{d^2x^\lambda}{d\tau^2} + \Gamma^\lambda_{\mu\nu}\frac{dx^\mu}{d\tau}\frac{dx^\nu}{d\tau} = 0 \tag{2.6}$$

and is called the geodesic equation [13]. The new introduced quantity is called the affine connection $\Gamma^\lambda_{\mu\nu}$ and defined by [3]

$$\Gamma^\lambda_{\mu\nu} = \frac{\partial x^\lambda}{\partial \xi^\alpha}\frac{\partial^2 \xi^\alpha}{\partial x^\mu \partial x^\nu} \tag{2.7}$$

If we compare equations (2.6) and (2.1), we can see that in the frame of the laboratory an additional term is present. In Newtonian theory, this term represents an external

[2] The coordinate system used is completely arbitrary and may be "accelerated, rotated, or curvilinear as well" [13].

[3] Although $\Gamma^\lambda_{\mu\nu}$ looks like a tensor it is not, as can be shown by coordinate transformations [1].

force, so one could guess that this extra term containing the affine connection is the field that determines the gravitational force. For light-like particles like photons the proper time in equation (2.6) is zero and therefore has to be replaced [4] by a different parameter. The geodesic equation describes how the spatial coordinates x^i and the coordinate time $t = x^0/c$ are changed with respect to the proper time τ.

2.1.2 The weak field limit

Now we want to consider slowly moving (compared to the speed of light) particles in static, weak gravitational fields. From the first demand we conclude, that

$$\frac{dx^i}{d\tau} \ll \frac{dt}{d\tau} \tag{2.8}$$

must be true. Our geodesic equation therefore reduces to

$$\frac{d^2x^\lambda}{d\tau^2} + \Gamma^\lambda_{\mu\nu}\frac{dx^\mu}{d\tau}\frac{dx^\nu}{d\tau} \overset{(2.8)}{=} \frac{d^2x^\mu}{d\tau^2} + \Gamma^\mu_{00}\left(\frac{dt}{d\tau}\right)^2 = 0 \tag{2.9}$$

where a simple relabelling of indices was used in the last step. In order to proceed, we have to determine the affine connection and bring it in a relation with a quantity we already now, the metric tensor $g_{\mu\nu}$. It is an easy exercise to derive such a connection ([12],[13]) by simply taking the derivative of the metric tensor $g_{\mu\nu}$ with respect to the laboratory frame coordinates and work out the resulting consequences. The resulting expression only includes metric tensors and affine connections. We can use the symmetry properties of the connection [5] and the metric [6] and add and subtract in a clever way appropriate terms, so that the resulting expression for the affine connection looks like

$$\Gamma^\sigma_{\lambda\mu} = \frac{1}{2}g^{\sigma\nu}\left(\partial_\lambda g_{\mu\nu} + \partial_\mu g_{\nu\lambda} - \partial_\nu g_{\lambda\mu}\right) \tag{2.10}$$

The right hand side of (2.10) is also called Christoffel connection [7]. Let's have a look

[4] Look at [1] for more detail.

[5] Symmetric in lower indices because partial derivatives in the definition (2.7) commute.

[6] We can always define a symmetric metric, by simply demanding that the proper time interval is invariant.

[7] The derivation of the Christoffel connection use the inverse metric tensor, so this equation ensures the

back at the geodesic equation (2.6), $\frac{d^2x^\lambda}{d\tau^2} = -\Gamma^\lambda_{\mu\nu}\frac{dx^\mu}{d\tau}\frac{dx^\nu}{d\tau}$. In the Newtonian case, the right hand side is the gradient of a scalar potential ϕ. So it will be seen that the affine connection bears information about the gravitational force, and that the metric tensor(determines the proper time interval) replaces the gravitational potential. This can be argued by recognizing that the affine connection only contains the metric and their derivatives, so the derivative of the metric tensor determines the field $\Gamma^\sigma_{\mu\nu}$. With this relation between the affine connection and the metric, we can therefore move on to show that this generalization from a flat to a curved space-time is really able to describe gravity. We stopped in this project by equation (2.9), but know we know the missing relation between Γ^μ_{00} and the metric tensor

$$\Gamma^\mu_{00} = \frac{1}{2}g^{\mu\lambda}(\partial_0 g_{0\lambda} + \partial_0 g_{\lambda 0} - \partial_\lambda g_{00}) \tag{2.11}$$

By applying our requirement for a static (time independent) metric it reduces to

$$\Gamma^\mu_{00} = -\frac{1}{2}g^{\mu\lambda}\partial_\lambda g_{00} \tag{2.12}$$

Now we work with a metric in a coordinate system that is almost cartesian, because there we can make most use of our third condition, the weakness of the field. From this weakness we conclude that the general metric should not vary much from the Minkowski metric in flat space and we can write

$$g_{\mu\nu} = \eta_{\mu\nu} + h_{\mu\nu} \tag{2.13}$$

Were the matrix $(h_{\mu\nu})$ describes a small perturbation from the Minkowskian form. We therefore require its components to be small, $|h_{\mu\nu}| \ll 1$. The inverse metric $g^{\mu\nu}$ is determined by the condition $g^{\mu\nu}g_{\nu\sigma} = \delta^\mu_\sigma$, resulting in (to first order in h)

$$g^{\mu\nu} = \eta^{\mu\nu} - h^{\mu\nu} \tag{2.14}$$

existence of the inverse metric tensor.

where we defined $h^{\mu\nu} \equiv \eta^{\mu\lambda}\eta^{\nu\theta}h_{\lambda\theta}$. Putting this in the geodesic equation (2.9) for a static, weak gravitational field we end up (to first order) with

$$\frac{d^2x^\mu}{d\tau^2} = -\Gamma^\mu_{00}\left(\frac{dt}{d\tau}\right)^2 = \frac{1}{2}\eta^{\mu\sigma}\partial_\sigma h_{00}\left(\frac{dt}{d\tau}\right)^2 \tag{2.15}$$

The time component (static field, $\partial_0 h_{00} = 0$) and the space-components are thus

$$\frac{d^2t}{d\tau^2} = 0 \tag{2.16}$$

$$\frac{d^2\vec{x}}{d\tau^2} = -\frac{1}{2}\left(\frac{dt}{d\tau}\right)^2 \nabla h_{00} \tag{2.17}$$

resulting in

$$\frac{d^2\vec{x}}{dt^2} = -\frac{1}{2}\nabla h_{00} \tag{2.18}$$

Comparing this to the Newtonian result [8], $\frac{d^2\vec{x}}{dt^2} = -\nabla\phi$, and using equation (2.13) we get

$$g_{00} = (1 + 2\phi) \tag{2.19}$$

So in the Newtonian limit the curvature of space-time is all we need [9] to describe gravity. From that we are also able to derive how a weak gravitational field affects time. According to the equivalence principle, at a given point in a arbitrary gravitational field we can find a locally inertial coordinate system, where the laws of special relativity applies. In a locally inertial frame that is subject to gravity, the space-time interval of the ticks of a clock are given by

$$d\tau = \sqrt{\eta_{\alpha\beta}d\xi^\alpha d\xi^\beta} \tag{2.20}$$

[8] $\phi = -\frac{GM}{r}$

[9] h_{00} used to derive the metric is actually -2ϕ+constant. But we get rid of the constant by demanding that far away from a gravitating body the metric should be Minkowsian (flat space) again (therefore the perturbation h_{00} vanishes) and that the potential ϕ we used for comparison is also zero at infinity.

Transforming this to an arbitrary coordinate system with the use of the metric tensor $g_{\mu\nu} = \eta_{\alpha\beta}\frac{\partial \xi^\alpha}{\partial x^\mu}\frac{\partial \xi^\beta}{\partial x^\nu}$ we have

$$d\tau = \sqrt{g_{\mu\nu}dx^\mu dx^\nu} = \sqrt{g_{\mu\nu}\frac{dx^\mu}{dt}\frac{dx^\nu}{dt}}dt \tag{2.21}$$

where dt is the differential of the coordinate time (influenced by gravity). If the clock is at rest in the gravitational field, we can write

$$d\tau = \sqrt{g_{00}}\,dt = \sqrt{1+2\phi}\,dt = \sqrt{1-\frac{2GM}{r}}dt \tag{2.22}$$

where I have used the potential as given by the Poissonian equation. From this, one can see that in the weak field limit the coordinate time t is the proper time of a clock very far away from the mass distribution, because in the case $|r| \to \infty$ the potential ϕ vanishes. This also means that clocks inside a gravitational field ticks slower as compared to ones located far away from the massive object. In general the metric component g_{00} has different values at different locations in space.

2.1.3 Field equation and Schwarzschild solution

The field equation of general relativity is given by Einstein's equation

$$R_{\mu\nu} - \frac{1}{2}g_{\mu\nu}R + g_{\mu\nu}\Lambda = \frac{8\pi G T_{\mu\nu}}{c^4} \tag{2.23}$$

where $R_{\mu\nu} = R^\lambda_{\mu\lambda\nu}$ is the Ricci-Tensor, that can be obtained by contracting the Riemann-tensor $R^\kappa_{\mu\lambda\nu} = \partial_\nu\Gamma^\kappa_{\mu\lambda} - \partial_\lambda\Gamma^\kappa_{\mu\nu} + \Gamma^\rho_{\mu\lambda}\Gamma^\kappa_{\rho\nu} - \Gamma^\rho_{\mu\nu}\Gamma^\kappa_{\rho\lambda}$, R is the Ricci-scalar, Λ is the cosmological constant and $T_{\mu\nu}$ is the stress-energy tensor. This equation relates geometrical properties of space-time to the energy and momenta of bodies within this space-time ([13]).

The last missing part of general relativity that is needed for this thesis is to find a simple solution of Einstein's field equation. The derivation of this so called Schwarzschild line-element is of great importance to understand its validity and is done in the appendix (section 7.1). It is valid only for homogeneous, non-rotating and not charged spherical bodies and, after putting the speed of light back into the equation, is given by

$$ds^2 = c^2 d\tau^2 = \left(1 - \frac{2GM}{c^2 r}\right) c^2 dt^2 - \left(1 - \frac{2GM}{c^2 r}\right)^{-1} dr^2 - r^2(d\theta^2 + sin^2\theta d\phi^2) \quad (2.24)$$

2.2 Fiber optics

In this chapter a short introduction to the basic principles of fiber optics is given and the applications and limitations of their use for the proposed experiment in [7] is discussed. Optical fibers allow for low loss transmission of light over long distances or inside long fibers coiled up on fiber spools with small dimensions, which makes this type of waveguide perfectly suited to test for gravitationally induced phases in a laboratory. We are only interested in single-mode step-index fibers, which do not suffer modal dispersion as step-index multi-mode fibers do and also have the additional benefits of lower power attenuation and no modal noise (interference of different modes in multi-mode fibers) [14].

2.2.1 Ray and wave model

Optical fibers are cylindrical dielectric waveguides with the ability to guide a light beam from one place to another (see for example [15]). Optical fibers can be divided into single-mode or multi-mode and furthermore subdivided into step-index and graded-index fibers. A step-index fiber consists of a cylindrical dielectric core with constant refractive index and is surrounded by a cladding with a material of slighlty lower refractive index. To understand why this is necessary, we need to understand total internal reflection.

Total internal reflection

In dielectric media, light has a different velocity compared to its propagation in free space. This difference is captured in the refractive index

$$n = \frac{c_0}{c} \quad (2.25)$$

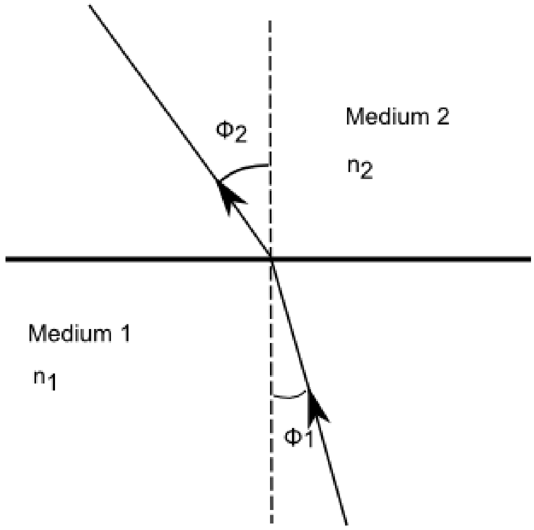

Figure 2.1: Refraction of a light ray at the boundary between two media with different refractive indices.

defined as ratio between two velocities where c_0 is the speed of light in vacuum and c is the speed of light in the considered material. Because light propagates slower in a medium than it does in vacuum, and because the above equation is a ratio between velocities, the refractive index has no dimension and is always [10] greater than one. This change of speed by going from one medium into the other is the origin of refraction, and can be described by Snell's law although to fully understand it one needs to consider wave properties of light. Figure (2.1) shows a light ray propagating through a medium (for example glass) with refractive index n_1 unless it enters a material of different refractive index with $n_1 > n_2$.

The bending clearly depends on the materials used and the angle of incidence. The angle of incidence ϕ_1 and the angle of refraction ϕ_2 are defined with respect to the normal to the surface area. So Snell's law provides the relationship

$$n_1 sin\phi_1 = n_2 sin\phi_2 \tag{2.26}$$

[10]What is meant here is the speed of information transfer, the phase velocity of light can be bigger than that of light in vacuum in some materials.

Equation (2.26) reveals, that by increasing the angle of incidence (ϕ_1) at the boundary between the two media, the angle of refraction (ϕ_2) is also increasing and in some limit results in $\phi_2 = \frac{\pi}{2}$ meaning that the light propagates on the boundary. This angle is called critical angle ϕ_c and is given by

$$sin\phi_{1,critical} \equiv sin\phi_c = \frac{n_2}{n_1} \tag{2.27}$$

The critical angle is only a property of the media. Increasing the angle of incidence beyond the critical angle results, instead of refraction, in reflection of light back into the medium where it comes from. This is called total internal reflection and happens for incidence angles $\phi_1 > \phi_c$: Light is guided in the core of an optical fiber by total internal reflection. If we would include electromagnetic theory in this description we would see that still some light can escape into medium 2. The wave leaving the material is called evanescent wave and carries away energy, which is a very useful effect for some purposes like transporting energy from one optical fiber into another.

Angle of acceptance and numerical aperture

Because light has to get somehow into the core, we can ask for the fibers acceptance angle. This is defined as the maximal angle over which light entering the fiber will be guided inside the core through total internal reflection. Of course this angle must be different than the critical angle, because light enters the fiber in general from a different material (in most cases air with a refractive index of $n_a \approx 1$). Figure (2.2) shows a geometric picture of this situation using the ray model.

We see that a light ray incident from the air will bend towards the normal because it goes from a medium with lower refractive index (air) to a medium with higher refractive index (e.g. silica). Inside the core, the ray propagates until it hits the core-cladding boundary at an angle ϕ. For the ray to be confined inside the fiber and guided to the other end of that fiber through total internal reflection the relation $\phi \geq \phi_c$ must hold. Using snells law, one can find a relation for θ_{conf}, the complementary angle to ϕ_c, and half the acceptance angle α_{conf}

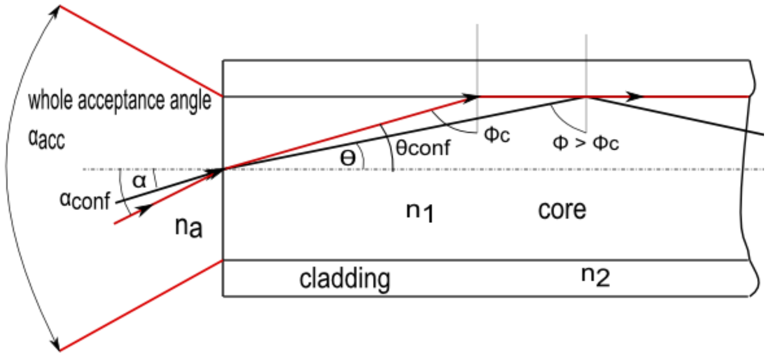

Figure 2.2: Ray propagation in a step-index fiber. The red line indicates the acceptance angle, for which light is guided through the fiber.

$$
\begin{aligned}
sin\alpha_{conf} &= \frac{n_1}{n_a} sin\theta_{conf} = \frac{n_1}{n_a} sin(\frac{\pi}{2} - \phi_c) && (2.28)\\
&= \frac{n_1}{n_a} cos\phi_c = \frac{n_1}{n_a}(1 - sin^2\phi_c)^{\frac{1}{2}} && (2.29)\\
&= \frac{n_1}{n_a}\left(1 - \frac{n_2^2}{n_1^2}\right)^{\frac{1}{2}} && (2.30)\\
&= \frac{\sqrt{n_1^2 - n_2^2}}{n_a} && (2.31)
\end{aligned}
$$

where I have used in the first line the requirement for total internal reflection ($\phi \geq \phi_c$) and in the third equation (2.27) was used. Because of total internal reflection, the condition for light to be guided through the fiber is $\alpha \leq \alpha_{conf}$, meaning that the acceptance cone is given by $\alpha_{acc} = 2\alpha_{conf}$. Note that this is only a function of the refractive indices, and is therefore fixed by the chosen materials for the core and the cladding. We can define the numerical aperture (NA) as a measure of this light-collecting property of a given fiber by

$$NA = n_a sin\alpha_{conf} = \sqrt{n_1^2 - n_2^2} = n_1\sqrt{2\Delta} \tag{2.32}$$

where in the last step the relative refractive index $\Delta = \frac{\sqrt{n_1^2 - n_2^2}}{2n_1^2}$ was used [14].

Modes in optical fibers

Because the ray model we have used up to now is not accurate enough for the description of single-mode fibers, we have to take a look at the wave theory of light in waveguides. A detailed study can be found for example in references [14, 15, 16]. I will highlight the most important results, which are necessary to understand waveguide dispersion and the behaviour of single-mode fibers.

Using Maxwell's equations and boundary conditions for waveguides with cylindrical geometry, we get the electric and magnetic fields of guided waves as solution. Each of this solutions is referred to as a mode, and each mode has a distinct propagation constant β, distinct field distributions and two independent polarization states. The modes in cylindrical waveguides are called LP modes. In the weakly guiding approximation, where the two refractive indices are assumed to be almost identical ($n_1 \approx n_2$), each of the transverse components of the monochromatic electric and magnetic fields satisfy the scalar wave equation [15]. By making the ansatz $\psi(r, \phi, z, t) = u(r, \phi)e^{i(\omega t - \beta z)}$ and using the scalar wave equation in cylindrical coordinates together with the method of separation of variables ($u(r, \phi) = U(r)S(\phi)$) we get

$$\frac{r^2}{U}\left(\frac{d^2U}{dr^2} + \frac{1}{r}\frac{dU}{dr}\right) + r^2\left(n^2(r)k_0^2 - \beta^2\right) = -\frac{1}{S}\frac{d^2S}{d\phi^2} = l^2 \tag{2.33}$$

where $k_0 = \frac{2\pi}{\lambda}$ is the free space propagation constant, l is a constant and $\beta = \frac{\omega\, n}{c_0}$ the propagation constant in the material. The r dependence of the above equation reads

$$\frac{d^2U}{dr^2} + \frac{1}{r}\frac{dU}{dr} + \left(n^2(r)k_0^2 - \beta^2 - \frac{l^2}{r^2}\right)U = 0 \tag{2.34}$$

As can be shown [14], the only solutions which results in guided waves are those with the following relation for the propagation constant

$$k_0^2 n_1^2 > \beta^2 > k_0^2 n_2^2 \tag{2.35}$$

This means that the propagation constant has to be smaller than those of the core (with refractive index n_1) and bigger than those of the cladding (with n_2). The solutions $\beta^2 < k_0^2 n_2^2$ are called radiation modes, that can even propagate within the cladding. Because we want real and positive values for the propagation constants inside the core and the cladding, we may define due to the above requirement for guiding modes [14]

$$\begin{aligned} k_T^2 &= k_0^2 n_1^2 - \beta^2 \\ \gamma^2 &= \beta^2 - k_0^2 n_2^2 \end{aligned} \tag{2.36}$$

which, inserted into equation (2.34), gives two equations for the core and the cladding respectively

$$\begin{aligned} \frac{d^2U}{dr^2} + \frac{1}{r}\frac{dU}{dr} + \left(k_T^2 - \frac{l^2}{r^2}\right) U = 0 \qquad for \qquad 0 < r < a \\ \frac{d^2U}{dr^2} + \frac{1}{r}\frac{dU}{dr} - \left(\gamma^2 + \frac{l^2}{r^2}\right) U = 0 \qquad for \qquad a < r \end{aligned} \tag{2.37}$$

where a denotes the radius of the core. This differential equation has as solutions Bessel functions of the first (inside the core) and the second (inside the cladding) kind. The solutions for the core therefore oscillate like sine or cosine functions with decaying amplitude for increasing distance from the center of the core ($a = 0$). The solution for the cladding provides an exponentially decaying amplitude for large r and/or large γ. We can define the normalized waveguide parameter or fiber parameter V by a combination of k_T and γ through

$$V = a\sqrt{k_T^2 + \gamma^2} = k_0 a \sqrt{n_1^2 - n_2^2} = k_0\, a\, NA \tag{2.38}$$

where NA is the numerical aperture defined in equation (2.32). The relations for the number of modes and their exact behaviour can be found in the literature (for example [14, 15, 16]. It is important to note, that the fundamental LP_{01} mode is the only one which is guided through the core if $V < 2.405$ for step-index fibers. Single mode step-index fibers are therefore defined to have a V parameter smaller than the above number.

2.2.2 Attenuation and pulse dispersion

Attenuation and dispersion are the two main factors limiting the performance of optical fibers. The exponentially decreasing power of optical beams is usually measured in decibels (dB) and given by

$$\alpha' = 10\, log_{10} \frac{P_{in}}{P_{out}} \tag{2.39}$$

where α' is the attenuation coefficient in decibel, and P_{in} and P_{out} are the input and output powers respectively. This quantity can also be related to the attenuation per unit length, which is given by

$$\alpha = \frac{10}{L}\, log_{10} \frac{P_{in}}{P_{out}} \tag{2.40}$$

and α is now measured in decibels per kilometer (dB/km). From this relation we can calculate the output power at the end of a fiber with length L which is given by

$$P_{out} = P_{in} 10^{-\frac{L\alpha}{10}} \approx P_{in} e^{-0.23L\alpha} \tag{2.41}$$

where the last relation follows from a change in the basis of the logarithm.

The main constituents resulting in attenuation of optical power are [15]

1. Intrinsic absorption
2. Extrinsic absorption
3. Rayleigh scattering
4. Geometric imperfections

Intrinsic absorption is caused by interactions of the propagating wave inside the fiber and some of its constituents. This type of loss is strongly wavelength dependent, with

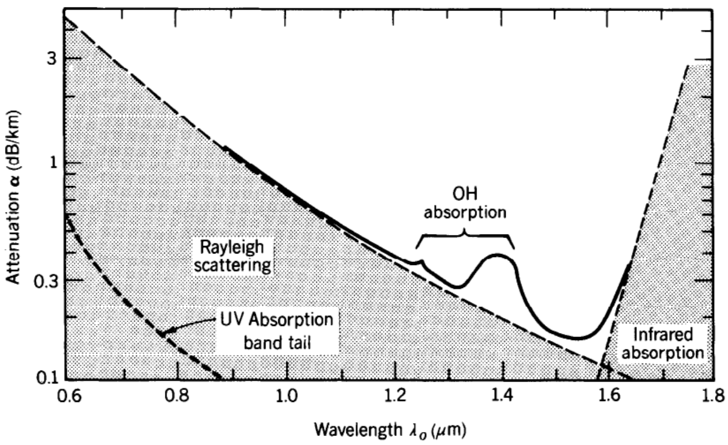

Figure 2.3: Loss spectrum of fused silica fibers. The infrared and the UV-absorption band are due to intrinsic absorption, whereas the extrinsic absorption is only represented by OH^--ion absorption. For higher frequencies the Rayleigh scattering is the most important limiting factor. The graphic is taken out of [14].

two strong absorption bands for fused silica (SiO_2) in the mid-infrared and ultraviolet part of the spectrum as can be seen in Fig. (2.3). There is a local minimum at a wavelength of around $1300nm$, and a global minimum around $1550nm$ which are best suited for low loss transfer of light and therefore used for telecommunication. Extrinsic absorption stems from tiny impurities (like OH^- or Fe^{2+} ions) in the material and are also strongly wavelength dependent (see Fig. (2.3)). Rayleigh scattering occurs due to inhomogeneities (which are small compared to the wavelength) in the material during the fabrication process. This inhomogeneities leads to density fluctuations which make the refractive index a function a position, therefore acting as small scattering centers. Losses due to Rayleigh scattering are proportional to λ_0^{-4} (were λ_0 is the central wavelength of the light pulse), which means that this type of loss is only important for high frequency transmission. Geometric effects like imperfect cylindrical shape, core-cladding interface irregularities or fiber bending can also introduce losses which limits the performance of optical fibers.

Dispersion is also one of the main limiting factors for fiber optic transmission of light. If a light pulse with a certain width in the time domain is launched into an optical fiber, the shape of the pulse (in the time domain) at the end of the fiber is changed due to dispersion. In [14], dispersive effects are divided into five principal sources

1. Modal dispersion
2. Material dispersion
3. Waveguide dispersion
4. Polarization-mode dispersion
5. Nonlinear dispersion

Because in this thesis only single-mode fibers with low input powers are under consideration, modal dispersion (which are caused by different travelling times for different modes) and nonlinear dispersion (intensity dependent refractive index) are of second rank importance and not discussed in detail.

Material dispersion is only present in dispersive media like optical fibers and results from the fact that every spectral component of a pulse will travel in such materials with a different group velocity. According to Fourier's fundamental theorem, every signal has a spectrum. So every pulse produced by a source has a certain spectral width $\Delta\nu$ centered around a central frequency ν_0. As long as this pulse travels through vacuum, its shape is unaltered but as soon as the pulse enters a dispersive medium it spreads out which results in pulse broadening. Because the amount of this broadening only depends on the material (and therefore characterizes the material), this type of dispersion is called material dispersion. To understand this effect, we first have a look at the group velocity of a pulse (wave packet) which is given by [11]

$$v_g \equiv (\frac{d\beta}{d\omega})^{-1}_{\omega=\omega_0} \tag{2.42}$$

[11] A derivation of the group velocity can be found in the appendix in section 7.2.

where the derivative has to be taken at the central angular frequency ω_0. In a non-dispersive medium, the group and the phase velocity are the the same, because the phase velocity $v_p = \frac{c_0}{n}$ is not a function of frequency and by inserting the above relation for a constant $\beta = \frac{\omega n}{c_0}$ we get

$$v_g = \frac{1}{\frac{d\beta}{d\omega}} = \frac{1}{\frac{n}{c_0}} = \frac{c_0}{n} = v_p \tag{2.43}$$

In a dispersive medium however, this statement is no longer true. To see the difference, one first calculates the derivative of the propagation constant with respect to the frequency

$$\frac{d\beta(\omega)}{d\omega} = \frac{\omega}{c_0}\frac{dn(\omega)}{d\omega}|_{\omega=\omega_0} + \frac{n(\omega)}{c_0} = \frac{1}{c_0}\left(n(\omega) + \omega\frac{dn(\omega)}{d\omega}|_{\omega=\omega_0}\right) \tag{2.44}$$

If we want to work in the wavelength domain (λ stands for the free space wavelength) and use the relationship $\omega = \frac{2\pi c_0}{\lambda}$ we get

$$\begin{aligned} \omega\frac{dn(\omega)}{d\omega} &= \omega\frac{dn}{d\lambda}\frac{d\lambda}{d\omega} \\ &= -\omega\frac{2\pi c_0}{\omega^2}\frac{dn}{d\lambda} \\ &= -\lambda\frac{dn(\lambda)}{d\lambda} \end{aligned} \tag{2.45}$$

so

$$\frac{d\beta(\omega)}{d\omega} = \frac{1}{c_0}(n(\omega) + \omega\frac{dn(\omega)}{d\omega}) \tag{2.46}$$

$$= \frac{1}{c_0}(n(\lambda) - \lambda\frac{dn(\lambda)}{d\lambda}) \tag{2.47}$$

Using this relationships and insert them in the definition of the group velocity (2.42) one ends up with a simple relation similar to that of the phase velocity

$$v_g = \frac{c_0}{n(\omega) + \omega \frac{dn(\omega)}{d\omega}} = \frac{c_0}{n(\lambda) - \lambda \frac{dn(\lambda)}{d\lambda}} = \frac{c_0}{N} \tag{2.48}$$

where the group refractive index is defined by

$$N \equiv n(\omega) + \omega \frac{dn(\omega)}{d\omega} = n(\lambda) - \lambda \frac{dn(\lambda)}{d\lambda} \tag{2.49}$$

With this we can calculate the time for a pulse to propagate through a fiber with length L by

$$t(\lambda) = \frac{L}{v_g} = \frac{L}{c_0} \left(n(\lambda) - \lambda \frac{dn(\lambda)}{d\lambda} \right) \tag{2.50}$$

So in a dispersive medium with a non linear relationship between the propagation constant and the angular frequency, each wavelength that constitutes to the envelope of the wave packet needs a different amount of time to propagate from one end to another resulting in a pulse broadening. If the spectral width of the pulse (FWHM), $\Delta\lambda$, is much smaller than the central wavelength λ_0, we can estimate the broadening of the pulse in the time domain by ([16])

$$\begin{aligned} \Delta\tau &= \frac{dt(\lambda)}{d\lambda} \Delta\lambda = \frac{L}{c_0} \left(\frac{d}{d\lambda} \left(n(\lambda) - \lambda \frac{dn(\lambda)}{d\lambda} \right) \right) \Delta\lambda \\ &= -\frac{L\lambda_0}{c_0} \frac{d^2 n}{d\lambda^2} \Delta\lambda \end{aligned} \tag{2.51}$$

Usually, this is written in a slightly different form by introducing the material dispersion parameter $D_m = -\frac{\lambda_0}{c_0} \frac{d^2 n}{d\lambda^2}$ resulting in

$$\Delta\tau = L D_m \Delta\lambda \tag{2.52}$$

where D_m has in general units of $\frac{ps}{nm\, km}$ and can either be positive (for silica-glass fiber and wavelength bigger than $\approx 1300nm$) or negative (if the central wavelength is shorter than $\approx 1300nm$). Silica-glass fiber has vanishing material dispersion around $1312nm$

[14].

The second kind of dispersion important for single-mode fibers is waveguide dispersion. Waveguide dispersion arises due to the dependence of the group velocity of the wavelength and is present even if the refractive indices of the core and the cladding are independent of λ. This can happen because the ratio of optical power travelling in the core and the cladding depends on the wavelength, and the phase velocities of the core and the cladding are different due to different refractive indices. We have seen, that one of the most important quantities characterising an optical fiber is the V parameter given by $V = k_0\, a\, NA = \frac{a\omega}{c_0} NA$, which is linearly dependent on the angular frequency even if no material dispersion is present (NA independent of ω) [17]. The time it takes for a pulse to go through a fiber of length L can again be described by $t_\omega = \frac{L}{v_g}$ and the group velocity, given by equation (2.42), is this time given by

$$v_g = \frac{d\beta}{d\omega} = \frac{d\beta}{dV}\frac{dV}{d\omega} = \frac{a \cdot NA}{c_0}\frac{d\beta}{dV} \tag{2.53}$$

The pulse broadening can again be approximated by [16]

$$\Delta\tau = \frac{dt(\omega)}{d\lambda}\Delta\lambda = D_\omega\, \Delta\lambda\, L \tag{2.54}$$

where $\Delta\lambda$ is the spectral width of the source and $D_\omega = \frac{d}{d\lambda} v_g^{-1} = -\frac{1}{2\pi c_o} V^2 \frac{d^2\beta}{dV^2}$.

The remaining effect resulting in pulse broadening important for single-mode fibers is polarization mode dispersion. Polarization mode dispersion is caused by fiber birefringence. As we have seen before, modes in optical fibers, even if they have perfect cylindrical geometry, always support two degenerate polarisation states. For perfect fibers, these two modes are degenerate and the pulses in both modes have the same group delay which is given by $t_i = \frac{N_i L}{c_0}$, where the index i refers to one of the two orthogonal polarization states and N_i is the corresponding group refractive index. Under real life conditions all fibers have some degree of asymmetry (e.g. from the manufacturing process or from external perturbations) which breaks the degeneracy of the modes resulting in optical birefringence. If a light pulse, with orientation such that the power equally excites both polarization modes, is launched into the fiber, the two modes travel with different group velocity through the fiber which results in polarization mode dispersion. We can define the beat length, which is the distance of propagation where a 2π difference between the modes is collected, by $L_b = \frac{\lambda}{\Delta N}$ where ΔN is the refractive index difference between the slow and the fast polarization mode [16]. For a short segment of the fiber, which can taken to be homogeneous, and the difference between the two propagation constants $\Delta\beta = \frac{\Delta N\,\omega}{c_0}$ between the modes, we can define the differential group delay by [18]

$$\begin{aligned} \Delta\tau &= \frac{L}{v_g} = L\frac{d(\Delta\beta)}{d\omega} \\ &= \frac{\Delta N}{c_0} + \frac{\omega}{c_0}\frac{d(\Delta n)}{d\omega} \end{aligned} \tag{2.55}$$

This formula can be used for uniform birefringence which is the case in short fibers. For long fibers however, each of the small segments either add or subtract from the total birefringence, and it can be shown that this behaviour leads to a square root-dependence from the length L of the fiber like in a random walk problem [19]. Therfore we my write [14]

$$\Delta\tau = D_{PMD}\sqrt{L} \tag{2.56}$$

for the average [12] rms-value of the pulse broadening due to polarization mode dispersion where D_{PMD} is the dispersion parameter which can be experimentally accessed for a given single-mode fiber with units of $\frac{ps}{\sqrt{km}}$. Additionally to pulse broadening, the center of the pulse can be displaced which would be dramatic for an experiment where a small physical effect (like the gravitational effects on single photon wave functions) should be resolved [18]. It is important to note, that all types of dispersion strongly depends on

[12]The actual values of the broadening are time dependent and can be much larger/smaller than the average value [20].

external perturbations like temperature or pressure because such effects would change the refractive index profile and therefore the pulse broadening.

2.2.3 Temperature and pressure dependence

A Mach-Zehnder interferometer with optical fibers can generally been used to resolve small phase shifts due to some external parameter like temperature or pressure (see for example [15]). In reverse, these effects can also cause unwanted phase shifts in the signal that effects the detection statistics. This situation is similar to gravitationally induced phase shifts. If one sets, for example, the lower arm (γ_2 in Fig. (1.1)) of the interferometer as a reference arm which is shielded to external perturbations, the other arm, which I refer to as sensing arm, is subject to a different gravitational potential which can be measured by the two detectors at the end of the interferometer. Therefore relative differences in external parameters can simulate the same effects as gravity and the desired information can not be extracted out of the signal. The phase in one arm is given by $\phi = \omega t = \frac{2\pi n_{eff} L}{\lambda}$ where n_{eff} is the effective refractive index of the fundamental mode, λ is the free space wavelength and L is the length of the fiber. A relative phase difference between the two arms can happen due to changes in the effective refractive index or change in the length of the fiber which can be represented mathematically by

$$\Delta\phi = \frac{2\pi}{\lambda}\left(n\Delta L + L\Delta n\right) \tag{2.57}$$

where I have replaced the effective refraction index n_{eff} by the refractive index of the material which is justified if the fiber V parameter is almost constant for a change in the effective refractive index [15]. To quantify the occurring phase change for a given length of fiber one is interested in the sensitivity defined as phase change per unit length per unit change of the external parameter as given by

$$\frac{\Delta\phi}{L\Delta X} = \frac{2\pi}{\lambda}\left(n\frac{\Delta L}{L\Delta X} + \frac{\Delta n}{L\Delta X}\right) \tag{2.58}$$

where ΔX refers to any external parameter that can influence the phase of light confined in the fiber like temperature. The relative phase change given by equation (2.58) depends on the material of the fiber, the external perturbation and the wavelength and the factors $n\frac{\Delta L}{L\Delta X}$ and $\frac{\Delta n}{L\Delta X}$ are different for every material and can be deduced experimentally. With this value given one can calculate the relative phase change between the two arms by

$$\Delta\phi = \frac{\Delta\phi}{L\Delta X}\, L\, X \tag{2.59}$$

This type of phase change can be reduced by special coatings of the optical fiber where the sensitivity can be either taken out of data sheets of the manufacturer or measured in the lab with e.g. a ordinary Mach-Zehnder interferometer for classical light. Because for example $\frac{\Delta\phi}{L\Delta T} \approx 100 rad/K/m$ ([15]) for an unshielded fiber, the temperature senstivity of the fiber is a very important parameter one has to take care of in an actual experiment. Because it is not possible to theoretically predict such external influences for very long single-mode fibers, one has to make experiments to reveal how the phase respond to a change of those external parameters under laboratory conditions.

3 Optical fiber for interference experiments inside earth's gravitational potential

The success of measuring a gravitationally induced phase shift crucially relies on the optical fiber used, therefore it is of great interest to find the best suited fiber for the experiment. We have seen in the last section that the main limiting factors by using optical fibers are dispersion and attenuation. Dispersion also applies for single photons described as wave packets and can have several effects on the detection. We have considered the three important dispersion processes that can occur in step-index single-mode fibers. Material dispersion, which was caused by the frequency dependence of the group velocity inside the fiber, is practically the same in both arms of the interferometer, and the resulting broadening of the pulse in the time domain does not affect the phase shift due to gravity. This would not be true, if one uses two different types of fibers acting as arms of the interferometer. In such a case, the envelopes of the single wavefunction amplitudes in superposition would not only have a different shape at the end of the fiber, but will also acquire a relative shift in the time domain making it impossible to detect a relative phase shift due to a gravitational potential difference. The same is true for waveguide dispersion, which is caused by the difference in group velocity in the core and the cladding. Both effects should, for identical fibers, not cover the gravitationally induced phase shift but only broaden the pulse in the time domain. A sketch of the broadening in the time domain due to this two types of dispersion, which are combined also referred to as chromatic dispersion, can be found in Fig. (3.1). To overcome chromatic dispersion and the resulting temporal broadening, one can use dispersion-shifted fibers (see for example [14]), which use the signs of the dispersion parameters D_m and

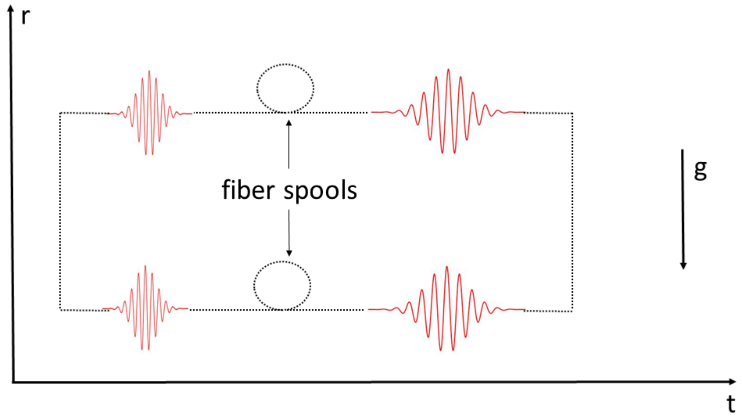

Figure 3.1: Sketch of the effect of chromatic dispersion on a single wave packet in superposition inside earth's gravitational potential. For identical fibers this type of dispersion results only in pulse broadening, which is the same for identical fibers and does not effect the introduced phase shift due to gravity.

D_ω in a way that the two effects compensate each other.

The effect of polarization mode dispersion is conceptually different. As was discussed in the last section, polarisation mode dispersion is a result of birefringence, where the two principal states of polarization evolves with different velocities inside the fiber resulting in a pulse spread at the end of the fiber proportional to the square root of its length (see equation (2.56)). Additionally to this broadening (see for example [18]), the center of the pulse can be shifted in the time domain which would cover the effect of gravity. A possible solution for this problem is the use of polarization maintaining fibers. These fibers have very high built-in birefringence, so light launched into one of the birefringent axes would not change its state of polarization and the pulse can propagate unaffected through the fiber.

Attenuation in fibers was also briefly discussed in section 2.2.2, where we have seen that the number of photons is exponentially decreasing with length L of the fiber. Therefore we need a bright single-photon source, capable of producing enough photons to achieve a meaningful measurement statistic which can be estimated by using equation (2.41) and the fact that the average optical power is directly proportional to the photon number. One of the photons of each produced pair is used as a trigger photon, which can reduce significantly the noise on the photon counts. An additional requirement for the source is the production of pairs with sufficiently large coherence length, which guaranties high quality interference. So a narrow-bandwidth single-photon source should be used which not only reduces the temporal broadening due to chromatic dispersion but also provides a large coherence length. To keep the photon losses at a minimum the source should be designed to produce photon pairs at $1550nm$. One possible realization of the source, which can be particular useful for implementation in fiber optic systems, is the use of a single-mode silica fiber with a second-order non-linearity which creates pairs of photons with parametric down-conversion [21]. Additional fiber Bragg-gratings at both ends of the source can act as mirrors, where the modes of the resulting cavity become the modes available for the emission of photons. With proper settings of their parameters the bandwidth can be tuned to the desired amount, which is in this case about $100MHz$, corresponding to a coherence length of about $2m$. With such a source provided, we can calculate the total amount of loss that occur at the end of the fibers. The coupling efficiency from the first beam splitter of the MZI (which is a fiber 3dB coupler) into the optical fiber is given similar to the attenuation in optical fibers by (see for example [16])

$$P_{coupling} = P_{in} 10^{-\frac{\alpha_{coupling}}{10}} \tag{3.1}$$

The usual values for $\alpha_{coupling}$ are smaller than $0.2dB$ [16], which corresponds to a worst case coupling efficiency of about 4.5% [1]. We have seen that in order to resolve a phase shift of $10^{-4}rad$ we need, by keeping the distance between the two arms $h = 1m$, a length $L = 1000km$ of fiber for both arms. We have also seen that the attenuation is an exponentially decreasing function in L, therefore we have to use a length which is one order of magnitude smaller which still provides a theoretical phase shift of $10^{-5}rad$.

[1] I have assumed that the coupling efficiency is the same for all types of fibers, which is not quite true and has to be tested for every fiber in the laboratory.

fiber type	**length [km]**	**# splicings**	**wavelength** [nm]	$\sim$ **power loss** [%]
SMF-28e+ LL	50.4	1	1310 and 1550	2.3
SMF-28 ULL	25.2	3	1310 and 1550	6.7
LEAF	25.2	3	1550	6.7
PANDA PM	10	9	1550	18.7

Table 3.1: Different types of optical fibers with different length and accordingly a different number of splicings to reach a total fiber length of about 100km. The values for length and wavelength are taken out from data sheets of the **Corning**-company. The LEAF fiber is a non-zero dispersion shifted fiber specialised for the use at 1550nm and PANDA PM-fibers denote polarization maintaining fibers. The resulting power attenuation only considers the worst case scenario for splicing (equation (3.3)), and within this model it is assumed that the value is the same for every type of fiber.

Because industrial standards does not allow for fibers to have a length of 100km, we also have to consider losses due to splicings. This splicings typically have a coupling parameter[2] of about

$$0.05dB \leq \alpha_{splicing} \leq 0.1dB \tag{3.2}$$

So we can calculate the losses resulting from the splicings by

$$P_{splicing} = P_{in} 10^{-\frac{\alpha_{splicing}}{10}} \tag{3.3}$$

or, by also considering the losses from the coupling calculated above [3]

$$P_{cs} = P_{in} 10^{-\frac{(\alpha_{coupling}+\alpha_{splicing})}{10}} \tag{3.4}$$

Because different types of fibers have different length, some of them has to be spliced more often than others. Table (3.1) summarizes the numbers one gets with different fibers for a resulting length of approximately 100 km.

The next attenuation effect resulting in lowering the signal intensity is due to the length of the fiber itself. The loss is proportional to the length of the fiber, which is in the end

[2]This values are taken out of Corining data sheets available at www.corning.com.

[3]This is justified by the assumed linearity of the power attenuation processes.

fiber type	**wavelength** [nm]	α_L $[\frac{dB}{km}]$	$\sim$ **power loss** [%]
SMF-28e+ LL	1310	$\leq$0.32	99.936
	1550	$\leq$0.18	98.41
SMF-28e ULL	1310	$\leq$0.31	99.92
	1550	$\leq$0.18	98.41
LEAF	1550	$\leq$0.19	98.73
PANDA	1550	$\sim$ 0.5	99.999

Table 3.2: The table shows the different attenuation coefficients for different types of optical fibers and the resulting worst case losses related to equation (3.5). The values are taken from Corning-data sheets.

one of the difficulties for the detection of small phase shifts. In order to resolve this tiny phases we need a fiber of roughly 100km length, but for this length the loss of photons is dramatically high, and is given according to equation (2.41) by

$$P_L = e^{-0.23\alpha_L L} \tag{3.5}$$

where L is in km and α_L in $\frac{dB}{km}$. The attenuation coefficient α_L varies for different types of fibers and different wavelength, which is summarized in Table (3.2).

Table (3.2) reveals that the PANDA fibers are almost out of question because of their inferior attenuation coefficient. The coupling efficiency of the second fiber beam splitter is assumed to be almost identical to the first one, which was about 4.5% in a worst-case scenario. So the average total amount of photons, reaching (in principle) a detector at the end of a fiber of length [4] $L = 100.8km$ after passing two fiber couplers (act as beam splitters) can be calculated by

$$P(L) = P_{in}\, 10^{-\frac{(2\alpha_{coupling}+n\alpha_{splicing})}{10}}\; e^{-0.23\alpha_L L} \tag{3.6}$$

with n meaning the number of splices. The total attenuation values for the different types of fiber are summarized in Table (3.3).

This table shows, that in order to resolve a phase shift that is experimentally detectable one can work with standard single-mode fibers or non-zero dispersion shifted fibers for

[4] This length is due to limited industrial standards.

fiber type	**wavelengths** [nm]	**~total loss** [%]	**~photons(detector)** $[\frac{photons}{second}]$
SMF-28e+ LL	1310	99.94	60
	1550	98.58	1420
SMF-28 ULL	1310	99.93	70
	1550	98.64	1360
LEAF	1550	98.92	1080
PANDA	1550	99.9992	~ 0

Table 3.3: Total loss for different types of optical fibers with length $L = 100.8km$ after passing through two optical fiber couplers and various splices. The estimated number of photons reaching the detectors at the end of those fibers are calculated assuming an initial pair-production rate of 10^5 photons per second.

$1550nm$ but even their use is accompanied by various problems for the detection. In what follows, an initial pair production rate of the source of about 10^5 photon pairs per second is assumed. Now suppose, that all of the photons (in the best case $\sim$ 1500/s) reach the two detectors. There are several measurement strategies that can be used, and a deep analysis of which one of them is the best suited for the experiment is out of the scope of this thesis. One major problem of the low photon rate ($\sim$ 1500 for the Corning SMF-28e+ LL fiber) at the end of the second fiber beam splitter is to extract the desired information out of the signal. In a classical experiment one can align the phase shifter of the MZI such, that both of the detectors will have an (theoretically) equal count rate, because the sensitivity is best for this splitting ratio. Afterwards the MZI can be rotated around one of his arms, resulting in a difference in gravitational potential and therefore an additional relative phase between the arms is introduced. This results in an unequal count rate for the two detectors as compared to the horizontal position. All of this sounds very pleasing, but the real detection process for slow photon number has to deal with several imperfections such as dark count rates (DCR), imperfect quantum efficiencies of and couplings to the detector and principle sources of noise (like shot-noise).

Up to now, the calculations about the photon count rate at the output does not take gravity into account. As stated in [6], the difference in proper time results in a different count rate at the end of the detector. I now want to analyse this in greater depth.

According to [7] the detection probabilities for the photons are given by [5]

$$P_{f\pm} = \frac{1}{2}\left(1 \pm \int_{\Delta\nu} d\nu |f(\nu)|^2 cos(\nu\Delta\tau + \phi)\right) \tag{3.7}$$

where the mode function $f(\nu)$ is normalized to one [6], $\int_{\Delta\nu} d\nu |f(\nu)|^2 = 1$, and will depend strongly on how the photons are created, and therefore on the source. The proper time difference $\Delta\tau$ was given by $\Delta\tau = \frac{lghN}{c^3}$ taking into account the propagation through the optical fiber. As mentioned there, this expression has two limits, but I am only considering gravitational induced phases here, which corresponds to the case where $\Delta\tau \ll \Delta\nu$, with $\Delta\nu$ the relevant frequency range of integration. In this case, the cosine function in the integrand can be taken as a constant within the relevant range of angular frequencies. The resulting integration gives, due to the normalization condition and with ν_0 as the central wavelength of the mode function

$$P_{f\pm} = \frac{1}{2}\left(1 \pm cos(\nu_0\Delta\tau + \phi)\right) = \frac{1}{2}\left(1 \pm cos(\nu_0 \frac{lghN}{c^3} + \phi)\right) \tag{3.8}$$

Note, that within this limit the visibility of fringes remains maximal due to neglidible gravitational time dillation. This regime can also be seen as a test for mass-energy equivalence between the energy of the photon and its gravitational mass [7]. Equation (3.8) reveals the behavior of ideal detectors at the end of a MZI placed in a gravitational potential. In the situation of a horizontal MZI, time flows for both possible trajectories at the same rate, $\Delta\tau = 0$, and results accordingly in detection probabilities for ideal detectors

$$P_{f\pm} = \frac{1}{2}\left(1 \pm cos(\phi)\right) \tag{3.9}$$

meaning that all photons arrive at detector D_+ if $\phi = 0$, and an equal ration between D_+ and D_- if the phase shifter provides a relative phase of $\frac{\pi}{2}$ as in classical detection strategies. Now we rotate the interferometer around his lower arm by an angle of $\frac{\pi}{2}$

[5] With an additional phase between the two arms denoted by ϕ.
[6] I assumed that the parts of the frequency spectrum outside this relevant range are neglidible.

and analyse the consequences in terms of photon count rates according to $\Delta\tau = \frac{lghN}{c^3}$. Inserting the length $l = 100.8km$, $h = 1m$ and the group refractive index [7] $N = 1.4682$ we can calculate the proper time difference $\Delta\tau$ which can be inserted in equation (3.8). The maximal difference is given for a interferometer placed vertically inside earth's gravitational potential. For this angle and a relative phase of $\phi = \frac{\pi}{2}$, the resulting detection probability for D_- is approximately $P_{D_-} = 0.5000644$. This is not a very high difference in detection probability compared to a horizontal MZI, which has under the same conditions a detection probability of 1/2. So on average it will roughly take 7800 photons at the end of the second beam splitter, that the difference in count rates for the two detectors is one photon. With a rate of $\sim$ 1500 photons/second at the output of the second beam splitter, this one photon difference requires the experiment to run 5.2 seconds on average. This rough estimation does not include imperfect detectors and does not include variations in temperature or pressure which can influence the performance of the fiber and therefore the counting statistics. The solution of this problems in terms of detection strategies is out of the scope of this thesis, but in the next chapters I will present slight modifications to the original proposal, which may increase the physical effects on the photons and therefore the phase shift which makes it easier to analyse the photon statistics.

[7] Taken from **CORNING** data sheets.

4 Testing mass-energy equivalence with a Michelson interferometer

4.1 Inertial mass-energy equivalence

In order to test the validity of the mass-energy equivalence principle by quantum interference effects, one can use as a first step a simpler device where gravitational effects don't influence the outcome of the experiment and only inertial mass-energy effects occur. One possible scheme for this inertial equivalence hypothesis to test is to make use of a Michelson interferometer with its arms located at different radii of a horizontally rotating disc (Figure (4.1)) instead of a static Mach-Zehnder interferometer. A Michelson interferometer consists of only one beam splitter and the photon amplitudes are reflected back and recombine at the output ports of the interferometer. The set-up is placed horizontally inside earth's gravitational field, allowing us to observe phase shifts due to the centripetal potential of the rotation without disturbance from gravity.

4.1.1 Mathematical model

Because gravitational effects on this disc are approximately the same for both arms of the interferometer, we can work in Minkowski space time and the metric in the preferable cylindrical coordinates is given by

$$ds^2 = c^2dt^2 - \left(dr^2 + r^2d\phi^2 + dz^2\right) \tag{4.1}$$

which can be transformed to a uniform rotating coordinate system ($\phi \to \phi' = \phi - \omega t'$)

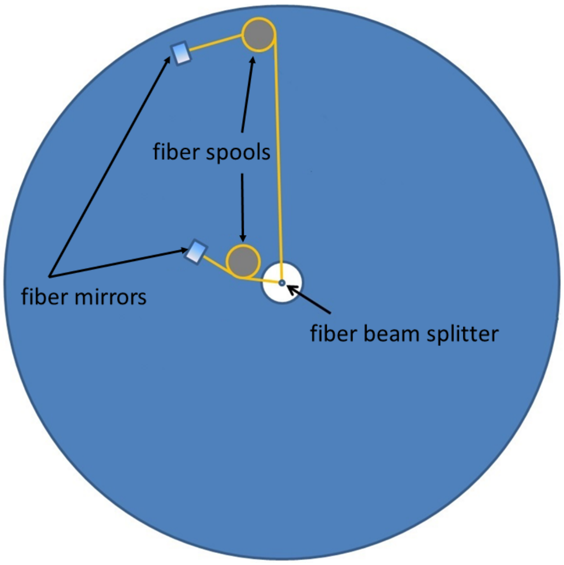

Figure 4.1: Sketch of a rotating Michelson interferometer placed horizontally inside earth's gravitational potential. This set-up allows to detect a phase shift due to the centripetal potential difference between the two arms, therefore testing inertial mass-energy equivalence. It consists in this simple form of a fiber beam splitter, two optical fiber spools and two fiber mirrors.

resulting in

$$ds^2 = \left(1 - \frac{\omega^2 r'^2}{c^2}\right) c^2 dt'^2 - 2r'^2 \omega d\phi' dt' - dr'^2 - r'^2 d\phi'^2 - dz'^2 \tag{4.2}$$

where the prime coordinates are those in the rotating frame. To simplify this metric, I assume the spools to be flat ($dz' = 0$) and that the radius of the spools is small compared to the distance of the center of rotation ($d\phi' = 0$) as well as negligible contribution for the small pieces of fiber connecting the center of the rotating disc with the spools located at different radii ($dr' = 0$)[1]. The spools should also have the same length l. Out of equation (4.2) we can extract the proper time of a clock at $r' \neq 0$, which is

$$\tau = \int_0^{t_f} \sqrt{1 - \frac{\omega^2 r'^2}{c^2}} dt' \tag{4.3}$$

[1]In a precise model, there are also terms including the rotations around the spool, but it turns out that they are three orders of magnitude smaller so only a simplified model is presented.

where t_f is a coordinate time in the rotating frame which can be expressed here by $t_f = \frac{lN}{c}$, with l as the length of the fiber coiled around the spools and N the group refractive index of that fiber. Expanding the square root in (4.3) to first order the proper time difference $\Delta\tau = \tau_2 - \tau_1$, where the index 2 refers to the spool closer to the center of rotation, is given by

$$\Delta\tau = \frac{lN\omega^2\left(r_1^2 - r_2^2\right)}{2c^3} \tag{4.4}$$

where the r_i are the distances of the spools from the center of rotation. Therefore the resulting phase shift reads

$$\begin{aligned}\Delta\phi = \Omega\Delta\tau &= \frac{2\pi c}{\lambda}\Delta\tau \\ &= \frac{\pi\, l\, N\, \omega^2(r_1^2 - r_2^2)}{c^2\lambda}\end{aligned} \tag{4.5}$$

with Ω as the central frequency of the wave packet.

4.1.2 Phase shift and possible realization

With help of equation (4.5) we can estimate the phase shift that occur in experiments similar to one as sketched in Fig. (4.1). As explained in section 3, we will work with photons at central wavelength of $1550nm$ which gives $N = 1.4682$ for the group refractive index of the fiber (CORNING-LL optical fiber) where the spool should again provide a total length of $l = 10^2km$ for back and forth motion between the center of rotation and the fiber mirror. For simplicity I assume furthermore for distance between the two spools a relation of $r_1^2 - r_2^2 = 1m^2$, which only leaves the angular velocity as a free parameter. A plot of the phase shift as a function of the angular velocity ω is shown in Fig. (4.2). We see from equation (4.5), that the phase shift for $\omega = 30\frac{rad}{s}$ is approximately $\Delta\phi = 3 \cdot 10^{-3}rad$, which is two orders of magnitude bigger than for gravitational effects as seen in section 1.1. In order to reduce noise during the measurement of the phase shift, one can try to modulate ω in time by a fixed frequency and achieve in a controllable way some

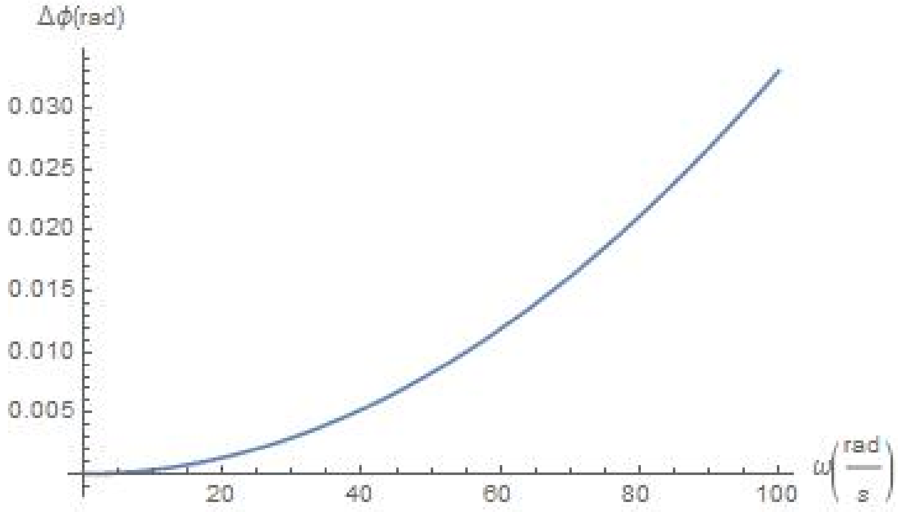

Figure 4.2: Dependence of the phase shift on the angular frequency of a rotating disc due to inertial mass-energy equivalence. The plot is given by equation (4.5) where $l = 10^5 m$, $N = 1.4682$, $(r_1^2 - r_2^2) = 1m^2$ and $\lambda = 1550nm$.

kind of AC-signal at the detectors which results in decreasing noise at the detectors by filtering out this modulation frequency. To connect the rotating fiber spools on the disc with fixed fibers in the laboratory without destroying them, we can use a rotating fiber coupler, e.g. from **PRINCETEL, Inc.** whose data sheet is printed in the appendix (see section (7.3)).

4.2 Gravitational mass-energy equivalence

Now I want to explore if a Michelson interferometer, placed vertically inside earth's gravitational potential, has any benefits compared to a Mach-Zehnder interferometer described in section 1.1, when using the same[2] fiber spools.

[2]The fiber spool for the Michelson interferometer has to provide only half the length of the spool for the MZI because of the back reflection at the fiber mirror. What is meant here is the total length the photon has to pass through.

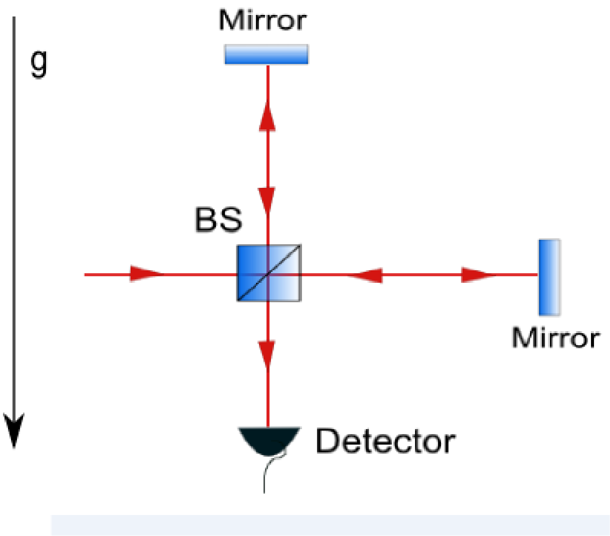

Figure 4.3: Sketch of a Michelson interferometer placed vertically in the earth's gravitational potential.

4.2.1 Mathematical model

We have seen, that the wave function of a single photon in superposition inside a Mach-Zehnder interferometer will arrive at the second beam splitter at different coordinate times due to different gravitational potentials. I will now derive the time dilation for the two spatial superpositions inside a Michelson interferometer, rotating it in such a way that in one of the arms the gravitational potential is approximately fixed, whereas the potential for the other arm is permanently changing. The situation is depicted in Fig. (4.3), and is equally valid for a continuous light beam and for single photons.

A single photon is put into a coherent superpositon along the horizontal and vertical path of the Michelson interferometer. Similar to the Mach-Zehnder case, the additional clock is implemented in the position degree of freedom of the photon. As a model for space-time we use the Schwarzschild line-element, derived in section 2.1.3 (equation (2.24)),

$$ds^2 = \left(1 - \frac{2GM}{c^2 r}\right) c^2 dt^2 - \left(1 - \frac{2GM}{c^2 r}\right)^{-1} dr^2 - r^2(d\theta^2 + sin^2\theta d\phi^2) \tag{4.6}$$
$$= \left(1 - \frac{r_s}{r}\right) c^2 dt^2 - \left(1 - \frac{r_s}{r}\right)^{-1} dr^2 - r^2(d\theta^2 + sin^2\theta d\phi^2) \tag{4.7}$$

where the Schwarzschild-radius $r_s \equiv \frac{2GM}{c^2}$ is introduced. Because this situation is geometrically different, we have to be careful while using this metric. The propagation in the horizontal direction is similar to the Mach-Zehnder case, and the above metric can be simplified by confining the motion into a plane with constant azimuthal angle ϕ ($d\phi = 0$) and approximately constant radial coordinate r ($dr = 0$) resulting in

$$ds^2 = \left(1 - \frac{r_s}{r}\right) c^2 dt^2 - r^2 d\theta^2 = 0 \tag{4.8}$$

where the last equality is true for light-like trajectories. Solving this for the horizontal propagation from the beam splitter to the mirror one gets

$$t_{h\rightarrow} = \frac{r}{c} \int_0^\theta \frac{1}{\sqrt{1 - \frac{r_s}{r}}} d\theta' \tag{4.9}$$
$$= \frac{\theta r}{c} \frac{1}{\sqrt{1 - \frac{r_s}{r}}} \tag{4.10}$$

Because of symmetry, the coordinate time $t_{h\leftarrow}$ for horizontal propagation from the mirror back to the beam splitter is the same as $t_{h\rightarrow}$. Thus the elapsed coordinate time for the full horizontal propagation is given by

$$t_h = \frac{2r\theta}{c} \frac{1}{\sqrt{1 - \frac{r_s}{r}}} \tag{4.11}$$

The proper length for the horizontal path can be calculated by [12]

$$dL = \sqrt{-ds^2}|_{dx^0=0} \tag{4.12}$$

where only the spatial coordinates are summed over. Inserting (4.8) in this relation yields

$$L = r\theta \tag{4.13}$$

For a photon travelling along the vertical axis, this formula does not apply because of the constantly changing potential. For this situation the polar angle θ and the azimuthal angle ϕ are constant and the metric reduces to

$$ds^2 = \left(1 - \frac{r_s}{r}\right) c^2 dt^2 - \left(1 - \frac{r_s}{r}\right)^{-1} dr^2 \tag{4.14}$$

again for a light-like propagation, $ds^2 = 0$ and we get a relation for the coordinate time of the photons path from a higher to a lower potential by

$$t_{v\uparrow} = \frac{1}{c} \int_r^{r+h} \frac{1}{1 - \frac{r_s}{r'}} dr' \tag{4.15}$$

and for the reverse path

$$t_{v\downarrow} = -\frac{1}{c} \int_{r+h}^{r} \frac{1}{1 - \frac{r_s}{r'}} dr' \tag{4.16}$$

where the minus takes care of the propagation against the positive radial direction. So the total elapsed coordinate time for the vertical trajectory is

$$t_v = \frac{2}{c} \int_r^{r+h} \frac{1}{1 - \frac{r_s}{r'}} dr' \tag{4.17}$$

Rewriting this integral (without the constant factor in front) in a form easy to integrate and inserting the new constant gives

$$
\begin{aligned}
\int_r^{r+h} \frac{r'}{r'-r_s} dr' &= \left[r_s log(r'-r_s) + r'\right]_r^{r+h} \\
&= r_s \left(log(r+h-r_s) - log(r-r_s)\right) + h \\
&= r_s log\left(1 + \frac{h}{r-r_s}\right) + h
\end{aligned}
\tag{4.18}
$$

This is quite a complicated expression, if we compare it to the horizontal one. Under the reasonable assumption that the vertical coordinate distance h is much smaller than the radial coordinate r, we can expand the logarithm to get

$$
r_s log\left(1 + \frac{h}{r-r_s}\right) + h \approx h\left(1 + \frac{r_s}{r-r_s}\right) = h\left(\frac{1}{1-\frac{r_s}{r}}\right) \tag{4.19}
$$

Inserting this back in equation (4.17) we finally arrive at an expression for the elapsed coordinate time for the vertical trajectory of a photon

$$
t_v = \frac{2h}{c(1-\frac{r_s}{r})} \tag{4.20}
$$

To compute the proper vertical length H we use $dH = \sqrt{-ds^2}|_{dx^0=0}$ which gives for $r_s \ll r$

$$
\begin{aligned}
H &= \int_r^{r+h} \frac{dr'}{\sqrt{1-\frac{r_s}{r'}}} \\
&= \int_r^{r+h} \left(1 + \frac{r_s}{2r'} + \mathcal{O}(\frac{r_s^2}{r'^2})\right) dr' \\
&= \left[r' + \frac{r_s}{2} log(r') + \mathcal{O}(\frac{r_s^2}{r'})\right]_r^{r+h} \\
&\approx h + \frac{r_s}{2} log(1 + \frac{h}{r})
\end{aligned}
\tag{4.21}
$$

Because in an experiment performed in the lab the two arms of the Michelson interferometer has the same physical length, the proper length of the two arms must be identical for a comparison of the elapsed coordinate times. From the requirement $H = L$ and equation (4.21) with the logarithm expanded to first order, we get a new relation for the vertical coordinate time

$$t_v = \frac{2h}{c(1-\frac{r_s}{r})} \approx \frac{2L}{c}\frac{1}{(1-\frac{r_s}{r})\,(1+\frac{r_s}{2r})} \tag{4.22}$$

With this the proper time difference as measured by an observer at coordinate position r is given by

$$\begin{aligned}\Delta\tau = \sqrt{1-\frac{r_s}{r}}(t_h - t_v) &\approx \frac{2L}{c}\left(1 - \frac{1}{\sqrt{1-\frac{r_s}{r}}\,(1+\frac{r_s}{2r})}\right)\\ &\approx \frac{l\,g\,G\,M}{c^5} \end{aligned}\tag{4.23}$$

where $l = 2L$ is the total distance (back and forth) between the mirrors and the beam-splitter for both trajectories, $g = \frac{GM}{r^2}$ is the earth's gravitational acceleration, G is the gravitational constant and m is the mass of the earth. Expression (4.23) is a second order [3] expansion for the proper time difference for a photon in a coherent superposition along the two arms of a Michelson interferometer inside the gravitational field of the earth. If we put in the same values for the parameters defined above as for the Mach-Zehnder interferometer we get for the proper time difference

$$\Delta\tau \approx 1.6 \cdot 10^{-22} s \tag{4.24}$$

which is orders of magnitude [4] smaller than those for the Mach-Zehnder interferometer. For this reason, using a Michelson interferometer instead of a Mach-Zehnder interferometer is not the path to go in order to test the gravitational mass-energy equivalence.

[3] The difference in coordinate times t_h and t_v is zero to first order.
[4] In the Mach-Zehnder case the proper time difference is of order 10^{-20}.

5 Modified Mach-Zehnder schemes for testing inertial and gravitational mass-energy equivalence

5.1 Mach-Zehnder interferometer using optical fiber spools

I present now a slightly modified version of the Mach-Zehnder setup proposed in [7]. Because general relativity allows to work in arbitrary coordinate systems and I want to make the calculations easier and more precise, I switch now to the Schwarzschild line-element in its isotropic form which is given by [22]

$$
\begin{aligned}
ds^2 &= A(R)^2 c^2 dT^2 - B(R)^2 (d\vec{X}^2) \\
&= \left(\frac{1 - \frac{r_s}{4R}}{1 + \frac{r_s}{4R}} \right)^2 c^2 dT^2 - \left(1 + \frac{r_s}{4R} \right)^4 \left(dX^2 + dY^2 + dZ^2 \right)
\end{aligned}
\tag{5.1}
$$

with the definion $R \equiv |\vec{X}| = \sqrt{X^2 + Y^2 + Z^2}$ made for a coordinate system (T, X, Y, Z). For simplicity, we ignore for now the rotation of the earth and look at the motion of a laboratory given within the defined coordinates by a world-line $T \rightarrow (T, 0, 0, Z_L)$. To get a better understanding of the occuring effects we can rescale our coordinates (T, X, Y, Z) by coordinates (t, x, y, z) so that the metric is Minkowskian at the position of the laboratory, $T \rightarrow (T, 0, 0, Z_L)$. This can be achieved by setting

$$x = B(R_L)X \qquad y = B(R_L)Y \qquad z = B(R_L)Z \qquad t = A(R_L)T \tag{5.2}$$

where $R_L \equiv |\vec{X_L}| = Z_L$ is defined with respect to the spatial position of the laboratory. Inserting this in equation (5.1) gives

$$\begin{aligned} ds^2 &= \left(\frac{(1-\frac{r_s}{4R})(1+\frac{r_s}{4R_L})}{(1+\frac{r_s}{4R})(1-\frac{r_s}{4R_L})}\right)^2 c^2 dt^2 - \left(\frac{1+\frac{r_s}{4R}}{1+\frac{r_s}{4R_L}}\right)^4 \left(dx^2 + dy^2 + dz^2\right) \\ &= \phi^2 c^2 dt^2 - \psi^2 d\vec{x}^2 \end{aligned} \tag{5.3}$$

with the useful definitions

$$\phi \equiv \left(\frac{(1-\frac{r_s}{4R})(1+\frac{r_s}{4R_L})}{(1+\frac{r_s}{4R})(1-\frac{r_s}{4R_L})}\right) \qquad \psi \equiv \left(\frac{1+\frac{r_s}{4R}}{1+\frac{r_s}{4R_L}}\right)^2 \tag{5.4}$$

One can easily check that this reduces to the metric of special relativity at the position of the laboratory. The goal now is to derive the proper time difference for an experiment, that can be performed in a laboratory. Therefore I consider again photons travelling inside optical fiber spools, resulting (due to dispersion) in velocities smaller the speed of light in vacuum. The photon moves along a world-line given by

$$t \to (t, vt, asin\,\theta + \rho\, sin\,\omega t, z_L + acos\,\theta + \rho\, cos\,\omega t) \tag{5.5}$$

This world-line describes a photon wave packet, which splits at the first beam splitter with spatial coordinates $(0, 0, z_L)$ and travels at a vertical distance $acos\theta$ inside an optical fiber spool of coordinate radius ρ. For convenience the coordinates used are depicted in Fig. (5.1).

The coordinate velocity of this particle is a composition of the velocity along the x-

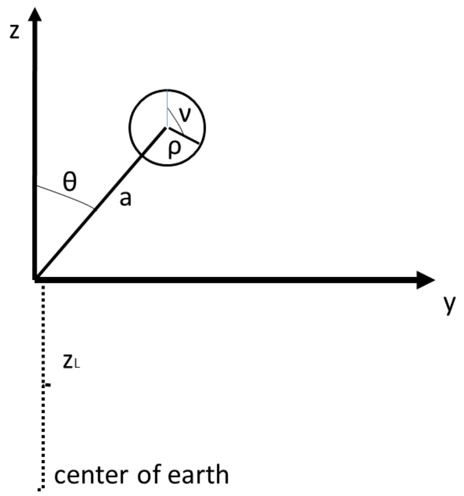

Figure 5.1: Sketch of the coordinates used in the world-line defined in (5.5), where the two angles are given at time t=0. The x-axis, which is aligned along the horizontal motion of the photons, is suppressed for better understanding and points out of the paper.

axis, $v_x = \frac{dx}{dt}$, and the velocity around the fiber spool represented by $v_\omega = \omega\,\rho$. For reasons that become clear later, there is also an angle θ between the coordinate z-axis and the vertical arms of the interferometer included. The coordinate length a can be parametrized to get the coordinate position of the photon at every instant of time. To get the proper time $\tau = \frac{ds}{c}$ we use equation (5.3) resulting in

$$\begin{aligned}
\tau &= \int_0^{t_f} \sqrt{\phi^2 - \frac{\psi^2}{c^2}\left(\left(\frac{dx}{dt}\right)^2 + \left(\frac{dy}{dt}\right)^2 + \left(\frac{dz}{dt}\right)^2\right)}dt \\
&= \int_0^{t_f} \sqrt{\phi^2 - \frac{\psi^2}{c^2}\,(v_x^2 + v_\omega^2)dt} \\
&= \int_0^{t_f} \sqrt{\phi^2 - \psi^2\left(\frac{v}{c}\right)^2}dt = \int_0^{t_f} \sqrt{\phi^2 - \psi^2\beta^2}dt \qquad (5.6)
\end{aligned}$$

where t_f represents an arbitrary final coordinate time and the definitions $v \equiv \sqrt{v_x^2 + v_\omega^2}$ and $\beta \equiv \frac{v}{c}$, where $v = \frac{d\vec{x}}{dt}$ is the coordinate velocity, were made. A physical velocity can be defined by means of proper time τ and proper length l by [12]

$$u = \frac{dl}{d\tau} = c \tag{5.7}$$

The last equality is of course only valid for massless particles in free space. As we have seen, a clock inside a gravitational field at some given position shows a differential time $d\tau = \sqrt{g_{00}}dt$ and at the same position one can measure a differential length $dl = \sqrt{-g_{mn}dx^m dx^n}$, so this definition is very natural. On the other hand one can define a physical velocity with respect to the elapsed coordinate time (the proper time of a clock far away from the source of the gravitational field) by

$$w = \frac{dl}{dt} \tag{5.8}$$

With this we are able to determine the relationship between these two velocities by

$$w = \frac{dl}{dt} = \frac{dl}{d\tau}\frac{d\tau}{dt} = u\sqrt{g_{00}} \tag{5.9}$$

and additionally the relation for a pure coordinate velocity can be taken out from

$$\frac{dl}{dt} = \sqrt{-g_{mn}\frac{dx^m}{dt}\frac{dx^n}{dt}} = \sqrt{-g_{ii}(v^i)^2} \tag{5.10}$$

$$\overset{(5.9)}{=} u\sqrt{g_{00}} \tag{5.11}$$

where the second equality is only valid if all non-diagonal components of the metric are equal to zero. So for the velocity seen by a far away observer we get

$$\vec{v} = u\sqrt{-\frac{g_{00}}{g_{11}}}\vec{e_v} \tag{5.12}$$

with the unit vector $\vec{e_v}$ pointing along the direction of propagation. The reason I go through this carefully is because a constant physical velocity is obviously not the same as a constant coordinate velocity. So in our case a constant physical velocity might require a non constant coordinate velocity. The same is true for the coordinate radius ρ, and the requirement of a constant geometrical radius in the laboratory might need a non-constant ρ. But fortunately it turns out that such effects can be neglected within the required accuracy of the calculations, so I will not worry about them in what follows from now on. If higher accuracies are needed one has to take this point into account.

Going back to equation (5.6), $d\tau = \int_0^{t_f} \sqrt{\phi^2 - \psi^2 \frac{v^2}{c^2}} dt$, we see that we can expand the metric components ϕ and ψ in terms of space-time coordinates at the location of the first beam splitter. Because we already know that these two functions will only depend on the modulus of the coordinate vector $|\vec{x(t)}|$, where $\vec{x(t)} = (vt, a sin\, \theta + \rho\, sin\, \omega t, z_L + a cos\, \theta + \rho\, cos\, \omega t)^T$, we can expand these function around the space-position of the first beam splitter which gives

$$\phi(|\vec{x(t)}|) = \phi(r_L) + \phi'(r_L)(|\vec{x(t)}| - |\vec{x_L}|) + \frac{\phi''(r_L)}{2}(|\vec{x(t)}| - |\vec{x_L}|)^2 + \mathcal{O}\left(\phi'''(r_L)\frac{a^3 + \rho^3 + v_x^2 t^2}{z_L^2}\right) \tag{5.13}$$

where ϕ' means the derivative with respect to $|\vec{x}|$ and z_L is the modulus of the vector $\vec{x_L}$ describing the position of the first beam-splitter $(0, 0, z_L)$ [1]. As a next step, assuming $\rho, a > 0$ and $\rho, a \ll z_L$, one can expand $|\vec{x(t)}|$ to second order which gives

$$\begin{aligned} |\vec{x(t)}| &= z_L \sqrt{1 + \frac{2(a\, cos\theta + \rho\, cos\, \omega t)}{z_L} + \frac{a^2 + \rho^2 + v_x^2 t^2 + 2\, a\, \rho\, cos(\theta - \omega\, t)}{z_L^2}} \\ &= z_L \left(1 + \frac{a\, cos\theta + \rho\, cos(\omega\, t)}{z_L} + \frac{(a\, sin\theta + \rho\, sin\omega\, t)^2 + v_x^2 t^2}{2 z_L^2} \right. \\ &\quad \left. + \, \mathcal{O}\left(\frac{v_x^2 t^2 + a^3 + \rho^3}{z_L^3}\right)\right) \end{aligned} \tag{5.14}$$

using this expansion and $\phi(r_L) = 1$ which is a result of our construction of a Minkowskian metric at the position of the beam-splitter, equation (5.13) gives

[1] Numerically, $r_L = |\vec{x_L}|$ and z_L are of course identical.

$$\phi(|x\vec{(t)}|) = 1 + \phi'(r_L)\,(a\,cos\theta + \rho\,cos(\omega t)) \\ + \mathcal{O}\left(\frac{\phi'(r_L)((a\,sin\theta + \rho\,sin\omega t)^2 + v_x^2\,t^2)}{z_L}\right) \tag{5.15}$$

With help of equation (5.14), it is straight forward to get a higher precision if needed. The square of the metric component required to calculate the proper time dilation can now be written as

$$\phi^2(|x\vec{(t)}|) = 1 + 2\phi'(r_L)\,(a\,cos\theta + \rho\,cos(\omega t)) + \mathcal{O}\left(\frac{\phi'(r_L)(a^2 + \rho^2 + v_x^2\,t^2)}{z_L}\right) \tag{5.16}$$

Because the expansion for ψ is exactly the same, we can express the integrand in equation (5.6) by substituting the above results and expand the square root which gives for the proper time [2]

$$\begin{aligned}\tau &= \int_0^{t_f} \sqrt{\phi^2(|x\vec{(t)}|) - \beta^2\psi^2(|x\vec{(t)}|)}dt \\ &= \sqrt{1-\beta^2}\int_0^{t_f}\left(1 + \frac{(\phi'(r_L) - \beta^2\psi'(r_L))}{1-\beta^2}\,(a\,cos\theta + \rho\,cos(\omega t))\right. \\ &+ \left.\mathcal{O}\left(\frac{(\phi'(r_L) - \beta^2\psi'(r_L))\,(a^2 + \rho^2 + v_x^2 t^2)}{(1-\beta^2)\,z_L}\right)\right) dt \\ &= \sqrt{1-\beta^2}\left(t_f + \frac{(\phi'(r_L) - \beta^2\psi'(r_L))}{1-\beta^2}\left(a\,t_f\,cos\theta + \frac{\rho}{\omega}\,sin(\omega t_f)\right)\right) \\ &+ \left(\mathcal{O}\left(\frac{(\phi'(r_L) - \beta^2\psi'(r_L))\,(a^2\,t_f + \rho^2\,t_f + v^2 t_f^3)}{\sqrt{1-\beta^2}z_L}\right)\right)\end{aligned} \tag{5.17}$$

Which is the final expression for the proper time of a photon taking a space-time trajectory around a fiber spool in a Mach-Zehnder interferometer, that is placed inside earth's gravitational field with an angle θ between the vertical arms and the z-axis. The purpose

[2] I only make an expansion to first order in ψ' and ϕ', because the resulting error is order $10^{-32}s$, which is not experimentally resolvable.

of keeping all the orders inside the equations is to have them at hand when going to higher accuracies if needed. Now lets compare the proper time of a photon in spatial superposition flying along the two paths. Because the vertical trajectory is the same, it cancels out of the equations and only the horizontal paths are left. Assuming that the two fiber spools have the same constant coordinate radii ρ [3] and that the frequencies of rotation ω around the spool are equal, the proper time difference for the lower arm ($a = 0$), denoted by τ_l, and the upper arm, denoted by τ_u, is given to first order by

$$\Delta\tau = \tau_l - \tau_u \approx \frac{\phi'(r_L) - \beta^2\psi'(r_L)}{\sqrt{1-\beta^2}} a\, t_f\, cos\theta \tag{5.18}$$

To calculate the proper time with respect to the length of the fiber measured at the position of the lab, one uses the equation for the physical velocity with respect to the coordinate time, $\frac{dl}{dt} = \frac{\sqrt{\psi(|x(\vec{t})|)^2 (d\vec{x})^2}}{dt}$. By doing so, we can rewrite t_f by its physical length and make the approximation that the metric components along the trajectory which is integrated over does not change much, so we can write using l to denote the physical length of the fiber

$$\Delta\tau \approx \frac{\phi'(r_L) - \beta^2\psi'(r_L)}{\sqrt{1-\beta^2}} \frac{a\, l\, cos\theta}{\beta\, c} \tag{5.19}$$

The reason why an angle θ between the vertical axis and the short arms of the interferometers where introduced in the world line of the photon is simply to modify the observed phase shifts. Remember that in a horizontal Mach-Zehnder interferometer the statistics observed by the two detectors only depends on the relative phase between the two arms, introduced by a phase shifter. In the vertical situation, the relative phase not only arises because of the phase shifter, but additionally by the amount of potential difference between the two arms. The simplest strategy to extract the information of the gravitationally induced phase shift out of the obtained measurement statistics is to first calibrate the Mach-Zehnder set-up in the horizontal position with the help of the

[3] corrections to that can be calculated to first order by the physical length $L = \int_0^a \sqrt{g_{mn} \frac{dx^m}{d\lambda} \frac{dx^n}{d\lambda}} d\lambda$, where $\lambda \in [0, a]$ is a parameter describing the coordinate length a at every instant of time t.

phase shifter. Afterwards, one might rotate the whole set-up in a vertical position and would see, in the ideal case, a change in the statistics due to gravitational influence. So why would we need a modification of the gravitational effect? One of the problems lies in the fact, that gravity is by far the weakest of the four known forces of nature. In our case this can be seen by putting some numbers in equation (5.19). For this, one has to calculate the derivative [4] of the metric components ϕ and ψ, which are

$$\begin{aligned}\phi'(R) &= \left(\frac{(1-\frac{r_s}{4R})(1+\frac{r_s}{4R_L})}{(1+\frac{r_s}{4R})(1-\frac{r_s}{4R_L})}\right)' \\ &= \left(\frac{1+\frac{r_s}{4R_L}}{1-\frac{r_s}{4R_L}}\right)\left(\frac{8\,r_s}{(r_s+4R)^2}\right) \\ &\approx \frac{8\,r_s}{(r_s+4R)^2}\end{aligned} \tag{5.20}$$

and

$$\begin{aligned}\psi'(R) &= \left(\left(\frac{1+\frac{r_s}{4R}}{1+\frac{r_s}{4R_L}}\right)^2\right)' \\ &= -\frac{\psi\,r_s}{2R^2(1+\frac{r_s}{4R})}\end{aligned} \tag{5.21}$$

We want to have a number for this expression at the position of the first beam splitter, $\phi'(R = r_L)$, $\psi'(R = r_L)$. The average value for the radius of the earth is given by $6,371 * 10^6$m, with can be taken approximateley as the coordinate distance r_L. The Schwarzschild radius r_s for the earth is about $8,87 * 10^{-3}$m and ψ is by construction equal to 1 at the position in question. With this we get

$$\phi'(r_L) \approx 1,093 * 10^{-16} m^{-1} \approx -\psi'(r_L) \tag{5.22}$$

[4] With respect to the modulus of the spatial coordinate vector $|\vec{x}| = R$, which is approximately the same as in old coordinates $(\vec{X})$ because the metric-components are equal to 1 at the position of the first beam splitter and very close to 1 in a neighbourhood of it.

Looking back to equation (5.19) reveals, that the difference in proper time is very small for small length l of the optical fibers, as has already been mentioned in [7]. Just for convenience one can compare the values achieved with the two different coordinates. Using isotropic coordinates ends to first order in the relation

$$\begin{aligned}\Delta\tau &\approx \frac{\phi'(r_L) - \beta^2\psi'(r_L)}{\sqrt{1-\beta^2}}\frac{a\, l\, cos\theta}{\beta\, c} \\ &\overset{\phi'(r_L)=-\psi'(r_L)}{\approx} 3,64 * 10^{-25}\frac{1+\beta^2}{\sqrt{1-\beta^2}}\frac{l}{\beta}\end{aligned} \tag{5.23}$$

where the parameters a and $\cos\theta$ were set equal to 1. So an observer on the upper arm of the Mach-Zehnder interferometer would measure a proper time difference that depends on $\beta = \frac{v}{c}$ (and therefore on the type of fiber) and the length of the fiber within this description. Looking back to the definition of $\beta = \frac{\sqrt{v_x^2+v_\omega^2}}{c} = \frac{\sqrt{v_x^2+\omega^2\rho^2}}{c}$ we see, that this function depends on the coordinate velocity v_x along the x-axis (this axis coincides with the axis of the fiber spool) and the velocity of the photon around the fiber spool. The latter can be easily calculated [5] by using the coordinate radius ρ and the speed of light inside a fiber, which is roughly $\frac{2c}{3}$. The coordinate velocity in the x-direction is approximated by the distance a photon has to travel along the x-axis going exactly once around the spool and the time needed to do so [6]. With this, one gets for β a value of approximately $\frac{2}{3}$. Choosing the length of the optical fiber to be the same as suggested in section 3, $l = 10^5$m, we get as approximation of the proper time difference up to first order

$$\Delta\tau \approx 1.06 * 10^{-19}s \tag{5.24}$$

Comparing this with the result of [7], we see that they does not coincide perfectly. One of the reasons is, that the calculations here are done by using optical fiber spools confined within a small region of space, whereas in [7] the calculations were made for extended

[5] I am not considering the difficulties arising from non constant physical velocities during propagation.

[6] The distance in x-direction for one full rotation equals the diameter of the optical fiber coating, which is roughly $245\mu m$.

path's where the occurring time dilation is smaller for paths further away from the center of gravitation. So again we are faced with the problem of resolving a very small physical effect.

5.2 Dynamical rotation of a Mach-Zehnder interferometer

We have seen in the last chapter, that a rotation of the MZI around one of his arms by an angle θ results in a modification of the proper time difference along the paths and therefore in a measurable change in the photon statistics at the two detectors. But various unwanted physical effects from temperature/pressure change in optical fibers to noise in the detection process itself produces phase shifts, that are much bigger than the gravitational one we wish to observe. So we can ask the question if there are modifications of the proposed scheme that allows for extracting the information about gravitational effects more accurately. The rotation around an axis as introduced before was done in a static way, meaning that we first made the rotation, fix the arms at that position and make the measurements afterwards. To enhance the experiment, one can think about a dynamical rotation of the MZI. Within this scheme one of the arms is rotated around the other with a variable frequency during the whole time of the measurement process, resulting in a sinusoidal signal at the detectors. I proceed by giving a mathematical deviation of this effect and work out the consequences in what follows.

5.2.1 Proper time of a particle in a rotating Mach-Zehnder interferometer

As before, we want to describe our particle by a world-line in the coordinates we have chosen in section 5.1. We want our photon to move with constant coordinate velocity around a fiber spool of constant coordinate radius ρ aligned along the x-coordinate. Again we neglect effects that may arise because constant coordinate velocity and a constant radius does in general not imply constant physical velocity and radii. Different to the case of a static rotating MZI we now replace the constant angle θ by a time varying argument in the world line given by

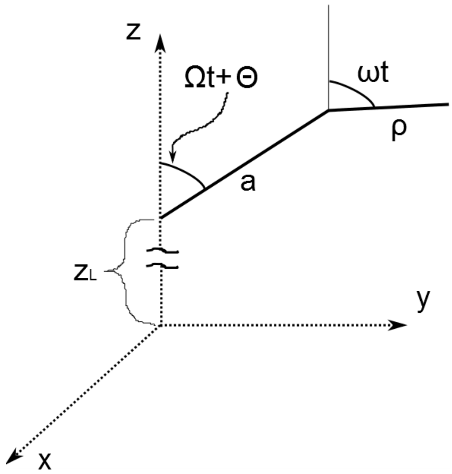

Figure 5.2: A sketch of the coordinates used for the world-line given by (5.25). The coordinate position z_L refers to the position of the first beam splitter of a Mach-Zehnder interferometer (MZI). The coordinates a and ρ are the distance between the two arms of the MZI and the radius of the spool respectively. Ω describes the angular velocity of one of the spools around the other whereas ω is the angular velocity of the photon around the fiber spool.

$$t \to (t, v_x\, t, a\, sin(\Omega\, t + \Theta) + \rho\, sin(\omega\, t), z_L + a\, cos(\Omega\, t + \Theta) + \rho\, cos(\omega\, t)) \tag{5.25}$$

where Θ is a parameter introduced to assign for a possible phase difference between the rotation around the spool and the rotation around one of the arms. The coordinates of this world-line are depicted for convenience in Fig. (5.2).

The proper time elapsed along the trajectories is given by

$$\begin{aligned}
\tau &= \int_0^{t_f} \sqrt{\phi^2(|\vec{x(t)}|) - \frac{\psi^2(|\vec{x(t)}|)}{c^2}\left(\left(\frac{dx}{dt}\right)^2 + \left(\frac{dy}{dt}\right)^2 + \left(\frac{dz}{dt}\right)^2\right)}\, dt \\
&= \int_0^{t_f} \sqrt{\phi^2(|\vec{x(t)}|) - \psi^2(|\vec{x(t)}|)\left(\frac{v_x^2 + \Omega^2 a^2 + \omega^2\rho^2 + 2\,\Omega\,\omega\, a\,\rho\, cos((\Omega-\omega)t + \Theta)}{c^2}\right)}\, dt \\
&= \int_0^{t_f} \sqrt{\phi^2(|\vec{x(t)}|) - \psi^2(|\vec{x(t)}|)\left(\zeta^2 + \frac{2\,\Omega\,\omega\, a\,\rho\, cos((\Omega-\omega)t + \Theta)}{c^2}\right)}\, dt
\end{aligned} \tag{5.26}$$

with the definition $\zeta \equiv \frac{\sqrt{v_x^2+\Omega^2 a^2+\omega^2\rho^2}}{c}$. Here I have assumed, that the rotation around the axis does not affect the coordinate velocity of the photon in the rotating arm. Whether this is assumption is valid or not has to be tested out in the laboratory. We proceed similar to the non rotating case (equation (5.13)) and expand the metric component of $\phi(|x\vec{(t)}|)$ (where $x\vec{(t)}$ is given by the spatial part of the world line in (5.25)) to second order by

$$\phi(|x\vec{(t)}|) = \phi(r_L)+\phi'(r_L)(|x\vec{(t)}|-|\vec{x_L}|)+\frac{\phi''(r_L)}{2}(|x\vec{(t)}|-|\vec{x_L}|)^2+\mathcal{O}\left(\phi'''(r_L)\frac{a^3+\rho^3+v_x^2t^2}{r_L^2}\right) \tag{5.27}$$

The modulus of the spatial position vector is given by [7]

$$\begin{aligned} |x\vec{(t)}| &= z_L + \rho\, cos(\omega\, t) + a\, cos(\Omega\, t + \Theta) \\ &+ \frac{v_x^2 t^2 + (a\, sin(\Omega\, t + \Theta) + \rho\, sin(\omega\, t))^2}{2 z_L} \\ &+ \mathcal{O}\left(\frac{v_x^2 t^2 + a^3 + \rho^3}{r_L^2}\right) \end{aligned} \tag{5.28}$$

with $r_L = z_L = |\vec{x_L}|$ as the modulus of the coordiante position vector of the first beam splitter, $\vec{x_L} = (0, 0, z_L)^T$. Inserting this in the expansion for $\phi(|x\vec{(t)}|)$ and remembering, that we have rescaled the metric to get $\phi(0, 0, z_L) = 1$ at the position of the beam splitter, gives for the square

$$\begin{aligned} \phi^2(|x\vec{(t)}|) &= 1 + 2\phi'(r_L)\left(\rho\, cos(\omega\, t) + a\, cos(\Omega\, t + \Theta)\right) \\ &+ \mathcal{O}\left(\frac{\phi'(r_L)(v_x^2 t^2 + \rho^2 + a^2)}{r_L}\right) + \mathcal{O}\left(\phi''(r_L)(\rho^2 + a^2 + \frac{v_x^2 t^2}{r_L})\right) \end{aligned} \tag{5.29}$$

The expansion for $\psi(|x\vec{(t)}|)$ is exactly the same and we can write the integrand in equation (5.26) as

[7] After expanding the square root to second order as in equation (5.14).

$$
\begin{aligned}
&\sqrt{\phi^2 - \psi^2 \left(\zeta^2 + \frac{2\,\Omega\,\omega\,a\,\rho\,cos((\Omega-\omega)t+\Theta)}{c^2}\right)} = \\
&= \sqrt{1-\zeta^2}\left(1 + \frac{(\phi'(r_L) - \zeta^2\psi'(r_L))(\rho\,cos(\omega\,t) + a\,cos(\Omega\,t+\Theta))}{1-\zeta^2}\right. \\
&- \frac{\Omega\,\omega\,a\,\rho\,cos((\Omega-\omega)t+\Theta)}{c^2(1-\zeta^2)} + \mathcal{O}\left(\frac{(\phi'(r_L)-\zeta^2\psi'(r_L))(v_x^2t^2+\rho^2+a^2)}{(1-\zeta^2)r_L}\right) \\
&\left. + \mathcal{O}\left(\frac{\Omega^2\omega^2a^2\rho^2}{(1-\zeta^2)^2c^4}\right)\right) \qquad (5.30)
\end{aligned}
$$

where the square root was expanded to first order only [8]. With this, the integral in equation (5.26) can be easily solved to give

$$
\begin{aligned}
\tau &= \int_0^{t_f} \sqrt{\phi^2 - \psi^2\left(\zeta^2 + \frac{2\,\Omega\,\omega\,a\,\rho\,cos((\Omega-\omega)t+\Theta)}{c^2}\right)}\,dt \\
&= \sqrt{1-\zeta^2}\,t_f + \frac{(\phi'(r_L)-\zeta^2\psi'(r_L))\left[\frac{\rho}{\omega}\,sin(\omega\,t_f) + \frac{a}{\Omega}(\,sin(\Omega\,t_f+\Theta) - sin(\Theta))\right]}{\sqrt{1-\zeta^2}} \\
&- \frac{\Omega\,\omega\,a\,\rho\,(sin((\Omega-\omega)t_f+\Theta) - sin\Theta)}{c^2\sqrt{1-\zeta^2}(\Omega-\omega)} + \mathcal{O}\left(\frac{(\phi'(r_L)-\zeta^2\psi'(r_L))(v_x^2t_f^3+\rho^2t_f+a^2t_f)}{\sqrt{1-\zeta^2}r_L}\right) \\
&+ \mathcal{O}\left(\frac{\Omega^2\omega^2a^2\rho^2t_f}{(1-\zeta^2)^{3/2}c^4}\right) \qquad (5.31)
\end{aligned}
$$

This is a first order equation for the proper time of a photon following a trajectory around a fiber spool of coordinate radius ρ. This spool rotates with frequency Ω around the axis defined by the first beam splitter and is displaced by a coordinate distance a from the same axis.

5.2.2 Consequences of the proper time difference

Now lets work out the consequences of this dynamically rotating interferometer. As a first step, one has to calculate the proper time difference between the two different paths

[8]The expansion is justified by the small values for $\phi'(r_L)$ and $\psi'(r_L)$ which where calculated in section (5.1) to be $\mathcal{O}(10^{-16})$.

γ_1 and γ_2 [9]. For γ_2, the coordinate distance $a = 0$ and therefore it is hard to subtract the proper times due to our definition of ζ. To solve this problem we expand the function $\sqrt{1-\zeta^2}$ to first order and use the definitions made for ζ and β[10]

$$\begin{aligned}\sqrt{1-\zeta^2} &= \sqrt{1-\beta^2}\sqrt{1-\frac{a^2\Omega^2}{c^2(1-\beta^2)}} \\ &= \sqrt{1-\beta^2}\left(1-\frac{a^2\Omega^2}{2c^2(1-\beta^2)}+\mathcal{O}\left(\frac{a^4\Omega^4}{c^4}\right)\right)\end{aligned} \tag{5.32}$$

By inserting this in equation (5.31) and assuming $\frac{a^2\Omega^2}{c^2}\psi'(r_L) \ll \frac{a^2\Omega^2}{c^2} \ll 1$, one gets as first order approximation for the proper time difference between the two paths

$$\begin{aligned}\Delta\tau = \tau_2 - \tau_1 \approx\; & \frac{\phi'(r_L)-\beta^2\psi'(r_L)}{\sqrt{1-\beta^2}}\left(\frac{a}{\Omega}\left(sin(\Omega\,\frac{l}{\beta\,c}+\Theta)-sin(\Theta)\right)\right)-\frac{a^2\Omega^2}{2c^2\sqrt{1-\beta^2}}\frac{l}{\beta\,c} \\ & -\frac{\Omega\,\omega\,a\,\rho}{c^2\sqrt{1-\beta^2}(\Omega-\omega)}\left(sin((\Omega-\omega)\frac{l}{\beta\,c}+\Theta)-sin(\Theta)\right) \\ & \equiv A-B-C\end{aligned} \tag{5.33}$$

Where τ_1 and τ_2 are the proper times corresponding to the paths γ_1 and γ_2 respectively and the coordinate time t_f was again replaced by the expression $t_f \approx \frac{l}{\beta\,c}$, with l the length of the optical fiber as measured by an observer in the laboratory. To see if the above equation makes sense at all, we start by analysing the first term. For small Ω, we can rewrite A as

$$A_{static} = \frac{\phi'(r_L)-\beta^2\psi'(r_L)}{\sqrt{1-\beta^2}}\frac{a\,l}{\beta\,c}cos(\Theta) \tag{5.34}$$

which is exactly the same as in the case of a non rotating interferometer, equation (5.19), as it should. For a given fiber spool with constant values for l and β, the range of the first term in equation (5.33) can be modulated in principle by the distance off-axis a,

[9] I denote the paths exactly like in section 1.1, where γ_2 defines the path that coincides in x-direction with the axis of rotation.

[10] $\zeta^2 = \beta^2 + \frac{a^2\Omega^2}{c^2}$

the angular velocity Ω and the out-of-phase angle Θ. In the type of experiment that is now under investigation, we want to fix $a \equiv 1m$. Ω is in principle a function of time, but we are dealing with the proper time difference between two coherent superpositions of a wavefunction for one single photon. We can calculate with help of section (1.1), that in the static case the estimated time a photon spends inside the fiber is of order $10^{-4}s$. So we can argue that within this small time interval the frequency of rotation and therefore Ω is constant [11]. Later in this chapter we will see that Ω is bounded due to industrial standards to approximately $200\frac{rad}{s}$, which is still not a very realistic value to realize because we have a big moment of inertia for a one meter displaced outer spool. In what follows I assume that we deal with an angular velocity of $30\frac{rad}{s}$. We have seen that Θ is the angle of displacement from the z-axis (in z-y-plane) for $t = 0$, accounting for the two involved rotations to be out of phase. For consecutive photons, the angle Θ is different for dynamical rotations due to the constantly rotating outer spool, so we can vary Θ and see for which value we get the biggest $\Delta\tau$. Because the physical values $\beta \approx \frac{2}{3}$, $a \equiv 1m$ and $\phi'(r_L) \approx -\psi'(r_L) \approx 1,093 \cdot 10^{-16}\frac{1}{m}$ are constants in this case, we are left with the function

$$A(\Omega, \Theta) = \kappa(\Omega)\left((sin(\lambda(\Omega) + \Theta) - sin(\Theta))\right) \tag{5.35}$$

that includes information about the maxima and minima for the first term in equation (5.33) for a given fiber spool. The two functions $\kappa(\Omega) = \frac{\phi'(r_L)(1+\beta^2)\,a}{\Omega\sqrt{1-\beta^2}}$ and $\lambda = \frac{\Omega\,l}{\beta\,c}$ are pure numbers for a given Ω. Within a small range $0 < \Omega < 100$, the maxima and minima of this function with respect to Θ are almost unaltered due to the fact that the argument of the sine function is $\ll 1$, meaning that in an expansion the Ω's in the nominator and denominator would almost cancel each other. So to analyse the position of the maxima and minima for fixed $\Omega = 30\frac{rad}{s}$, we make the first derivative of equation (5.35) with respect to Θ and set this equal to zero. The question now is the following: When is a cosine-function of a variable plus a constant equal to the cosine-function of

[11] In the final experiment one can of course vary Ω in time to get a AC-signal at the detectors and extract the gravitational information. But here we are dealing with the proper time difference for a **single** photon, where Ω is approximately fixed for the whole motion inside the fiber spool.

the variable? This can only occur in a neighbourhood of the maxima/minima of an ordinary cosine-function, or in mathematical terms the condition for the first maximum is

$$cos(x + 2n\pi) = cos(-x) \tag{5.36}$$

with $n \in \mathbb{N}$. This must be compared to the requirement that the first derivative of equation (5.35) must be zero

$$cos(\lambda + \Theta + 2n\pi) = cos(-\Theta) \tag{5.37}$$

Equating the arguments gives finally $\Theta = -\frac{\lambda}{2}$, as condition for the maximum. The minimum is just shifted by π. With the values we have chosen above, we get the extrema at positions

$$\Theta_{max} = -0.0075 + 2\pi n \qquad \Theta_{min} = \pi - 0.0075 + 2\pi n \quad n \in \mathbb{N} \tag{5.38}$$

The values corresponding to this point for a fixed $\Omega = 30\frac{rad}{s}$ are

$$A_{max} = 1.06 * 10^{-19}s \qquad A_{min} = -1.06 * 10^{-19}s \tag{5.39}$$

for the maximum and the minimum respectively. A plot of the Θ dependence of the first term in equation (5.33) is shown in Figure (5.3).

Now one can ask the question why the maxima and minima for dynamical rotations are not located at the same place as the maxima and minima for static "rotations". In the static case the outer arm is fixed while the photon is inside the fiber. For that reason the extremal positions are clearly at $\Theta = 0$ - which corresponds to the topmost position of the arm - and $\Theta = \pi$ corresponding to the bottommost position. For dynamical rotations the situation is different due to the constantly moving arm while the photon is inside the fiber. Simple geometry reveals, that the positions of the arm where the height difference between the two arms inside the gravitational field is least affected, corresponds to

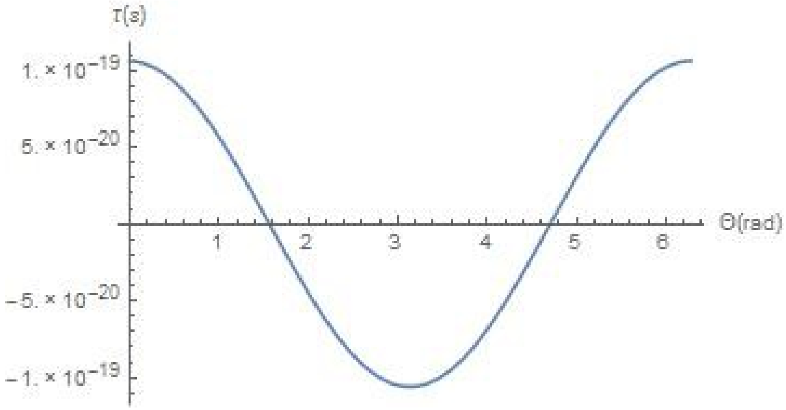

Figure 5.3: A plot of the function $\frac{\phi'(r_L)-\beta^2\psi'(r_L)}{\sqrt{1-\beta^2}}\left(\frac{a}{\Omega}\left(sin(\Omega\,\frac{l}{\beta\,c}+\Theta)-sin(\Theta)\right)\right)$ where the Θ dependence is on the x-axis and the resulting proper time dependence is on the y-axis. The plot corresponds to $\Omega = 30\frac{rad}{s}$.

the point before and after the extremal positions. This intuitively pleasing argument coincides with our mathematical description, and indicates the validity of the formula. Because this term only accounts for relative height difference, the value for proper time difference at the extremal positions should not be different to the static case. Indeed, if one uses equation (5.34) and inserts for $\Theta = 0$ and $\Theta = \pi$, the values for maximal and minimal proper time dilation coincides with the values for the dynamical case.

The second term in equation (5.33), $B = -\frac{a^2\Omega^2}{2c^2\sqrt{1-\beta^2}}\frac{l}{\beta\,c}$ is not there for static MZI's and arises only due to the rotation of one spool around the other. The displacement of one of the spools by a distance **a** generates a centripetal potential $\frac{a^2\Omega^2}{2}$, that either increases or decreases the proper time difference, depending on the position of the spool. The minus sign indicates, that it increases this difference (defined by equation (5.33)) only in the lower half of the circle which is defined by the motion of the outer spool (spool 1). If the spool moves around the upper half-circle, the proper time is decreased which is something we would have expected. Although term A as discussed before is, within a small range, not very much affected by a change in Ω, B is quadratic in this variable and we expect a parabolic behaviour. This suggests to make Ω as large as possible in order to increase the proper time difference. Calculating the effect one would expect for this term at an angular velocity of $\Omega = 30\frac{rad}{s}$ as before

$$B_{max} \approx -3,35 \cdot 10^{-18} s \tag{5.40}$$

which is one order of magnitude bigger than the pure gravitational term A.

The remaining part of the equation for the proper time difference,

$$C = -\frac{\Omega\, \omega\, a\, \rho}{c^2 \sqrt{1-\beta^2}(\Omega-\omega)} \left(sin((\Omega-\omega)\frac{l}{\beta\, c} + \Theta) - sin(\Theta) \right) \tag{5.41}$$

accounts for the relative motion between the two different rotations. The rotation of the outer spool combined with the rotation of the photon due to the fiber aligned within this spool changes the relative position between the wavefunctions for the two trajectories because the centred spool has only one type of rotation. In the limit where Ω and ω are the same quantity, the term for this part in equation (5.41) reduces to

$$C_{static} = -\frac{\Omega\, \omega\, a\, \rho}{c^2 \sqrt{1-\beta^2}} \frac{l\, cos(\Theta)}{\beta\, c} \tag{5.42}$$

This means that there is no relative difference in the two rotations and the difference remains constant during the rotation for one photon. This is because in this limit every point of the spool rotates in phase with the arm the spool is attached to. Under real life conditions this limiting case could never occur: The angular velocity of the photon inside the fiber is always bigger that the angular velocity of the rotation of the arm. Although the terms **A** and **C** look quite similar, we have a stronger Ω-dependence of **C** in the proper time difference due to the additional Ω in the nominator of this term, which makes it harder to analyse the behaviour we expect to be almost linear in Ω. Again we seek for the extremal points for this function which means, because for a given fiber spool the parameters ω,l,β and ρ are constants,

$$C(\Omega,\Theta) = -\kappa \frac{\Omega}{\Omega-\omega} \left(sin((\Omega-\omega)\frac{l}{\beta\, c} + \Theta) - sin\Theta \right) \tag{5.43}$$

with $\kappa = \frac{\omega\, a\, \rho}{c^2 \sqrt{1-\beta^2}}$. For the dependence on Θ we can again use the symmetry property of the cosine-function, $cos(x + 2n\pi) = cos(-x)$ which leads in this case to

$$\Theta_{extr} = -\frac{(\Omega - \omega)l}{2\,\beta\,c} + n\pi \tag{5.44}$$

as position for the extremal points with $n \in \mathbb{N}$, where odd n correspond to maximal- and even n to minimal values for **C**. Inserting this back into equation (5.41) we get the corresponding values for **C**

$$\begin{aligned} C_{min} &= -\frac{2\,\Omega\,\omega\,a\,\rho}{c^2\sqrt{1-\beta^2}(\Omega-\omega)}\left(sin(\frac{(\Omega-\omega)l}{2\beta\,c} + 2\pi n)\right) \\ C_{max} &= -\frac{2\,\Omega\,\omega\,a\,\rho}{c^2\sqrt{1-\beta^2}(\Omega-\omega)}\left(sin(\frac{(\Omega-\omega)l}{2\beta\,c} + (2n+1)\pi)\right) \end{aligned} \tag{5.45}$$

As mentioned above, we expect **C** to be a monotonic increasing function with Ω which means that there is no global maxima or minima; The higher the angular velocity of the rotation around one arm of the interferometer, the bigger is the contribution of this term for the total proper time difference as can be seen in Figure (5.4)
We can now put in the numbers we have used for the other terms to find the values for Θ at which the function is maximal/minimal as well as to search for the values for the proper time difference that stem from term **C** at this angles. To be consistent with the other two terms I insert in this expressions for the angular velocity of the arm $\Omega = 30\frac{rad}{s}$ resulting in

$$\begin{aligned} &\Theta_{min} \approx 2,963rad + 2\pi n & &C_{min} \approx -1,66 \cdot 10^{-17}s \\ &\Theta_{max} \approx 2,963rad + (2n+1)\pi & &C_{min} \approx 1,66 \cdot 10^{-17}s \end{aligned} \tag{5.46}$$

Having analysed all the terms step by step I can explain why I have done this so carefully. What we want is an experiment able to extract information of the gravitational

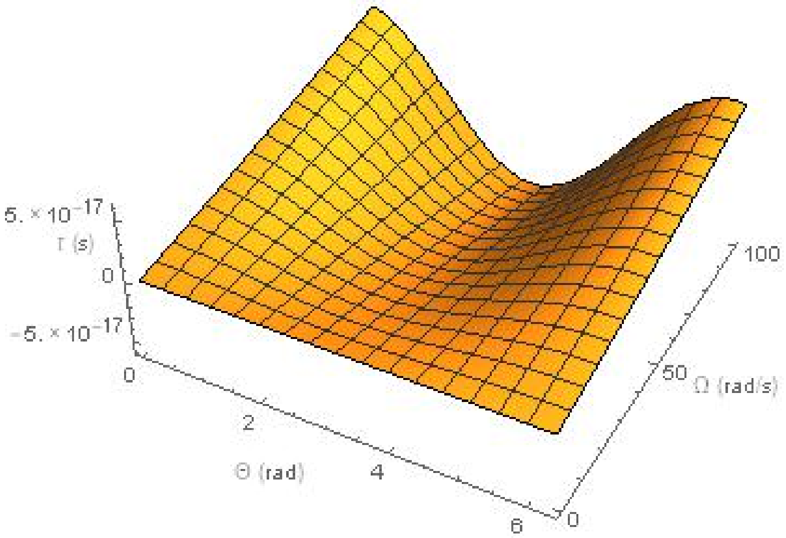

Figure 5.4: A plot of the function $C(\Omega,\Theta) = -\frac{\Omega\,\omega\,a\,\rho}{c^2\sqrt{1-\beta^2}(\Omega-\omega)}\Big(sin((\Omega-\omega)\frac{l}{\beta\,c}+\Theta) - sin(\Theta)\Big)$ which shows that the maxima and minima are monotonic increasing with the angular velocity Ω of the rotation around one of the arms of the MZI. The Θ-dependence is given by a cosine-function, with minima at $\Theta = -\frac{(\Omega-\omega)l}{2\,\beta\,c} + 2\pi n$ and maxima at $\Theta = -\frac{(\Omega-\omega)l}{2\,\beta\,c} + (2n+1)\pi$.

influence of the earth on a test particle, in our case a photon. We have seen that term **A**, which we have interpreted to account for the gravitational potential difference of the two trajectories, is of order $10^{-19}s$. The second term (**B**), that was generated by the rotational potential was already one order of magnitude bigger and the term accounting for the relative motion between the two involved rotations was two orders of magnitude bigger than **A**. Now it is important to note that **B** and **C** can also be derived to first order without including gravity, just by taking the metric of Minkowskian space-time, which is shown in the appendix (section 7.4). Therefore this experiment does not increase the effect of gravity alone, it just increases the proper time difference due to the additional rotation of one of the arms. But what this type of experiment can show is the mass-energy equivalence for photons that arise through a combination of gravitational and centripetal potential. Mass-energy equivalence here stands for the equivalence of the photons energy and its gravitational and inertial mass. But as said before, the contribution of gravitational mass of the photon to the total proper time difference can't be extracted out of the signal, due to the overwhelming effect of the rotation of one of the arms.

5.2.3 Possible experimental realization

An experiment for testing this type of effect has to include all the features of the world-line defined by (5.25). The fiber spools that can be used here may be from **CORNING**, and provide the specifications as shown in section 3. A rotation around one of the arms of the interferometers would result in a twist of the fiber, which would lead to its destruction after a short amount of time. Therefore we need a kind of fiber rotary joint. Several types of this rotary joints are produced by **PRINCETEL**, which provides superior devices concerning single-mode performance. The best suited device is a **FORJ: Single-channel fiber optic rotary joint RPT** with an insertion loss $< \pm 0,25dB$ for $1550nm$. This rotary joints can be used up to $\approx 200\frac{rad}{s}$, which is more than enough to perform the experiment. After this rotary joint a fiber optic beam splitter is used to generate the two different paths followed by one of the fiber spools for each path. The two trajectories are recombined by an identically constructed fiber optic beam splitter followed by another rotary joint, which is responsible for the decoupling. A SolidWorks sketch of the proposed experiment is shown in Fig. (5.5).
The arms of the interferometer are implemented by two fiber spools: One of them is located on the top of the frame and the other one on the axis of rotation. To suppress the inevitable vibrations due to mass imbalance around the axis of rotation as good as possible, a system composed of precise hydraulic cylinders can be used. This system is controlled by a laser-feedback system which is mounted on the frame around the interferometer with mirrors fixed on the rotating frame of the interferometer. Light is coupled into and out of the interferometer with help of rotary joints, where the stator is fixed to the pedestal and the rotor is attached to the rotating frame. Due to mechanical vibrations, this type of interferometer introduces additional noise that affects the signal by creating unwanted phase shifts. To keep this vibrations to a minimum, not the full frequency range of the rotary joints should be used.

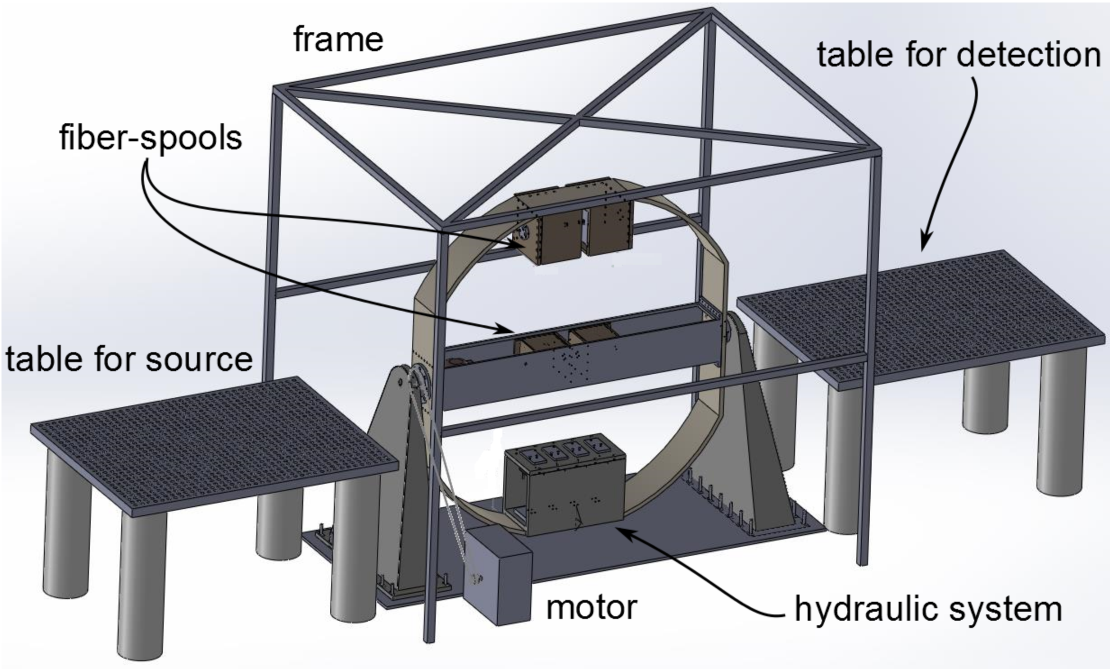

Figure 5.5: A sketch of a possible realization of a dynamical rotating Mach-Zehnder interferometer. The setup for the source can be placed on the left optical table, where light is coupled in a single-mode fiber which is connected to the first rotary joint. One of the fiber spools is placed on the axis of rotation whereas the other is fixed on one of the arms. After passing through the interferometer it is coupled out by a rotary joint and led to the optical table provided for the detection setup. At the opposite side of the frame a precise hydraulic system is mounted which can be controlled by a laser-feedback system.

5.3 Rotating Mach-Zehnder interferometer with an additional degree of freedom

We have seen, that a rotating interferometer can be beneficial for a measurement of a phase shift in the photons wavefunction and therefore a test for mass-energy equivalence for combined intertial and gravitational mass. The reason was the constantly changing position of one of the fiber spools which in turn provides a controllable change of the gravitational potential as well as a centripetal potential for one of the trajectories. But we can still do better than that by also varying the position of the central fiber spool in vertical direction by, lets say, a harmonic motion with a controllable frequency. With such a technique, the potential difference between the two spools can be increased for a certain period of time, which in turn increases the proper time difference for both trajectories and therefore the detectable phase shift. Furthermore a strategy like this should allow for extracting out the phase shift that stems from gravitational effects only. We want to refer in what follows to the rotating spool as spool 1, and for the spool moving within this radius of rotation as spool 2 as sketched in Fig. (5.6). This section starts with a mathematical model for the proper time difference between the two paths followed by a discussion of the effects together with a sketch of a possible experimental realization.

5.3.1 Mathematical model

Our starting point is again the world-line of a particle (our photon) which in this case is not dramatically different from the previous one and reads

$$t \to (t, v_x t, a\, sin(\Omega\, t + \Theta) + \rho\, sin(\omega\, t), z_L + a\, cos(\Omega t + \Theta) + b\, cos(\epsilon t + \nu) + \rho cos(\omega\, t)) \tag{5.47}$$

where now ϵ is the angular frequency for a motion along the vertical axis (z-axis), and ν is a phase that covers the case of out-of-phase dynamics between the two different

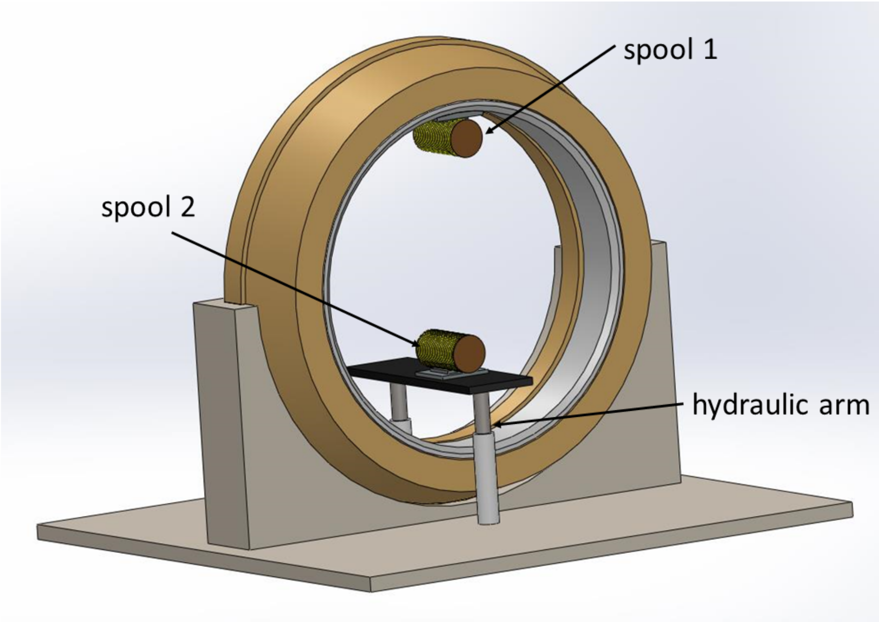

Figure 5.6: Sketch of a possible experimental configuration of the world-line defined in (5.47). Spool 1 is rotating with frequency Ω around spool 2, which makes a harmonic motion with amplitude b and frequency ϵ along the z-direction.

rotations and the newly introduced harmonic motion. We require $\nu = \frac{\pi}{2}$ at the position of the first beam-splitter (z_L) in order to agree with the results of the last section. The coordinate distance b acts as an amplitude, which in this case is the maximal possible displacement of the inner fiber spool from its central position (z_L). As before we can write for the elapsed proper time between a coordinate interval $t \in [0, t_f]$

$$\begin{aligned}\tau &= \int_0^{t_f} \sqrt{\phi^2(|\vec{x(t)}|) - \frac{\psi^2(|\vec{x(t)}|)}{c^2} \left(\frac{d\vec{x(t)}}{dt}\right)^2} dt \\ &= \int_0^{t_f} \sqrt{\phi^2(|\vec{x(t)}|) - \psi^2(|\vec{x(t)}|)\,(\xi^2 + \chi^2)} dt \qquad (5.48)\end{aligned}$$

where I made the definitions

$$\xi^2 \equiv \frac{v_x^2 + \rho^2\omega^2 + a^2\Omega^2}{c^2} \tag{5.49}$$

$$\chi^2 \equiv \frac{b^2\epsilon^2 sin^2(\epsilon t+\nu) + 2a\rho\Omega\omega cos((\Omega-\omega)t+\Theta)}{c^2} + \frac{2b\epsilon sin(\epsilon t+\nu)\left(a\Omega sin(\Omega t+\Theta) + \rho\omega sin(\omega t)\right)}{c^2} \tag{5.50}$$

The expansion for the function $\phi^2(|x\vec{(t)}|)$ around the position of the first beam splitter is done only to first order and is calculated by using the first order expansion for the spatial distance calculated from the world-line (5.47) [12]

$$|x\vec{(t)}| = r_L + acos(\Omega t+\Theta) + bcos(\epsilon t+\nu) + \rho cos(\omega t) + \mathcal{O}\left(\frac{v_x^2t^2 + (a+\rho+b)^2 - b^2}{r_L}\right) \tag{5.51}$$

With this $\phi^2(|x\vec{(t)}|)$ is given by

$$\phi^2(|x\vec{(t)}|) = 1 + 2\phi'(r_L)\left(acos(\Omega t+\Theta) + bcos(\epsilon t+\nu) + \rho cos(\omega t)\right) + \mathcal{O}\left(\frac{\phi'(r_L)(v_x^2t^2 + (a+b+\rho)^2 - b^2)}{r_L}\right) \tag{5.52}$$

The expansion for $\psi^2(|x\vec{(t)}|)$ has exactly the same form with $\phi'(r_L)$ replaced by $\psi'(r_L)$. We are now able to expand the integrand in equation (5.48). We assume in this expansion that

$$\frac{a\,\rho\,\Omega\,\omega}{c^2} \ll 1, \qquad \frac{a\,\Omega\,b\,\epsilon}{c^2} \ll 1, \qquad \frac{\rho\,\omega\,b\,\epsilon}{c^2} \ll 1 \qquad r_L \gg 1 \tag{5.53}$$

which leads us to the following term for the proper time

[12] The expansion is similar to the expansions of the previous sections and only valid if $v_x\,t \ll z_l, \rho \ll z_l, a \ll z_l, b \ll z_l$.

$$
\begin{aligned}
\tau =& \int_0^{t_f} \sqrt{\phi^2(|x(\vec{t})|) - \psi^2(|x(\vec{t})|)\,(\xi^2+\chi^2)}dt \\
=& \sqrt{1-\xi^2}t_f - \frac{\Omega\,\omega\,a\,\rho\,(sin((\Omega-\omega)t_f+\Theta) - sin(\Theta))}{c^2\sqrt{1-\xi^2}(\Omega-\omega)} \\
&+ \frac{(\phi'(r_L) - \xi^2\psi'(r_L))\,(\frac{a}{\Omega}\,(sin(\Omega t_f+\Theta) - sin(\Theta)) + \frac{\rho}{\omega}\,(sin(\omega t_f)))}{\sqrt{1-\xi^2}} \\
&+ \frac{(\phi'(r_L) - \xi^2\psi'(r_L))\frac{b}{\epsilon}\,(sin(\epsilon t_f+\nu) - sin(\nu))}{\sqrt{1-\xi^2}} + \frac{b^2\epsilon^2\,(sin(2(\epsilon\,t_f+\nu)) - 2\,\epsilon\,t_f - sin(2\nu))}{8c^2\sqrt{1-\xi^2}} \\
&- \frac{b\epsilon\rho\omega}{2c^2\sqrt{1-\xi^2}}\left(\frac{sin((\epsilon-\omega)t_f+\nu) - sin(\nu)}{\epsilon-\omega} - \frac{sin((\epsilon+\omega)t_f+\nu) - sin(\nu)}{\epsilon+\omega}\right) \\
&- \frac{b\epsilon a\Omega}{2c^2\sqrt{1-\xi^2}}\left(\frac{sin((\epsilon-\Omega)t_f+\nu-\Theta) - sin(\nu-\Theta)}{\epsilon-\Omega} - \frac{sin((\epsilon+\Omega)t_f+\nu+\Theta) - sin(\nu+\Theta)}{\epsilon+\Omega}\right) \\
&+ \mathcal{O}\left(\frac{\phi'(r_L)(v_x^2t_f^3 + (a+b+\rho)^2t_f - b^2t_f}{r_L\sqrt{1-\xi^2}}\right) + \mathcal{O}\left(\frac{\psi'(r_L)(v_x^2t_f^3 + (a+b+\rho)^2t_f - b^2t_f)}{r_L\sqrt{1-\xi^2}}\right) \\
&+ \mathcal{O}\left(\frac{a^2\rho^2\Omega^2\omega^2}{c^4(1-\xi^2)^{3/2}}\right) + \mathcal{O}\left(\frac{b^2\epsilon^2a^2\Omega^2}{c^4(1-\xi^2)^{3/2}}\right) + \mathcal{O}\left(\frac{b^2\epsilon^2\omega^2\rho^2}{c^4(1-\xi^2)^{3/2}}\right) \qquad (5.54)
\end{aligned}
$$

As can easily be seen, the first three terms in this rather long expression correspond to the case we had in section 5.2.1 as it must [13]. The additional degree of freedom of spool 2 added quite complicated expressions which affects the proper time difference between the two spools. Because for the trajectory of spool 1 nothing has changed, it is again described by a world-line as in the previous section. The trajectory of spool 2 however, now consists of an additional harmonic motion along the vertical axis. If the expansion $\xi^2 = \zeta^2 = \sqrt{1-\beta^2}\left(1 - \frac{a^2\Omega^2}{2c^2(1-\beta^2)} + \mathcal{O}\left(\frac{a^4\Omega^4}{c^4}\right)\right)$ is made for a better comparison of the two trajectories and $\frac{\Omega^2a^2\psi'(r_L)}{c^2} \ll \frac{\Omega^2a^2}{c^2} \ll 1$ is required, we get for the proper time difference between the two arms

[13] ξ^2 of this section and ζ^2 of section (5.2.1) are of course the same functions.

$$
\begin{aligned}
\Delta\tau = \tau_2 - \tau_1 \approx \\
&\frac{(\phi'(r_L) - \beta^2\psi'(r_L))\frac{a}{\Omega}\left(sin(\Omega\frac{l}{\beta c} + \Theta) - sin(\Theta)\right)}{\sqrt{1-\beta^2}} - \frac{\Omega^2 a^2}{2c^2\sqrt{1-\beta^2}}\frac{l}{\beta c} \\
&- \frac{\Omega\,\omega\,a\,\rho(sin((\Omega-\omega)\frac{l}{\beta c} + \Theta) - sin\Theta)}{c^2(\Omega-\omega)\sqrt{1-\beta^2}} - \frac{(\phi'(r_L) - \beta^2\psi'(r_L))\frac{b}{\epsilon}\left(sin(\epsilon\frac{l}{\beta c} + \nu) - sin(\nu)\right)}{\sqrt{1-\beta^2}} \\
&+ \frac{b\,\epsilon\,\rho\,\omega}{2c^2\sqrt{1-\beta^2}}\left(\frac{sin((\epsilon-\omega)\frac{l}{\beta c} + \nu) - sin(\nu)}{\epsilon-\omega} - \frac{sin((\epsilon+\omega)\frac{l}{\beta c} + \nu) - sin(\nu)}{\epsilon+\omega}\right) \\
&- \frac{b^2\epsilon^2(sin(2(\epsilon\frac{l}{\beta c} + \nu)) - 2\epsilon\frac{l}{\beta c} - sin(2\nu))}{8c^2\sqrt{1-\beta^2}} && (5.55) \\
&\equiv A + B + C + D + E + F && (5.56)
\end{aligned}
$$

where I suppressed the higher orders in this expression for simplicity. In the last line the terms in this formula was given a label, which makes it easier to refer to them in the next section where I want to give them an interpretation.

5.3.2 Analysis of the proper time difference

In analysing expression (5.55) we recognize, that the first three terms (A,B,C) are exactly of the same form as in the last section, where we have studied the behaviour without the additional harmonic motion of spool 2 in z-direction. We interpreted there, that A takes care of the relative height difference of the two spools inside the earth's gravitational field. B and C would be also present without any gravitational effect and correspond to the upcoming centripetal potential for spool 1 and the relative motion between the two occurring rotations of the trajectories respectively. But now we are faced with three additional terms, that may allow us to extract the gravitational information out of the signal at the detectors. In the limit where spool 2 is fixed, we should recover the equation for the proper time difference obtained in the last section, equation (5.33). So in what follows we will make for each term a short check if this is really the case.

The first additional term looks pretty much like A, which suggests that this term corrects for the gravitational height difference that occur between the two spools due to the harmonic motion of spool 2. Indeed in the limit of no motion, $\epsilon \to 0$, we get

$$D_{static} = -\frac{\phi'(r_L)\,(1+\beta^2)\,b\,l}{\beta\sqrt{1-\beta^2}\,c} cos(\nu) \tag{5.57}$$

which goes to zero for $\nu = \frac{(2n+1)\pi}{2}$ and is the wanted result because we required ν to be $\frac{\pi}{2}$ at the position of the first beam-splitter ($z_L = r_L$). To find the extrema of this function, we first observe that D is linearly related to the amplitude b, meaning that we want to make b as large as possible. We are only restricted by technical limitations and because we have chosen $a = 1m$ for the distance off-axis, we set arbitrarily $b = 0.6m$ to be confined inside the circle defined by spool 1. So for a given fiber spool we are left with

$$D(\epsilon,\nu) = \kappa\,\frac{b(sin(\frac{\epsilon\,l}{\beta\,c}+\nu) - sin(\nu))}{\epsilon} \tag{5.58}$$

with $\kappa \equiv -\frac{\phi'(r_L)\,(1+\beta^2)}{\sqrt{1-\beta^2}}$. Because of the same argument as for A, this term is, within a small range, almost independent of the frequency of the motion, so for simplicity we ignore the tiny ϵ dependence of this term and differentiate with respect to ν to get the extremal points. This results in the condition for the extremal points

$$\nu_{min} = -\frac{\epsilon\,l}{2\,\beta\,c} + 2\pi n \qquad \nu_{max} = -\frac{\epsilon\,l}{2\,\beta\,c} + (2n+1)\pi \qquad n \in \mathbb{N} \tag{5.59}$$

with the maxima and minima for the proper time contribution of D as given by

$$D(\epsilon,\nu)_{min} = \frac{2\,\kappa\,b}{\epsilon} sin(\frac{\epsilon\,l}{2\,\beta\,c} + 2\pi n) \tag{5.60}$$

$$D(\epsilon,\nu)_{max} = \frac{2\,\kappa\,b}{\epsilon} sin(\frac{\epsilon\,l}{2\,\beta\,c} + (2n+1)\pi) \tag{5.61}$$

$$\tag{5.62}$$

To get an idea about the quantitative effect of C, we put in the same values as in section

5.2.2. To choose our angular frequency, we have to keep in mind what is technically possible. The difficulty of high ϵ lies in the fact that it is technically hard to connect two spools that are in relative harmonic motion to each other when one of them additionally rotates around an axis. As mentioned before, $\mathsf{D}(\epsilon,\nu)$ is almost independent of ϵ within a small range and therefore we can freely choose it out of a small interval. But for the next terms, as we will see, this is not the case and in order to make comparisons we have to make a convenient choice. With $\epsilon = \frac{2\pi}{s}$ we get for the minima and maxima

$$\begin{aligned} \nu_{min} &\approx -\frac{\pi}{2000} rad + 2\pi n & D_{min} &\approx -6.35 \cdot 10^{-20} s \\ \nu_{max} &\approx \pi(1 - \frac{1}{2000}) rad + 2\pi n & D_{max} &\approx 6.35 \cdot 10^{-20} s \end{aligned} \tag{5.63}$$

The next term, $E = \frac{b\,\epsilon\,\rho\,\omega}{2c^2\sqrt{1-\beta^2}}\left(\frac{sin((\epsilon-\omega)\frac{l}{\beta c}+\nu)-sin(\nu)}{\epsilon-\omega} - \frac{sin((\epsilon+\omega)\frac{l}{\beta c}+\nu)-sin(\nu)}{\epsilon+\omega}\right)$, is again a function of the angular frequency ϵ and the phase-angle ν for a given fiber spool. The amplitude is again fixed to a value $b = 0.6m$. This term can be interpreted to describe proper time differences between the motion around the fiber spools in the two arms and the harmonic up- and down-motion of spool 2. Lets see what we get from this. First we can observe that this function depends almost linear on ϵ due to the additional factor in the nominator. This means that we clearly have the biggest contributions to the proper time difference when ϵ has the largest possible value. So for a given fiber spool, E is only a function of ν and we can calculate the extremal points by taking the first derivative with respect to ν which gives

$$\nu_{min} = arctan\left(-\frac{\epsilon sin(\frac{\epsilon\, l}{\beta\, c})sin(\frac{\omega\, l}{\beta\, c}) + \omega(cos(\frac{\epsilon\, l}{\beta\, c})cos(\frac{\omega\, l}{\beta\, c}) - 1)}{\epsilon cos(\frac{\epsilon\, l}{\beta\, c})sin(\frac{\omega\, l}{\beta\, c}) - \omega sin(\frac{\epsilon\, l}{\beta\, c})cos(\frac{\omega\, l}{\beta\, c})}\right) + 2\pi n \qquad n \in \mathbb{N} \tag{5.64}$$

$$\nu_{max} = arctan\left(-\frac{\epsilon sin(\frac{\epsilon\, l}{\beta\, c})sin(\frac{\omega\, l}{\beta\, c}) + \omega(cos(\frac{\epsilon\, l}{\beta\, c})cos(\frac{\omega\, l}{\beta\, c}) - 1)}{\epsilon cos(\frac{\epsilon\, l}{\beta\, c})sin(\frac{\omega\, l}{\beta\, c}) - \omega sin(\frac{\epsilon\, l}{\beta\, c})cos(\frac{\omega\, l}{\beta\, c})}\right) + (2n+1)\pi \qquad n \in \mathbb{N} \tag{5.65}$$

To get a feeling how this quantity may affect the experiment, we put in the values that we have already used throughout this chapter and additionally choose with $\epsilon = \frac{2\pi}{s}$ a reasonable value for the angular frequency. With this, we get for the critical points and the corresponding proper time differences

$$\begin{aligned} \nu_{min} &\approx 4.76rad + 2\pi n \qquad E_{max} \approx 3.56 \cdot 10^{-19}s \\ \nu_{max} &\approx 1.62rad + 2\pi n \qquad E_{min} \approx -3.56 \cdot 10^{-19}s \end{aligned} \tag{5.66}$$

The last additional term, $F = -\frac{b^2\epsilon^2(sin(2(\epsilon\frac{l}{\beta c}+\nu))-2\epsilon\frac{l}{\beta c}-sin(2\nu))}{8c^2\sqrt{1-\beta^2}}$, for given spools and fixed amplitude b is only a function of the angular frequency ϵ and the phase angle ν. Similar to the case of a rotating spool, where the photon is subject to a centripetal potential, this term describes how the test particle gets affected by a harmonic motion which includes a constantly changing acceleration. After making the first derivative with respect to ν we can write as a condition for the extremal points

$$\nu_{min} = -\frac{\epsilon\, l}{\beta\, c} + n\pi \qquad \nu_{max} = -\frac{\epsilon\, l}{\beta\, c} + \frac{(2n+1)\pi}{2} \qquad n \in \mathbb{N} \tag{5.67}$$

Because term $F(\epsilon, \nu)$ is a monotonic increasing function of ϵ we want to make it as large as possible to maximize the proper time difference this term contributes to the total one. To get a feeling for the orders of magnitude, we choose as before $\epsilon = \frac{2\pi}{s}$ and take the same values for the spools and the amplitude b. We evaluate F at the extremal points which gives

$$F_{max} = 3,33 \cdot 10^{-19}s \qquad F_{min} = 2,73 \cdot 10^{-25}s \tag{5.68}$$

5.3.3 Possible experimental realizations

With equation (5.55) for the proper time difference we have everything we need to calculate the detection probabilities at the two detectors. But still, we have a great amount of possibilities in realizing an experiment with the degrees of freedom that were introduced. So in order to find the best experimental realization, we see what the additional harmonic motion is giving us in different situations.

Option 1: harmonic motion with one spool fixed

We now deal with the situation, where spool 1 is fixed at one position on a ring that does not rotate at all. The inner spool moves in harmonic motion along the z-axis with frequency ϵ. For this situation only three of the terms of equation (5.55) remains

$$\begin{aligned}
\Delta\tau \approx\ & \frac{(\phi'(r_L) - \beta^2\psi'(r_L))\, l}{\sqrt{1-\beta^2}\beta\, c}\,(a\, cos(\Theta) - b\, cos(\nu)) \\
& + \frac{b\,\epsilon\,\rho\,\omega}{2c^2\sqrt{1-\beta^2}}\left(\frac{sin((\epsilon-\omega)\frac{l}{\beta c}+\nu) - sin(\nu)}{\epsilon-\omega} - \frac{sin((\epsilon+\omega)\frac{l}{\beta c}+\nu) - sin(\nu)}{\epsilon+\omega}\right) \\
& - \frac{b^2\epsilon^2(sin(2(\epsilon\frac{l}{\beta c}+\nu)) - 2\epsilon\frac{l}{\beta c} - sin(2\nu))}{8c^2\sqrt{1-\beta^2}} \qquad (5.69) \\
& \equiv A' + B' + C' \qquad (5.70)
\end{aligned}$$

where the first term, A', is a result of terms A and B in the limit $\Omega \to 0$ and for very small ϵ. Again I want to emphasize what is meant by the phase angles Θ and ν. Looking back to the world-line that was defined at the beginning of this chapter, we see that Θ is the angle that spool 1 (because $a = 0$ for spool 2) makes with the positive z-axis at $t = 0$. This means that this angle describes the position of the spool at the time the photon enters the fiber spool and is therefore the out-of-phase angle between the two rotations. Similarly, ν describes the position of spool 2 at time $t = 0$, which means the moment before the photon enters spool 2. For both angles the short fiber segments before and after the spool were neglected. We have also argued, that this world-line is only valid for a single photon, and within its motion through the fiber the frequency ϵ is constant for that photon.

Now we can distinct two different cases, depending on what we aim for. We can go for the mass-energy equivalence principle that stems from both, inertial and gravitational mass, or we can really try to look for gravity only. We know from the last subsection, where the terms was analysed in great detail, that only term A' bears information about gravity. The other terms account only for the acceleration and deceleration of spool 2 and the relative motion between this movement and the rotation inside the fiber spool. Because we want to fix spool 1 for now, we have to choose a Θ that makes the proper time difference as large as possible for a good resolution of the gravitational effect at the detectors. This corresponds to the case where $\Theta = n\pi$, because there A' has its largest value. Furthermore, if $n \in \mathbb{N}$ is an even number, we have a positive sign meaning that, with the values for a and b as given before, spool 1 is above spool 2 and lies on the z-axis, whereas if n is odd spool 1 lies on the negative z-axis and is below spool 2.

By fixing spool 1 at $\Theta = \pi$, the lowest possible position on the ring, we have to ensure for the resolution of gravity that ϵ is small because the other non-gravitational terms are linear and even quadratic in ϵ. We don't even need to vary ϵ in time because we already have a modulation due to the harmonic up and down motion, so for what follows we may fix $\epsilon = 0.1[\frac{1}{s}]$ arbitrarily. With this, terms B' and C' are negligible for given spools and an amplitude $b = 0,6m$ because inserting that values at the extremal positions given by equations (5.67), (5.64) and (5.65) results in orders of magnitude of about 10^{-21} and 10^{-24} respectively. Lets say we start at a position, where $\nu = 0$ corresponding to the largest vertical displacement of the spools. The corresponding proper time difference at this position, neglecting B' and C', is $\Delta\tau \approx -1,7 \cdot 10^{-19}$. Now spool 2 is slowly moving down, resulting in a constant change of ν which means a constantly changing proper time difference. At the lowest position along the z-axis, the other extremal point, we get $\Delta\tau \approx -4,24 \cdot 10^{-20}$. The reason why this function is not symmetric lies in the fact that we have chosen $a = 1m$ and $b = 0.6m$, and therefore we have always a negative sign at the extremal points with that particular value for Θ. This change in $\Delta\tau$ for a full motion of spool 2, back and forth between its extremal points, results in a change of the phase shift at the detectors. Due to the linear relationship between these two quantities, a change of one order of magnitude in the proper time results in a one order of magnitude change in the phase shift. Quantitatively this results, by using $\Delta\phi = \nu_0 \Delta\tau$ with $\nu_0 \approx 1,22 * 10^{15} \frac{rad}{s}$ as central angular frequency of the wave packet, in a change of the phase-shift from $\Delta\phi \approx 2,1 \cdot 10^{-4} rad$ to $\Delta\phi \approx 5,2 \cdot 10^{-5} rad$. This difference should, in principle, be experimentally resolvable and due to the modulation we get a kind of AC-signal at the output that may or may not be bigger than the noise introduced by temperature, vibrations and other sources. For a given radius a of the outer ring one can also try to increase the amplitude b of the harmonic motion and may even go out of the ring for this purpose resulting in a larger proper time difference and a corresponding better signal at the two detectors. Different situations for identical fiber spools and fixed a with neglected contributions from B' and C' are depicted in Figure (5.7). This particular experimental situation is similar to the an experiment performed with one of the spools fixed inside an elevator. We have fixed spool 1 on a floor ($\Theta = \pi$) and let the other spool move in a harmonic way along the z-axis like an elevator moves up and down along different floors of large a building. The bigger the amplitude b the bigger is the experienced time dilation and therefore the linear related relative phase shift between the two trajectories. Through the harmonic motion it is also possible to create a kind of AC-signal at the detectors, which can be used to reduce the noise in the detection process.

The second kind of experiment, with spool 1 fixed at a defined position, aims to show the mass-energy equivalence that stems from both, inertial and gravitational mass. The advantage of this type of experiment lies in the fact that the resolvable phase shift is orders of magnitude larger than in the situation where spool 2 is slowly moving up and down. I want to give a short insight in this type of experiment in what follows.

We now want to increase the speed of motion of spool 2, while keeping spool 1 again fixed at $\Theta = \pi$ to get the biggest contribution from gravity. Again we don't want to change ϵ in time, because we already have a modulation due to the harmonic motion.

A reasonable value for the angular frequency that seems to be technically possible is $\epsilon = \frac{2\pi}{s}$. By taking this value and keeping the other values in equation (5.55) as they where before, we get for the different terms a proper time difference at the extremal

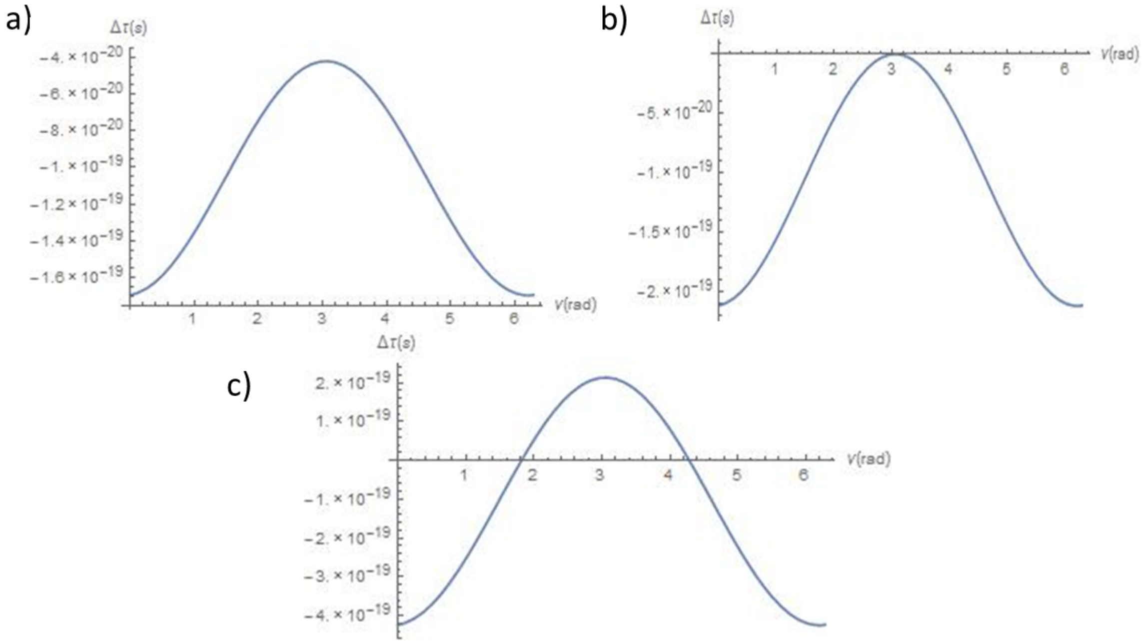

Figure 5.7: The proper time difference of two fiber spools, 1 and 2, where spool 1 is fixed at $\Theta = \pi$ and spool 2 does a very slow ($\epsilon < \frac{1}{s}$) harmonic motion along the z-axis starting at the highest possible position inside earth's gravitational field with $\nu = 0$. The amplitudes b are chosen to be $0.6m, 1m, 3m$ for pictures a),b) and c) respectively. In a) the proper time can't be zero because spool 2 and spool 1 can never be at the same height. Picture b) shows the case where the proper time difference between the two paths is zero at $\nu = \pi$, where the spools are next to each other. In c) spool 2 is slowly moving down until it is at the same height, but moving onwards due the the larger amplitude. After reaching the lowest point the spool moves up, reaching spool 1 where the proper time difference is again zero, and continues its motion until it reaches the highest possible point again. It can be seen, that we can increase the proper time difference and the linear related relative phase difference between the two paths by increasing the amplitude b.

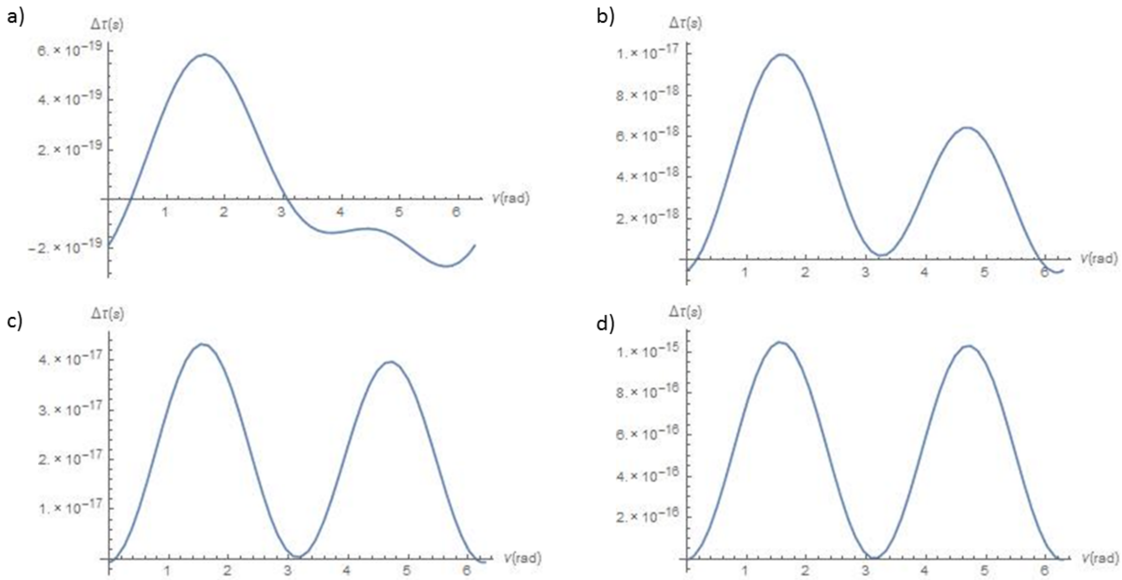

Figure 5.8: Proper time difference between two paths that are realized by a fixed spool at $\Theta = \pi$ and a spool oscillating with frequency ϵ along the z-axis. a): This plot corresponds to $b = 0.6m$ and $\epsilon = \frac{2\pi}{sec}$. As can be seen, the proper time difference varies within order 10^{-19}, which does not make an improvement to the slowly oscillating spool. b): ϵ is the same as in a), but $b = 3$ resulting in a gain for the phase-shift of two orders of magnitude. c): the amplitude is the same as in a), but the frequency of the harmonic motion is $\frac{10\pi}{sec}$. The effects are almost the same as those for case b). d): The values for $\epsilon = \frac{10\pi}{sec}$ and $b = 3m$ result in a huge amplification of the observable phase-shift and sinusoidal modulation of the signal that covers three orders of magnitude.

points [14] all of order 10^{-19}, which is not an improvement to the situation of slow ϵ. But as is shown in Figure (5.8), we can increase the effect by either increasing the amplitude b or increasing the angular frequency ϵ or doing both.

For example the proper time difference for $b = 3m$ and $\epsilon = \frac{10\pi}{sec}$ varies between 10^{-15} at the maximum and 10^{-18} at the minimum. The corresponding phase shift therefore lies between 10^{0} and 10^{-3}, which not only increases the phase shift and therefore the resolution but also gives a very large sinusoidal variation of the signal, which could be

[14] given by equations (5.59),(5.65) and (5.67)

used to protect against noise.

Option 2: harmonic motion and additional rotation

Now we want to take additionally a rotation of spool 1 into consideration and see if this is beneficial for our purposes. Again the situation is analysed for two different cases: The first case deals with the question if we can set the specifications of our introduced device to extract out only the gravitational effect on the wave packets, whereas in the second case we look for a combined effect of gravitational and inertial mass like in section 5.3.3. The proper time difference in this case is the full proper time difference as in equation (5.55) and reads

$$
\begin{aligned}
\Delta\tau \approx\ & \frac{(\phi'(r_L) - \beta^2\psi'(r_L))}{\sqrt{1-\beta^2}} \left(\frac{a}{\Omega} \left(sin(\Omega \frac{l}{\beta c} + \Theta) - sin(\Theta) \right) - \frac{b}{\epsilon} \left(sin(\epsilon \frac{l}{\beta c} + \nu) - sin(\nu) \right) \right) \\
& - \frac{\Omega^2 a^2}{2c^2\sqrt{1-\beta^2}} \frac{l}{\beta c} - \frac{\Omega\, \omega\, a\, \rho(sin((\Omega-\omega)\frac{l}{\beta c} + \Theta) - sin\Theta)}{c^2(\Omega-\omega)\sqrt{1-\beta^2}} \\
& + \frac{b\, \epsilon\, \rho\, \omega}{2c^2\sqrt{1-\beta^2}} \left(\frac{sin((\epsilon-\omega)\frac{l}{\beta c} + \nu) - sin(\nu)}{\epsilon-\omega} - \frac{sin((\epsilon+\omega)\frac{l}{\beta c} + \nu) - sin(\nu)}{\epsilon+\omega} \right) \\
& - \frac{b^2\epsilon^2(sin(2(\epsilon\frac{l}{\beta c} + \nu)) - 2\epsilon\frac{l}{\beta c} - sin(2\nu))}{8c^2\sqrt{1-\beta^2}} && (5.71) \\
\equiv\ & A'' + B'' + C'' + D'' && (5.72)
\end{aligned}
$$

Test for the gravitational mass-energy equivalence principle

We have seen in section (5.3.3), that extracting gravitational effects out of the signals at the detectors requires a low angular frequency of spool 2. Here we are dealing additionally with a spool attached to a ring which rotates with angular velocity Ω around the central position of spool 2 ($\nu = \frac{\pi}{2}$). Because the maxima and minima of the proper time difference of term A" are of order 10^{-19} we can put in values for ϵ in terms $B'' = -\frac{\Omega^2 a^2}{2c^2\sqrt{1-\beta^2}} \frac{l}{\beta c}$ and $C'' = \frac{\Omega\, \omega\, a\, \rho(sin((\Omega-\omega)\frac{l}{\beta c}+\Theta)-sin\Theta)}{c^2(\Omega-\omega)\sqrt{1-\beta^2}}$ and search for an angular velocity that gives contributions to the total proper time difference that are at least one order of magnitude smaller than that of term A". By doing so we can find that C" requires

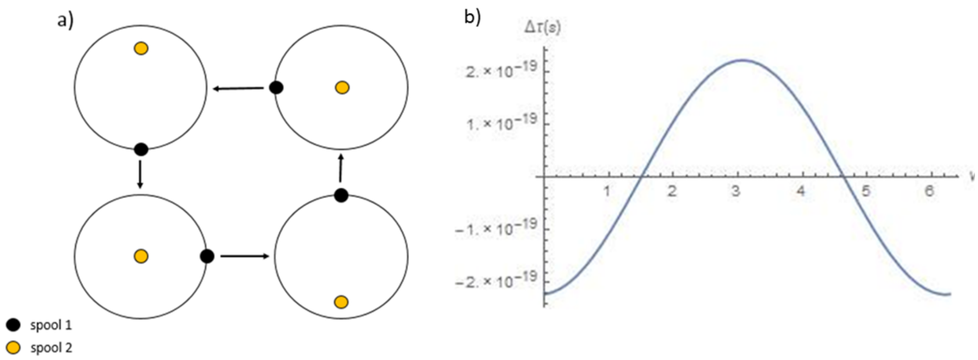

Figure 5.9: Possible positions of the two fiber spools to test gravitational effects on single photons are shown in a), where the spools are moving with the same value for their angular velocities/frequencies. In b) the proper time difference resulting from the motion described in a) is shown. The phase-angle ν for harmonic motion is shown on the horizontal axis. The phase-angle Θ is included because for this special motion it is always $\nu + \pi$.

an Ω of order 10^{-1}, which corresponds to a very slow rotation of spool 1. We can set arbitrarily $\Omega = \frac{0.1rad}{sec}$ and take the same numerical value for ϵ, which makes it easier to analyse the occurring effects. To make the gravitational proper time difference as large as possible, the experiment should start for example at $\nu = 0$ and $\Theta = \pi$, which corresponds to the highest possible position of spool 2 and the lowest of spool 1 with respect to the positive z-axis. We start with an amplitude for spool 2 of about $b = 0.6m$ and will compare this to the case of a fixed spool 1.

Figure (5.9) shows some of the possible positions of the spools and the proper time difference that occurs due to the rotation of spool 1. Part b) of the figure shows, that the proper time difference due to the relative motion of both spools is still of order of $10^{-19}s$. Inserting the values corresponding to the optical fibers and the fiber spools in equation (5.71) gives for the periodic maxima and minima of this function and the corresponding phase-shift

$$\Delta\tau_{max} \approx \pm 2,2 \cdot 10^{-19} s \qquad \Delta\phi = 2.7 \cdot 10^{-4} rad \tag{5.73}$$

This shows, that an additional rotation of spool 1 does not increase the effect that occurs due to gravity by a remarkable amount. Because of the slow motions of both spools, and the fact that a photon roughly needs $5 \cdot 10^{-4} s$ to pass through one of the spools, it is not necessary to block some of them to receive the curves shown in Fig. (5.9). By playing around with equation (5.71) one can find, that in order to increase the phase shift by one order of magnitude, the radius a of rotation as well as the amplitude b of the harmonic motion have to be increased to approximately $4m$. This results are also intuitively very pleasing because in both cases (static and a rotating spool 1) the proper time difference should only depend on the height difference inside the gravitational potential provided by the earth, which cannot be dramatically different for the two cases. The only reason why the proper time differences at the extremal point, where the distance between both spools is maximal, is not exactly the same is due to the small contribution that results from the rotation. But compared to the static spool we now deal with a periodic sinusoidal function, that is symmetric around zero proper time difference, whereas in the case of a static spool the function was not symmetric and was oscillating between 10^{-19} and 10^{-20}.

Test for gravitational and inertial mass-energy equivalence

Now we want to see if this type of arrangement for the fiber spools can increase the phase shift that stem from inertial and gravitational mass and therefore test the mass-energy equivalence principle for both type of masses. We want to analyse the proper time difference between the two possible trajectories which can be calculated with help of equation (5.71). Similar to the last section we start the experiment at a position where the distance between the spools is maximal, e.g. $\nu = 0$ and $\Theta = \pi$. Because we have seen in section 5.3.2 that in order to increase the gravitational effect we have to go to as high as possible angular frequencies and angular velocities, we may choose again $\epsilon = \frac{2\pi}{s}$ as a realistic value. Because a modulation of this frequency would not enhance the effect, we keep this value fixed during the whole experiment. But what we can vary in time with a noticeable effect is the angular velocity Ω, that was chosen due to the rotary joints not to be higher than $\frac{200rad}{s}$. Lets first investigate the resulting proper time difference for fixed radius a and amplitude b but varying Ω starting from a realistic maximal value of $\frac{30rad}{s}$. Because the leading term including Ω is C" [15], we estimate the extremal values of this function to be very close to the values provided by equation (5.44). Due to the small value of ϵ and the small amplitude of b, the proper time difference is almost independent of the position of spool 2 before a photon enters the interferometer as can be seen by inserting the values for the spool and the above values for ϵ and Ω. Because we want some kind of AC-signal at the detectors and spool 1 rotates pretty fast additionally to our demand for constant Ω, we can also fix ν for a defined time window by using the same technique as in the last section. So we may start with $\nu = 0$, measure for a certain amount of time, and change the shutter for a next definite ν and proceed. A graphical visualization for different values of Ω can be found in Fig. (5.10), where Ω was chosen to be time independent and ν was chosen to be equal to π.

As can bee calculated by using equation (5.71), the values for the proper time difference at the extremal points for $\Omega = \frac{30rad}{s}$, $a = 1m$ and $b = 0.6m$ are approximately

$$\Delta\tau_{min} \approx -2 \cdot 10^{-17} \qquad and \qquad \Delta\tau_{max} \approx 1,3 \cdot 10^{-17} \tag{5.74}$$

which is not an obvious improvement to the case where one of the spools was fixed at $\Theta = \pi$ (Fig. (5.7) a)). However if we choose higher frequencies of rotation for spool 2, we can improve the effect that now stems mostly from the rotation and therefore from the difference in centripetal potential. If we compare these results with section 5.3.3 where the second spool was fixed, we see that we reach almost the same orders of magnitude although with different realizations and physical effects. In section 5.3.3 we was considering different amplitudes b, resulting mostly in a gravitational contribution to the acquired relative phase, and different frequencies ϵ for the harmonic rotation of

[15]The contribution of this term is two orders of magnitude higher than that from A".

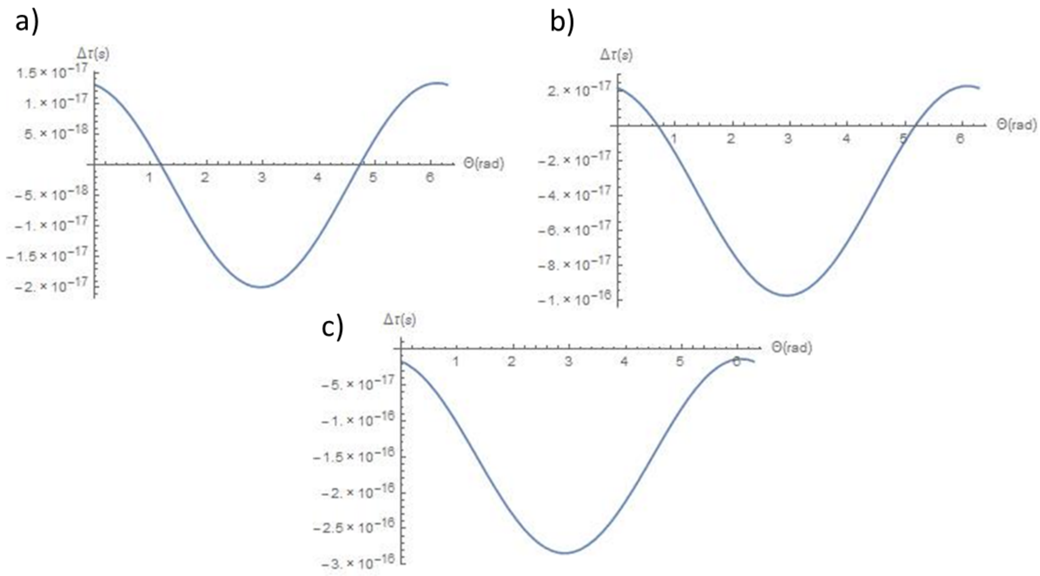

Figure 5.10: Proper time difference depending on the out-of-phase angle Θ with $\epsilon = \frac{2\pi}{s}$ and $b = 0.6m$ where the angular velocities are chosen to be $\frac{30rad}{s}$, $\frac{100rad}{s}$ and $\frac{200rad}{s}$ for graphs a),b) and c) respectively.

the inner spool which contributes to the phase due to inertial effects. The benefit of this method lies in the fact that it is easier to confine a rotating ring with varying frequency of rotation and fixed radius in a laboratory, than a set-up with a fast moving fiber spool with huge radius.

6 Conclusion and outlook

We have seen in chapter 1.1, that in order to test for gravitationally induced relative phases for single-particle wave functions interferometers with big areas are needed. Optical fibers operating at a wavelength of $1550nm$ were introduced (section 3) as ideally suited system to implement the arms of the interferometers. But several external effects like temperature or pressure can limit the performance of the fibers and therefore introduces unwanted noise that can suppress the effects introduced by gravity or non-inertial motion. This effects can be a major hindrance to the experiment and has to be minimized by use of a combination of clever detection schemes (not presented in this thesis) and by enhancing the effect with help of increasing the measurable phase shifts. Michelson interferometers (section 4) can provide feasible playgrounds for testing inertial mass-energy equivalence but are not beneficial for measurements of gravitational induced phases due to the smaller proper time difference. The use of rotating Mach-Zehnder interferometers can increase inertial effects on the wave function and, by increasing the vertical distance between the two arms, also the proper time difference due to gravity as shown in section5.2. Additional degrees of freedom (section 5.3) allows to test more accurately the effect of gravity alone as well as the combined effects of gravity and inertia by modulating the proper time difference with help of a linear oscillating inner spool that provides sinusoidal counting statistics after measurement. Thus this schemes makes it possible to test inertial mass-energy equivalence through a Michelson interferometer, gravitational mass-energy equivalence by use of a static MZI with big separation of the arms or additional vertical degree of freedom of one of the spools, or testing a combination of both with the help of rotating Mach-Zehnder interferometers with or without additional harmonic motion of one of the spools.

In order to improve the test for gravitational effects alone one can either increase the gravitational potential difference by bigger vertical separation of the spools and/or use additionally different detection schemes. One very promising method is the use of weak measurements with post-selection instead of strong (projective) measurements as presented for example in [23]. There the birefringent element takes the role of gravity. This type of measurement can be beneficial if one can control the birefringence in optical fibers and stabilize the experiment for long times because by using weak measurement one has to pay the price of low photon count rates as compared to projective measurements [24].

7 Appendix

7.1 Derivation of the Schwarzschild line-element

To make it simpler, we switch from a cartesian coordinate system to a spherical one, and from the requirement for spherical symmetry we can conclude that non of the angles θ and ϕ is special. This implies, that we can replace in our metric $d\theta \to -d\theta$ (and likewise for ϕ) without changing the invariant proper time $d\tau^2$. This means that no mixed terms like $dtd\theta$ or $drd\phi$ etc. should appear. Another point that has to be taken into account is, that if t and r are both constant, the inner geometry of the surface of the sphere should not be different from that of a two-sphere, $d\tau^2 = r^2(d\theta^2 + sin^2\theta d^2\phi)$[1]. So the most general metric for spherical symmetry we can write down is given by

$$d\tau^2 = A(r,t)dt^2 - B(r,t)dtdr - C(r,t)dr^2 - r^2(d\theta^2 + sin^2\theta d\phi^2) \tag{7.1}$$

The constants A,B and C should only depend on r and t, otherwise the proper time would also depend on the angles even if $d\theta$ and $d\phi$ are zero. If we only consider static fields, the time dependence is not present any more and the invariant proper time is only a function of distance. Equation (7.1) includes an off diagonal metric term. To get rid of it, we redefine our time scaling by

$$t' = t + \lambda(r) \tag{7.2}$$

where λ is an arbitrary function of r. To get rid of g_{tr}, we set a condition on λ

[1]Because if $r = const$, $t = const \to dr = dt = 0$)

$$\frac{d\lambda}{dr} = -\frac{B(r)}{2A(r)} \tag{7.3}$$

therefore we get

$$dt = dt' + \frac{B(r)}{2A(r)}dr \tag{7.4}$$

inserting this in (7.1) gives

$$\begin{aligned} d\tau^2 &= A(r)dt'^2 + \frac{B(r)^2}{4A(r)}dr^2 + B(r)drdt' - B(r)drdt' \\ &\quad - \frac{B(r)^2}{2A(r)}dr^2 - r^2(d\theta^2 + sin^2\theta d\phi^2) \\ &= A(r)dt'^2 - D(r)dr^2 - r^2(d\theta^2 + sin^2\theta d\phi^2) \end{aligned} \tag{7.5}$$

where

$$D(r) = C(r) + \frac{B(r)^2}{2A(r)} \tag{7.6}$$

equation (7.5) is called the 'standard' form of the metric, and I surpress the prime on t' from now on. Our metric tensor (recall: $d\tau^2 \equiv -g_{\mu\nu}dx^\mu dx^\nu$) contains now only the diagonal terms

$$g_{tt} = -A(r) \quad grr = D(r) \quad g_{\theta\theta} = r^2 \quad g_{\phi\phi} = r^2 sin^2\theta \tag{7.7}$$

Looking at Einstein's field equation, (2.23), we see that it contains on the left side only terms containing the metric tensor, so we are almost there. To calculate the Ricci tensor, we need to know the affine connections out of equation (2.10) ($\Gamma^\sigma_{\lambda\mu} = \frac{1}{2}g^{\nu\sigma}(\partial_\lambda g_{\mu\nu} + \partial_\mu g_{\nu\lambda} - \partial_\nu g_{\lambda\mu}$), where only terms containing two identical indices survive[2]

[2]Because the affine connection is symmetric in the two lower indices, some of them are not written explicitely

$$
\begin{aligned}
\Gamma^r_{rr} &= \frac{1}{2D(r)}\frac{D(r)}{dr} & \Gamma^r_{\phi\phi} &= -\frac{r sin^2\theta}{D(r)} & \Gamma^r_{tt} &= \frac{1}{2D(r)}\frac{dA(r)}{dr} \\
\Gamma^r_{\theta\theta} &= -\frac{r}{D(r)} & \Gamma^\theta_{\theta r} &= \frac{1}{r} & \Gamma^\theta_{\phi\phi} &= -sin\theta cos\theta \\
\Gamma^t_{tr} &= \frac{1}{2A(r)}\frac{dA(r)}{dr} & \Gamma^\phi_{\phi r} &= \frac{1}{r} & \Gamma^\phi_{\phi\theta} &= \frac{cos\theta}{sin\theta}
\end{aligned}
$$

From that we simply get the symmetric Ricci tensor by contracting κ and λ

$$
R_{\mu\nu} = R^\lambda_{\mu\lambda\nu} = \partial_\nu \Gamma^\lambda_{\mu\lambda} - \partial_\lambda \Gamma^\lambda_{\mu\nu} + \Gamma^\rho_{\mu\lambda}\Gamma^\lambda_{\rho\nu} - \Gamma^\rho_{\mu\nu}\Gamma^\lambda_{\rho\lambda} \tag{7.8}
$$

If one calculates these quantities, the only remaining ones are those with equal indices ($\mu = \nu$) and read

$$
\begin{aligned}
R_{tt} &= -\frac{1}{2D(r)}\frac{d^2A(r)}{dr^2} - \frac{1}{rD(r)}\frac{dA(r)}{dr} \\
&\quad + \left(\frac{1}{4D(r)}\frac{dA(r)}{dr}\right)\left(\frac{1}{D(r)}\frac{dD(r)}{dr} + \frac{1}{A(r)}\frac{dA(r)}{dr}\right) \\
R_{rr} &= \frac{1}{2A(r)}\frac{d^2A(r)}{dr^2} - \frac{1}{rD(r)}\frac{dD(r)}{dr} \\
&\quad - \left(\frac{1}{4A(r)}\frac{dA(r)}{dr}\right)\left(\frac{1}{D(r)}\frac{dD(r)}{dr} + \frac{1}{A(r)}\frac{dA(r)}{dr}\right) \\
R_{\theta\theta} &= -1 + \frac{1}{D(r)} + \frac{r}{2D(r)}\left(-\frac{1}{D(r)}\frac{dD(r)}{dr} + \frac{1}{A(r)}\frac{dA(r)}{dr}\right) \\
R_{\phi\phi} &= sin^2\theta R_{\theta\theta}
\end{aligned} \tag{7.9}
$$

Now we have all the ingredients required for calculating a solution to the field equation. We are now interested in solutions in empty space, so we require $R_{\mu\nu} = 0$. Remember that we work with metric tensor in standard form given by equation (7.5), and the components of the Ricci tensor we calculated before should now set to be zero. Because $R_{\theta\theta}$ and $R_{\phi\phi}$ differ only by a multiplicative factor, it is sufficient to set one of them equal to zero.

Because the R_{rr} and R_{tt} components of the Ricci tensor look very similar, we can devide R_{rr} by D(r) and R_{tt} by A(r) and get a relation that will help to determine the coefficients A(r) and D(r)

$$\frac{R_{rr}}{D(r)} + \frac{R_{tt}}{A(r)} = -\frac{1}{rD(r)}\left(\frac{1}{A(r)}\frac{dA(r)}{dr} + \frac{1}{D(r)}\frac{dD(r)}{dr}\right) \tag{7.10}$$

Because R_{rr} and R_{tt} vanish independly, we can set the above sum equal to zero. From this we conclude, that the coefficients must satisfy

$$\frac{1}{A(r)}\frac{dA(r)}{dr} = \frac{1}{D(r)}\frac{dD(r)}{dr} \tag{7.11}$$

this statement can be rewritten, by recognizing that $\frac{d}{dr}\left(A(r)D(r)\right) = \frac{dA(r)}{dr}D(r) + \frac{dD(r)}{dr}A(r)$, so it follows

$$\frac{d}{dr}\left(A(r)D(r)\right) = 0 \rightarrow A(r)D(r) = constant \tag{7.12}$$

We can also impose boundary conditions, by demanding that the metric coefficient reduce to that of the Minkowsian one if we are very far away ($r \rightarrow \infty$) so

$$A(r)D(r) = 1 \tag{7.13}$$

we can use this to simplify the expression for $R_{\theta\theta}$ in equation (7.9) to get the relation

$$R_{\theta\theta} = 0 = -1 + A(r) + r\frac{dA(r)}{dr} = \frac{d}{dr}\left(rA(r)\right) - 1 \tag{7.14}$$

The solution of this differential equation is

$$A(r) = 1 + \frac{\kappa}{r} \tag{7.15}$$

To get the constant of integration κ, we recall that $g_{tt} = -A(r)$. This must reduce to the Newtonian case, $g_{tt} = -(1 + 2\phi)$, in the weak field limit where ϕ denotes the gravitational potential. Therefore $\kappa = -2GM$ and

$$A(r) = \left(1 - \frac{2GM}{r}\right) D(r) \qquad = \frac{1}{A(r)} = \left(1 - \frac{2GM}{r}\right)^{-1} \tag{7.16}$$

We now can insert this in equation (7.5) and have thus found the solution Karl Schwarzschild derived almost hundred years ago and was named after him as Schwarzschild-metric. With this the proper time reads

$$d\tau^2 = \left(1 - \frac{2GM}{r}\right) dt^2 - \left(1 - \frac{2GM}{r}\right)^{-1} dr^2 - r^2(d\theta^2 + sin^2\theta d\phi^2) \tag{7.17}$$

7.2 Derivation of the group velocity

We can represent a plane wave travelling through a medium in z-direction by

$$U = U_0 e^{i(\omega t - \beta z)} \tag{7.18}$$

where U_0 is a complex amplitude, $\beta = \frac{\omega n}{c_0}$ is the propagation constant, ω is the angular frequency and n is the refractive index for this particular frequency [3]. Because this wave is extended from minus infinity to infinity, it cannot transfer any information and is not the right mathematical description for a physical signal. A better description is a temporal pulse, and we can describe such wave packets by a function $U(z = 0, t)$, where the position $z = 0$ is chosen without any loss of generality. To study how this function evolves we represent it as a superposition of harmonic waves

$$U(0, t) = \int_{-\infty}^{\infty} U_0(\omega) e^{i\omega t} d\omega \tag{7.19}$$

where the complex amplitudes $U_0(\omega)$ are the inverse Fourier transforms at $z = 0$ and the frequency dependence takes care of the fact, that different frequencies may have different amplitudes. We can now note that every frequency component propagates according to (7.18), with its own propagation constant β, resulting in a total field at an arbitrary

[3] The complex amplitude can be decomposed in an amplitude an phase, $U_0 = |U_0|e^{i\phi}$.

point z given by

$$U(z,t) = \int_{-\infty}^{\infty} |U_0(\omega)| e^{i(\omega t - \beta(\omega) z + \phi(\omega))} d\omega \tag{7.20}$$

If we assume that $|U_0|$ is very sharply peaked in an interval $\Delta\omega$ around some central frequency ω_0 and negligible elsewhere, we can replace the integral over the whole frequency range by an integral over this small region $\Delta\omega$

$$U(z,t) = \int_{\omega_0 - \frac{1}{2}\Delta\omega}^{\omega_0 + \frac{1}{2}\Delta\omega} |U_0(\omega)| e^{i(\omega t - \beta(\omega) z + \phi(\omega))} d\omega \tag{7.21}$$

For weakly dispersive media, the refractive index $n(\omega)$ and therefore the propagation constant $\beta(\omega)$ and the phase of the complex amplitude $\phi(\omega)$ are slowly varying functions of the angular frequency, so we can make a Taylor expansion around the central frequency ω_0 (and neglect higher order terms) [4]

$$\beta(\omega) \approx \beta(\omega_0) + (\frac{d\beta}{d\omega})_{\omega=\omega_0}(\omega - \omega_0) \tag{7.22}$$

$$\phi(\omega) \approx \phi(\omega_0) + (\frac{d\phi}{d\omega})_{\omega=\omega_0}(\omega - \omega_0) \tag{7.23}$$

and insert this in equation (7.21) to get after some reorderings

$$\begin{aligned} U(z,t) &= e^{i(\omega_0 t - \beta_0 z + \phi_0)} \int_{\omega_0 - \frac{1}{2}\Delta\omega}^{\omega_0 + \frac{1}{2}\Delta\omega} |U_0(\omega)| e^{i(\omega-\omega_0)[t - (\frac{d\beta}{d\omega})_{\omega=\omega_0} z + (\frac{d\phi}{d\omega})_{\omega=\omega_0}]} && (7.24) \\ &= A(z,t) e^{i(\omega_0 t - \beta_0 z + \phi_0)} && (7.25) \end{aligned}$$

where we have defined the envelope

[4] This is justified for deriving the group velocity for weakly dispersive media, but if we want to describe e.g. optical solitons, we have to keep terms proportional to ω^2 in the expansion

$$A(z,t) \equiv \int_{\omega_0-\frac{1}{2}\Delta\omega}^{\omega_0+\frac{1}{2}\Delta\omega} |U_0(\omega)| e^{i(\omega-\omega_0)[t-(\frac{d\beta}{d\omega})_{(\omega=\omega_0)}z+(\frac{d\phi}{d\omega})_{\omega=\omega_0}]} \tag{7.26}$$

$$= \int_{\omega_0-\frac{1}{2}\Delta\omega}^{\omega_0+\frac{1}{2}\Delta\omega} |U_0(\omega)| e^{i(\omega-\omega_0)[t-\frac{z}{v_g}+(\frac{d\phi}{d\omega})_{(\omega=\omega_0)}]} \tag{7.27}$$

and finally the definition of the group velocity is made by

$$v_g \equiv \left(\frac{d\beta}{d\omega}\right)^{-1}_{(\omega=\omega_0)} \tag{7.28}$$

7.3 Data sheet of single-channel fiber optic rotary joint

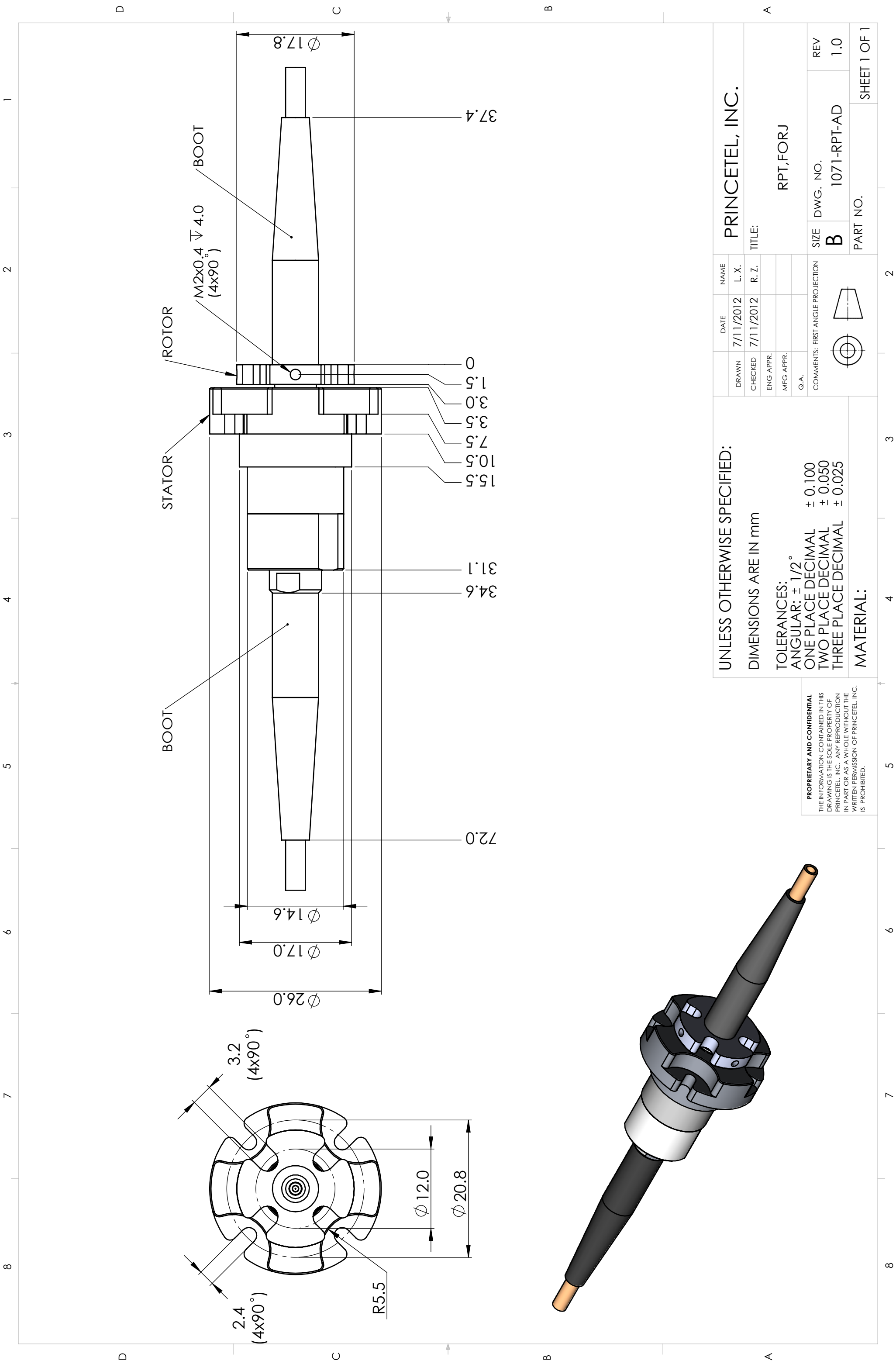

7.4 Rotating Mach-Zehnder interferometer in flat space-time

We consider the same world-line as in section 5.2.1 for the rotating interferometer in curved space-time given by

$$t \rightarrow (t, v_x\, t, a\, sin(\Omega\, t + \Theta) + \rho\, sin(\omega\, t), z_L + a\, cos(\Omega\, t + \Theta) + \rho\, cos(\omega\, t)) \tag{7.29}$$

We use the Minkowskian metric for flat space-time which reads

$$d\tau = \frac{1}{c}\sqrt{\eta_{\mu\nu}dx^{\mu}dx^{\nu}} = \sqrt{1 - \frac{1}{c^2}\frac{d\vec{x}^2}{dt^2}}dt \tag{7.30}$$

Using the coordinate velocity as given by making the derivative of the spatial part of world line (7.29) results in the following expression for the proper time

$$\begin{aligned} \tau &= \int_0^{t_f} \sqrt{1 - \left(\frac{v_x^2 + \rho^2\omega^2 + a^2\Omega^2}{c^2} + \frac{2\, a\, \rho\, \omega\Omega}{c^2} cos((\omega + \Omega)t + \Theta)\right)}dt \\ &\approx \sqrt{1 - \beta^2}t_f - \frac{a^2\Omega^2}{2c^2\sqrt{1 - \beta^2}}t_f - \frac{a\, \rho\, \omega\Omega}{(\Omega + \omega)c^2\sqrt{1 - \beta^2}}\left(sin((\omega + \Omega)t_f + \Theta) - sin(\Theta)\right) \end{aligned} \tag{7.31}$$

were the definition $\beta^2 = \frac{v_x^2 + \rho^2\omega^2}{c^2}$ was made and by assuming $\frac{a^2\Omega^2}{c^2} \ll \beta^2 < 1$ and $\frac{a\rho\omega\Omega}{c^2} \ll \beta^2 < 1$ only first order approximations were kept.

With this expression for the proper time we can calculate the proper time difference for the two spools using the same technique as in section 5.2.1 resulting in

$$\Delta\tau = - - \frac{a^2\Omega^2}{2c^2\sqrt{1 - \beta^2}}\frac{l}{\beta c} - \frac{a\, \rho\, \omega\Omega}{(\Omega + \omega)c^2\sqrt{1 - \beta^2}}\left(sin(\frac{(\omega + \Omega)l}{\beta c} + \Theta) - sin(\Theta)\right) \tag{7.32}$$

which is the same expression as given for the metric in isotropic form for a curved space-time, equation (5.33). Therefore, up to first order, these terms does not contribute to the gravitational proper time difference in curved space-time and the assumptions made in section 5.2.2 are valid.

Bibliography

[1] Steven Weinberg. *Gravitation and Cosmology*. 1st. New York: John Wiley and Sons, Inc, 1972. ISBN: 0-471-92567-5.

[2] R. V. Pound and G. A. Rebka. “Apparent Weight of Photons”. In: *Phys. Rev. Lett.* 4 (7 1960), pp. 337–341. DOI: 10.1103/PhysRevLett.4.337. URL: http://link.aps.org/doi/10.1103/PhysRevLett.4.337.

[3] J C Hafele and R E Keating. “Around-the-World Atomic Clocks: Predicted Relativistic Time Gains”. In: *Science (New York, N.Y.)* 177.4044 (July 1972), pp. 166–8. ISSN: 0036-8075. DOI: 10.1126/science.177.4044.166. URL: http://www.sciencemag.org/content/177/4044/166.abstract.

[4] Irwin I. Shapiro. “Fourth Test of General Relativity”. In: *Phys. Rev. Lett.* 13 (26 1964), pp. 789–791. DOI: 10.1103/PhysRevLett.13.789. URL: http://link.aps.org/doi/10.1103/PhysRevLett.13.789.

[5] S. A. Colella, R. and Overhauser, A. W. and Werner. “Observation of Gravitationally Induced Quantum Interference”. In: *Phys. Rev. Lett.* 34.23 (1975), pp. 1472–1474. DOI: 10.1103/PhysRevLett.34.1472. URL: http://link.aps.org/doi/10.1103/PhysRevLett.34.1472.

[6] Magdalena Zych et al. “Quantum interferometric visibility as a witness of general relativistic proper time”. In: *Nature communications* 2 (Jan. 2011), p. 505. ISSN: 2041-1723. DOI: 10.1038/ncomms1498. URL: http://dx.doi.org/10.1038/ncomms1498.

[7] Magdalena Zych et al. “General relativistic effects in quantum interference of photons”. In: *arXiv: 1206.0965v1 [quant-ph]* (2012), pp. 1–12. URL: `http://www.mendeley.com/research/general-relativistic-effects-quantum-interference-photons-3/`.

[8] N.D. Birrell and P.C.W. Davies. *Quantum fields in curved space*. Cambridge Univeristy Press, 1982.

[9] Nobuyuki Matsuda et al. “Observation of optical-fiber Kerr nonlinearity at the single-photon level”. In: (Nov. 2012). arXiv: `1211.3488`. URL: `http://arxiv.org/abs/1211.3488`.

[10] Isaac Newton. *Philosophiae Naturalis Principia Mathematica, trans. by Andrew Motte*. Ed. by University of California Press. New-York : Published by Daniel Adee, 1966.

[11] Thorne K.S. Misner C. W. and J. A. Wheeler. *Gravitation*. Ed. by Freeman. 1973.

[12] Eckhard Rebhan. *Theoretische Physik: Relativitätstheorie und Kosmologie*. Ed. by Andreas Rüdiger and Bianca Alton. 1st. Berlin/Heidelberg: Springer-Verlag, 2012, pp. 182–185. ISBN: 978-3-8274-2314-6. URL: `Springer.de`.

[13] Sean Caroll. *Spacetime and Geometry*. Ed. by Adam Black and Nancy Benton. 1st. San Franciso: Addison Wesley, 2004. ISBN: 0-8053-8732-3. URL: `www.aw.com/aw`.

[14] Teich M.C. Saleh B.E.A. *Fundamentals of photonics*. Ed. by Boston University Bahaa E.A. Saleh. second edition. John Wiley & Sons, Inc., Hoboken, New Jersey, 2007. URL: `www.wiley.com`.

[15] Ajoy Ghatak and Thyagarajan K. *Introduction to fiber optics*. Ed. by Cambrigde University Press. Press Syndicate of the University of Cambridge, 1998.

[16] R.P. Khare. *Fiber optics and optoelectronics*. 13th. Oxford University Press(YMCA Library Building, 1 Jai Singh Road, New Delhi 110001, India), 2004. ISBN: 978-0-19-566930-5.

[17] D Gloge. “Dispersion in weakly guiding fibers”. In: *Applied optics* 10.11 (Nov. 1971), pp. 2442–5. ISSN: 0003-6935. DOI: 10.1364/AO.10.002442. URL: http://ao.osa.org/abstract.cfm?URI=ao-10-11-2442.

[18] B. Huttner, C. Geiser, and N. Gisin. “Polarization-induced distortions in optical fiber networks with polarization-mode dispersion and polarization-dependent losses”. In: *IEEE Journal of Selected Topics in Quantum Electronics* 6.2 (Mar. 2000), pp. 317–329. ISSN: 1077-260X. DOI: 10.1109/2944.847767. URL: http://ieeexplore.ieee.org/lpdocs/epic03/wrapper.htm?arnumber=847767.

[19] J P Gordon and H Kogelnik. “PMD fundamentals: polarization mode dispersion in optical fibers”. In: *Proceedings of the National Academy of Sciences of the United States of America* 97.9 (Apr. 2000), pp. 4541–50. ISSN: 0027-8424. URL: http://www.pubmedcentral.nih.gov/articlerender.fcgi?artid=34323\&tool=pmcentrez\&rendertype=abstract.

[20] F. Heismann. “Polarization mode dispersion: fundamentals and impact on optical communication systems”. In: *Proc. ECOC, Madrid, Spain* (1998).

[21] Albert Canagasabey et al. “Broadly tunable second-harmonic generation in periodically poled silica fibers”. In: *Optics Letters* 32.13 (2007), p. 1863. ISSN: 0146-9592. DOI: 10.1364/OL.32.001863. URL: http://ol.osa.org/abstract.cfm?URI=ol-32-13-1863.

[22] Piotr T. Chrusciel. “A rotating interferometer”. In: (2014).

[23] Nicolas Brunner and Christoph Simon. “Measuring Small Longitudinal Phase Shifts: Weak Measurements or Standard Interferometry?” In: *Physical Review Letters* 105.1 (July 2010), p. 010405. ISSN: 0031-9007. DOI: 10.1103/PhysRevLett.105.010405. arXiv: 0911.5139. URL: http://arxiv.org/abs/0911.5139.

[24] Boaz Tamir and Eliahu Cohen. “Introduction to Weak Measurements and Weak Values”. en. In: *Quanta* 2.1 (May 2013), p. 7. ISSN: 1314-7374. DOI: 10.12743/quanta.v2i1.14. URL: http://quanta.ws/ojs/index.php/quanta/article/view/14.

Curriculum vitae

Personal data:

Name:	Christopher Karl Hilweg
Date of birth:	15.07.1988
Nationality:	Austria
Work adress:	Faculty of Physics, University of Vienna Boltzmanngasse 5 1090 Vienna Austria

---

Education:

03/2013 – Present	Master of Science: Physics University of Vienna Title Master thesis: Interferometric tests of quantum physics on curved space-time
10/2008 - 02/2013	Bachelor of Science: Physics University of Vienna Title Bachelor thesis: Die Rolle der negativen Entropie in der Quantenmechanik
09/2002 – 06/2007	Secondary collegue for mechanical engineering Klagenfurt, Lastenstraße
09/1998 - 07/2002	Secondary modern school Althofen
09/1994 - 07/1998	Elementary school Guttaring

Work experience:

09/2013 – 09/2014	University of Vienna, Faculty of Physics student assistant
10/2012 – 07/2014	University of Vienna, Faculty of Physics Student tutor
10/2013 – 02/2014	University of Natural Researches and Life Sciences, Vienna Mathematic instructor

10/2012 – 02/2013	University of Natural Researches and Life Sciences, Vienna Mathematic instructor
08/2007 – 09/2007	Treibacher Industrie AG Assistant in chemical laboratory
08/2006 – 09/2006	Treibacher Industrie AG Assistant in chemical laboratory

Languages and skills:

Mother tongue:	Deutsch
Other languages:	English (proficient), Slovak (basic)
Programms:	MS Office (very good) PRO Engineer Wildfire (good) SolidWorks (good) C++ (beginner)